

Electronic Thesis and Dissertation Repository

---

7-5-2011 12:00 AM

## Optical Power Splitting Techniques Using Photonic Crystal Line Defect Waveguides

Rajat Dey, *The University of Western Ontario*

Supervisor: Dr. Jayshri Sabarinathan, *The University of Western Ontario*

A thesis submitted in partial fulfillment of the requirements for the Doctor of Philosophy degree in Electrical and Computer Engineering

© Rajat Dey 2011

Follow this and additional works at: <https://ir.lib.uwo.ca/etd>



Part of the [Electromagnetics and Photonics Commons](#), and the [Nanotechnology Fabrication Commons](#)

---

### Recommended Citation

Dey, Rajat, "Optical Power Splitting Techniques Using Photonic Crystal Line Defect Waveguides" (2011). *Electronic Thesis and Dissertation Repository*. 192.  
<https://ir.lib.uwo.ca/etd/192>

This Dissertation/Thesis is brought to you for free and open access by Scholarship@Western. It has been accepted for inclusion in Electronic Thesis and Dissertation Repository by an authorized administrator of Scholarship@Western. For more information, please contact [wlsadmin@uwo.ca](mailto:wlsadmin@uwo.ca).

**OPTICAL POWER SPLITTING TECHNIQUES USING PHOTONIC CRYSTAL  
LINE DEFECT WAVEGUIDES**

**(Spine title: Optical Power Splitting Techniques Using Photonic Crystal Line  
Defect Waveguides)**

**(Thesis format: Monograph)**

**by**

**Rajat Dey**

**Graduate Program  
in  
Engineering Science  
Electrical and Computer Engineering**

A thesis submitted in partial fulfillment  
of the requirements for the degree of  
Ph.D

School of Graduate and Postdoctoral Studies  
The University of Western Ontario

**© Rajat Dey, 2011**

# Certification of Examination

THE UNIVERSITY OF WESTERN ONTARIO  
SCHOOL OF GRADUATE AND POSTDOCTORAL STUDIES  
CERTIFICATE OF EXAMINATION

Chief Advisor:

---

Dr. Jayshri Sabarinathan

Examining Board:

---

Dr. Anestis Dounavis

---

Dr. Xianbin Wang

---

Dr. Mahi Singh

---

Dr. Stephen Karrer O’Leary

The thesis by

**Rajat Dey**

entitled:

**Power Splitting Techniques Using Photonic Crystal Line Defect Waveguides**

Is accepted in partial fulfillment of the  
Requirements for the degree of  
Ph.D

Date: \_\_\_\_\_

---

Chair of Examination Board

# Abstract

“Photonic Crystals (PCs)” are dielectric structures with periodic spatial alternations of refractive index on the scale of the wavelength of light. Many optical devices, based on PCs, have been proposed. There are multiple ways by which equal amount of power of incoming signals can be divided into two, three and four output channels; for example using multiple coupled photonic crystal waveguides, directional coupling and cascaded multimode PC waveguides. Ideally, the splitter should divide the input power equally into the output channels without significant reflection or radiation losses and should be compact in size. In this thesis we have proposed different techniques of optical power splitting using (a) Y-junction, (b) PC line defect waveguides integrated with multimode interference (MMI) block, and (c) multiple line defect PC waveguides. The optical modeling of these proposed structures were investigated by finite difference time domain (FDTD) simulation. The goal was to achieve equal power at each output channel with broad spectrum around the target wavelength with low loss.

Using a new design of a 2-D slab based Y-junction scheme, we have achieved 84.4% power output from a 1×2 power splitter and 58.3% from a 1×4 power splitter configuration respectively. Then to improve the power transmission of 1×4 power splitter configuration, we have examined two more structures, one is 2-D slab PC line defect waveguides integrated with MMI block and another which is based on multiple line defect waveguides. The first structure transmits 75.7% power at the output with 46nm broad spectrum for a 2-D slab configuration whereas the second structure transmits 94.9% power at output with 32nm broad spectrum for 2-D configuration.

The advantages of PC line defect waveguides integrated with MMI block for 1×4 power splitter configuration over the Y-junction are ease of fabrication, broad output spectrum and high transmission power. The only disadvantage is the size of the device. The device is somewhat larger than other devices but still compact enough to compete with commercial on chip optical power splitters. In future multiple line defect PC waveguides will probably be able to achieve both compact size and high power.

**Keywords: Photonic crystal, Photonic crystal line defect waveguide, Multimode interference block, 60° bend waveguide, multiple line defect waveguide.**

# Acknowledgements

I would first like to express my thanks to my research advisor, Dr. Jayshri Sabarinathan, whose support, encouragement, creativity, and insight have guided me and helped me to develop my critical thinking skill. I am extremely fortunate to be her student, and I continue to admire her talent and personality.

I wish to thank my present and past members of the research group for their help and friendship. In particular, post doctoral fellow Dr. Aref Bakhtazad for his enormous help and suggestions from his sound bank of knowledge. Hao for his good humor, motivation, and initiative to help. Anil for his patience in helping with my fabrication work.

I would like to express my gratitude to Baolai Ge at Sharcnet of parallel computing for his suggestions and help in effectively using the simulation software to running the simulation on the server.

I extend my thanks to Tim Hawk, Todd Simpson, and Rick Glew for all their help at the Nanofabrication Laboratory.

My parents, and my sister Madhushree Dey, for their love, friendship, encouragement, and unconditional support during the course of my studies and also constantly serve to remind me of the great achievements that are always possible and of the remarkable opportunities that can always be found.

My wife Priyanka for her seemingly indispensable reserves of patience and encouragement, and for helping to make my time as a Ph.D student engaging and wonderful. I wish to express my gratitude and love for her prayers and support.

Last but not the least; I would like to thank God for all his/her blessings and grace. I thank him/her for all of the opportunities, experiences, and people he/she brought into my life, and I thank him/her for answered prayers and opened doors.

# Table of Contents

<b>Certification of Examination .....</b>	<b>ii</b>
<b>Abstract.....</b>	<b>iii</b>
<b>Acknowledgements .....</b>	<b>iv</b>
<b>List of Tables .....</b>	<b>viii</b>
<b>List of Figures.....</b>	<b>ix</b>
<b>Acronyms.....</b>	<b>xiv</b>
<b>1. Introduction.....</b>	<b>1</b>
1.1 Overview of Photonic Crystals.....	2
1.2 Overview of Photonic Crystal Splitter.....	4
1.3 Overview of Multi Mode Interference Splitter.....	6
1.4 Motivation.....	7
1.5 Challenges.....	11
1.6 Organization of Thesis.....	12
<b>2. 2-D Slab Photonic Crystal Based Power Splitter .....</b>	<b>14</b>
2.1 2D Slab Photonic Crystal.....	14
2.2 Defects in PC .....	16
2.2.1 Line defect waveguides.....	17
2.2.2 PC microcavity.....	19
2.3 2D Photonic Crystal in Splitter Application.....	21
2.3.1 2-D slab PC based Y-Junction Splitter .....	21
2.3.2 Ultracompact multiway beam splitter using photonic crystal dielectric rod ...	23
2.3.3 Photonic Crystal power-splitter based on directional coupling .....	25
2.3.4 Power splitter based on cascaded multimode photonic crystal waveguides....	27
2.4 Summery.....	28
<b>3. 2-D slab photonic crystal based Y-junction 1×2 and 1×4 power splitter .....</b>	<b>30</b>
3.1 FDTD Simulation .....	32
3.1.1 Basic aspect of 3-D FDTD.....	32
3.1.2 Simulation boundaries in 3-D FDTD.....	33
3.2 Description of Y-Junction Structure.....	34
3.3 Characterization of Y-Junction in 3-D FDTD .....	34
3.3.1 Simulation setup.....	35
3.3.2 Power transmission of unmodified structure .....	36
3.3.3 Modification of the design.....	37
3.3.4 Analysis of modified Y-junction .....	38
3.3.5 Design of 1×4 power splitter based on Y-junction .....	42
3.3.6 Improve transmission by changing slab thickness.....	44
3.4 Fabrication of 2-D Slab 1×2 Y-Junction Base Power Splitter.....	46

<b>4. Photonic Crystal Line Defect Waveguides Integrated with Multimode Interference Block based Power Splitter .....</b>	<b>50</b>
4.1 Design of 2-D Photonic Crystal Line Defect Waveguides Integrated with MMI for Power Splitter Application.....	52
4.1.1 Basic structure of MMI.....	52
4.1.2 Integration of MMI and photonic crystal line defect waveguides .....	53
4.1.3 FDTD simulation parameter for entire structure .....	54
4.1.4 Mode profile analysis.....	55
4.2 Optimization Process .....	55
4.2.1 Optimization of MMI length.....	56
4.2.2 Improvement of output power .....	57
4.2.3 Analysis of power spectrum.....	58
4.3 Design of 2-D Slab Photonic Crystal Line Defect Waveguides Integrated with MMI for Power Splitter Application .....	60
4.3.1 Basic structure of MMI.....	60
4.3.2 Device design.....	60
4.3.3 FDTD simulation parameter for entire structure .....	61
4.3.4 Mode profile analysis.....	62
4.4 Optimization Process .....	63
4.4.1 Optimization of MMI length.....	64
4.4.2 Optimization of conventional waveguide width .....	65
4.4.3 Analysis of overall result .....	66
<b>5. Multiple Line Defect Based Power Splitter .....</b>	<b>68</b>
5.1: Principles and Computational Methods.....	69
5.1.1 Maxwell's equations for PCs.....	69
5.1.2 Bloch's theorem.....	70
5.1.3 Plane wave expansion method .....	71
5.1.4 Effective refractive index.....	72
5.1.5 Finite Difference Time Domain (FDTD) method.....	73
5.2 Modeling of Multiple Line Defect Waveguides for 1×4 Power Splitter .....	74
5.2.1 2-D FDTD simulation parameter .....	75
5.2.2 Design of PC multiple line defect waveguides.....	76
5.2.2.1 Analysis of multimode PC line defect waveguides using self-imaging phenomenon.....	77
5.2.2.2 Design of power splitter structure.....	85
5.2.2.3 Determination of separation region .....	87
5.2.2.4 Merits and demerits of the multiple line defect waveguides structure .....	89
5.3 Modeling of Multiple Line Defect Waveguides for 1×3 Power Splitter .....	91
5.3.1 3-D FDTD simulation parameter .....	91
5.3.2 Design of multiple line defect waveguides on 2-D PC slab .....	92
5.3.2.1 Methodology of 1×3 power splitting technique.....	94
5.3.2.2 Analysis of 1×3 power splitter design .....	99
5.3.2.3 Advantage and disadvantage of multiple line defect waveguides structure	101

<b>6. Analysis and Comparison of Different Power Splitter Configuration.....</b>	<b>103</b>
6.1 Comparison of 1×2 Power Splitter on 2-D Slab Photonic Crystal Configuration	104
6.2 Comparison of 1×4 Power Splitter on 2-D Photonic Crystal Configuration.....	105
6.3 Comparison of 1×4 Power Splitter on 2-D Slab Photonic Crystal Configuration	106
<b>7. Conclusion and Suggestions for Future Work.....</b>	<b>108</b>
7.1 Summary.....	108
7.2 Suggestion for Future Work.....	110
<b>Bibliography.....</b>	<b>112</b>
<b>Appendix A: Gold deposition on alignment marks through lift off process.....</b>	<b>119</b>
<b>Appendix B: Photolithography with conventional waveguide and etching for conventional waveguide.....</b>	<b>120</b>
<b>Appendix C: E-beam Lithography.....</b>	<b>121</b>
<b>Appendix D: Recipe for Bosch etching.....</b>	<b>122</b>
<b>Curriculum Vitae.....</b>	<b>123</b>



# List of Tables

Table 5-1. Parameter used to calculate the folded images position of 7-PCLDWs at $0.264(a/\lambda)$ .....	83
Table 5-2. Parameter used to calculate the folded images position of 5-PCLDWs at $0.264(a/\lambda)$ .....	84
Table 5-3. Parameter used to calculate the folded images position of 3-PCLDWs at $0.264(a/\lambda)$ .....	84
Table 5-4. Multiple line defect waveguides transmitted output power.....	84
Table 5-5. Transmitted output power of the devices.....	87
Table 5-6. Parameter used to calculate the folded images of 3-PCLDWs at $0.258(a/\lambda)$ ...97	
Table 5-7. Parameter used to calculate the folded images of 5-PCLDWs at $0.258(a/\lambda)$ ...97	
Table 5-8. Multiple line defect waveguides transmitted output power.....	99
Table 5-9. Transmitted output power of $1\times 3$ splitter.....	101
Table 6.1 Comparison between Y-junction based power splitter and literature benchmark.....	104
Table 6.2 Comparison between proposed designs with literature benchmark.....	105
Table 6.3 Comparison between two proposed designs.....	106
Table A-1: recipe for gold deposition on alignment marks through lift off process.....	119
Table B-1: Recipe for conventional waveguide etching.....	120
Table C-1: Parameters of E-beam.....	121
Table D-1: Recipe for ICP etch... ..	122

# List of Figures

Figure 1.1 Schematic depiction of three types of photonic crystals (a)1-D, (b) 2-D and (c) 3-D. The different colours represent materials with different dielectric constants.....	2
Figure 1.2 (a) Electronic bandgap (b) Photonic bandgap.....	3
Figure 1.3 Schematic Y-junction power splitter based on photonic crystal.....	4
Figure 1.4 Schematic diagram of power splitter based on directional coupling with two branches.....	5
Figure 1.5 Illustration of a 1×4 MMI splitter.....	7
Figure 1.6 Optical signal distribution using PC line defect waveguides integrated with MMI block.....	11
Figure 2.1 2-D PCS with finite-height high-index slab surrounded by low index dielectric region.....	14
Figure 2.2 Simulated photonic band structures for bulk PC with finite height (a) Schematic of 2-D PCS triangular lattice structure; (b) Simulated photonic band structure of 2-D triangular lattice PCS, the shadow region marked the PBG.....	16
Figure 2.3 LDWG formed by (a) introducing a single defect inside a regular PC lattice breaks its periodicity and (b) band structure of corresponding PC LDW.....	18
Figure 2.4 Light transmissions in 90 degree waveguide.....	18
Figure 2.5 Schematic of (a) microcavity formed by removing a single air hole and (b) microcavity formed by removing 7 air holes at the center of PC.....	20
Figure 2.6 Structure and the TM field profile of an acceptor type point defect made by increasing the radius of the central hole.....	20
Figure 2.7 (a) Schematic of Y-junction power splitter based on 2-D slab PC; (b) Normalized transmission spectra (Measured and Simulation) of channel 1 and 2 between 1350nm-1600nm wavelengths.....	22
Figure 2.8 (a) Schematic diagram of beam splitters consist of the inout PCWs (a) 5-CPCWs; (b) 7- CPCWs and output PCWs. Modified rods are enclosed by rectangle.....	23
Figure 2.9 Output transmitted power is a function of the variable of CPCWs rods (a) in the 1×3 splitter and (b) in the 1×4 splitter.....	24

Figure 2.10 Schematic diagram of photonic crystal power splitter. The device is divided into two regions, as labeled on top. Black boxed area indicates super-cells. White holes represent air-holes.....	25
Figure 2.11 Normalized output power after FDTD computation, Grey area indicated spectrally flat coupling range.....	26
Figure 2.12 (a) Configuration of PC power splitter with cascade area-defect structure. (b) Optimized structure with radius of air holes in region 1 is set to $R_1 = 0.26a$ , the radius of air holes in region 2 is designed with a taper structure that $R_2$ decreases from $0.28a$ to $0.22a$ in contra-direction, and with the same displacement $d = 0.1a$ .....	27
Figure 2.13 Normalized output power transmission is indicated by solid-circle red line for proposed structure whereas square-blue line indicated the power transmission of the simple structure. Grey line indicates over 45% power is transmitted.....	28
Figure 3.1 Yee's cell used in 3-D FDTD simulation.....	32
Figure 3.2 Preliminary Y branch structure.....	34
Figure 3.3 3-D FDTD simulation setup for the designed Y-junction.....	35
Figure 3.4 3-D FDTD calculation of normalized output power transmission of an unmodified Y-junction structure.....	37
Figure 3.5 Modified Y branch structure.....	38
Figure 3.6 Normalized transmission of output power spectrum of modified Y-junction based power splitter.....	39
Figure 3.7 Normalized maximum transmitted output power of Y-junction based power splitter.....	40
Figure 3.8 FDTD simulation of the electric field distribution in the optimized Y-junction base power splitter when the incident wave arrives at the level of the additional holes...41	41
Figure 3.9 Architecture of 1 to 4 power splitter using Y-junction.....	42
Figure 3.10 Normalized transmitted output power of Y-junction based $1 \times 4$ power splitter .....	43
Figure 3.11 Normalized transmission of output power spectrum of modified Y-junction with 250nm slab thickness.....	44
Figure 3.12 Transmitted output power of Y-junction base $1 \times 4$ power splitter with 250nm slab thickness.....	45

Figure 3.13 Schematic diagram of a PC base 1×2 Y-junction power splitter fabrication on SOI platform.....	47
Figure 3.14 SEM image of Y-junction structure.....	49
Figure 4.1 Schematic diagram of MMI power splitter.....	52
Figure 4.2 Basic structure of proposed power splitter, consist of input conventional waveguide, multimode interference region and PC line defect waveguides.....	54
Figure 4.3 (a) Initial structure of MMI block integrated with conventional waveguide (b) FDTD simulation of electric field profiles at the output edge of MMI. The operating wavelength of this excitation is 1.55μm.....	55
Figure 4.4 Optimized structure of 1 to 4 power splitter with length of multimode region is 93.5μm. The width of the MMI region is 14.20μm.....	56
Figure 4.5 Normalized output transmission spectra at four channels with different $L_{\min}$ values and maximum energy transfer when $L_{\min} = 93.5\mu\text{m}$ .....	57
Figure 4.6 Normalized output transmission spectra at four channels with $L_{\min} = 93.5\mu\text{m}$ , $W_e = 14.20\mu\text{m}$ and varying conventional waveguide width from 0.5μm to 1.4μm.....	58
Figure 4.7 Normalized output transmitted power at each channel with respect to incident power.....	59
Figure 4.8 (a) Initial structure of 2-D slab MMI block integrated with conventional waveguide (b) FDTD simulation of electric field profiles at the output edge of MMI. The operating wavelength of this excitation is 1.55μm.....	61
Figure 4.9 (a) Basic structure of proposed power splitter, consist of input conventional waveguide, multimode interference region and PC line defect waveguides; (b) FDTD simulation setup for the entire structure.....	62
Figure 4.10 Optimized structure of 1 to 4 power splitter with length of multimode region is 56.2μm. The width of the MMI region is 11.08μm.....	64
Figure 4.11 Normalized output transmission spectra at four channels with different $L_{\min}$ values and maximum energy transfer when $L_{\min} = 56.2\mu\text{m}$ .....	65
Figure 4.12 Normalized output transmission spectra at four channels with $L_{\min} = 56.2\mu\text{m}$ , $W_e = 0.95\mu\text{m}$ and varying conventional waveguide width from 0.85μm to 1.2μm.....	66
Figure 4.13 Normalized output transmitted power at each channel with respect to incident power.....	66

Figure 5.1 2-D triangular lattice and its reciprocal lattice.....	70
Figure 5.2 2-D FDTD simulation setup.....	75
Figure 5.3 Geometry of photonic crystal multiple line defect waveguides power-splitters: (a) Combination of seven and one pair of three PCLDWs; (b) Combination of five and one pair of three PCLDWs and setup for the FDTD method. The device is divided into five regions, as labeled at the bottom. Black boxes indicated super-cell for PWE calculation. White holes represent air-holes etched on Si ( $n_{\text{eff}}=2.847$ ).....	77
Figure 5.4 The dispersion curves for (a) 7-PCLDWs (b) 5-PCLDWs and (c) 3-PCLDWs and computational super-cell (inset).....	79
Figure 5.5 Schematic diagrams of multiple line defect waveguides (a) 7-PCLDWs, (b) 5-PCLDWs (c) 3-PCLDWs with profile monitor on multimode region.....	80
Figure 5.6 FDTD simulated results of steady-state electric field distribution in the multi mode regions of (a) 7-PCLDWGs (b) 5-PCLDWs and (c) 3-PCLDWGs at $0.264(a/\lambda)$ ...81	
Figure 5.7 Input waveguide divided into two output channel with MR of (a) 7-PCLDWs, (b) 5-PCLDWs and (c) 3-PCLDWs.....	85
Figure 5.8 Transmitted output power of MRs after FDTD computation as a function of the number of periods: between 58 period to 78 period (a) in 7-PCLDWs , between 46 period to 60 period (b) in 5-PCLDWs, between 23 period to 45 period in (c) 3-PCLDWs.....	86
Figure 5.9 Schematic diagram of two $1\times 4$ power PC power splitter with same separation region; (a) combination of seven and one pair of three PCLDWs;(b) combination of five and one pair of three PCLDWs.....	87
Figure 5.10 Transmitted power at the output channels with variable separation region; (a) $1\times 4$ splitter denotes combination of 7-PCLDWs and one pair of 3-PCLDWs; (b) $1\times 4$ splitter denotes combination of 5-PCLDWs and one pair of 3-PCLDWs.....	89
Figure 5.11 Normalized output power of all the output ports with variable one pair of 3-PCLDWs of the proposed splitters: (a) $1\times 4$ splitter when 7-PCLDWs and SR period is fixed; (b) $1\times 4$ splitter when 5-PCLDWs and SR period fixed.....	89
Figure 5.12 Normalized output power after 2D FDTD computation of (a) combination of seven and one pair of three PCLDWs; (b) combination of five and one pair of three PCLDWs.....	90
Figure 5.13 (a) Schematic diagram of power splitter based on 2-D slab PC multiple line defect waveguides. It is a combination of three and five PCLDWs. (b) Design figure in FDTD simulation.....	93

Figure 5.14 The dispersion curves for (a) 3-PCLDWs and (b) 5-PCLDWs.....	95
Figure 5.15 Schematic diagrams of multiple line defect waveguides (a) 3-PCLDWs, (b) 5-PCLDWs with profile monitor on multimode region.....	96
Figure 5.16 FDTD simulated results of steady-state electric field distribution in the multi mode regions of (a) 3-PCLDWs and (b) 5-PCLDWs at $0.258(a/\lambda)$ .....	96
Figure 5.17 Input waveguide is divided into output channel with the help of MRs of (a) 3-PCLDWs and (b) 5-PCLDWs.....	98
Figure 5.18 transmitted output power of MRs after the FDTD computation as function of the number of periods: between 29 periods to 45 periods (a) 3-PCLDWs, between 29 periods to 46 period (b) 5-PCLDWs.....	98
Figure 5.19 (a) Transmitted power at the output channels with variable separation region of $1\times 3$ splitter combination of 3-PCLDWs and 5-PCLDWs; (b) Normalized output power of all the output channel with variable periods of 5-PCLDWs of $1\times 3$ splitter.....	100
Figure 5.20 Normalized output power after 3-D FDTD computation of combination of three and five PCLDWs with a separation region of $9^{\text{th}}$ periods.....	101
Figure 7.1 Multiple line defect waveguides integrated with MMI for $1\times 4$ power splitter application.....	110
Figure 7.2 2-D PC based MMI for $1\times 4$ power splitter application.....	111

# Acronyms

BPM	Beam propagation method
CWG	Conventional waveguide
CPCW	Coupled photonic crystal waveguide
CW	Continuous wave
EBL	Electron beam lithography
FDTD	Finite difference time domain
He	Helium
ICP	Inductively coupled plasma
IPA	Iso-Propyl-alcohol
LDW	Line defect waveguide
MMI	Multi mode interference
MR	Multimode region
MLDWG	Multiple line defect waveguide
1D	One- dimensional
PC	Photonic Crystal
PBG	Photonic bandgap
PCS	Photonic crystal slab
PCW	Photonic crystal waveguide
PIC	Photonic integrated circuits
PML	Perfect matched layer
PWEM	Plane wave expansion method
PWE	Plane wave expansion
PAA	Phased Antenna Array
RF	Radio frequency
SOI	Silicon on insulator
SEM	Scanning Electron Microscope
SR	Separation region

2D	Two- dimensional
3D	Three-dimensional
TIR	Total internal reflection
UPML	Uniaxial perfectly matched layers
UV	Ultraviolet

### **Units**

fs	Femtoseconds
$\mu\text{m}$	Micrometers
nm	Nanometers



# Chapter 1

## Introduction

“Photonic Crystals” (PC) are dielectric structures with periodic spatial alternations of the refractive index on the scale of the wavelength of the light [1, 2]. Due to this periodicity, a photonic bandgap (PBG) is formed and the propagation of electromagnetic waves is prohibited for all wave vectors within this bandgap. Over the past several years, various important scientific and engineering applications such as the control of light emission and propagation and the trapping of photons, have been realized the photonic bandgap and artificially introduced defects.

In this thesis, new power splitting techniques using 2-D and 2-D slab PC line defect waveguides are investigated. In order to achieve this, initially we investigated the Y-junction structure for  $1\times 2$  and  $1\times 4$  applications. In this scheme, we have improved the power transmission and output spectrum in  $1\times 2$  application which is better than published result where as in  $1\times 4$  applications the power transmission and output spectrum is not good enough for practical application point of view. So, in order to improve the power transmission and output spectrum we have investigated a new design where PC line defect waveguides are integrated with a multimode interference (MMI) block for  $1\times 4$  power splitting applications. Optical modeling is used to demonstrate that the power is equally divided at each output channel with a relatively broad spectrum. A structure is also considered where multiple line defect waveguides are used for  $1\times 4$  power splitter applications. In this scheme, we have investigated the two versions which

are a combination of five and one pair of three line defect waveguides and another one with seven and one pair three line defect waveguides. These two structures are more compact than the previous design but in terms of practical implementation the design on a 2-D slab need to be further explored for the  $1 \times 4$  application. Among those structures Y-junction based  $1 \times 2$  power splitter was fabricated which will subsequently be measured.

## 1.1 Overview of Photonic Crystals

PCs are defined as structures with periodically varying dielectric constant in specific symmetric direction with periodicity of the order of the wavelength of the light in the material that the PCs are made of. According to the dimensions of the periodicity, PCs are classified into one-dimensional (1D), i.e. where the dielectric variation is along one direction. Similarly two-dimensional (2D) and three-dimensional (3D) PC are defined when the dielectric constant varies along two and three direction respectively. Schematic samples of different types of PCs are shown in Figure 1.1.

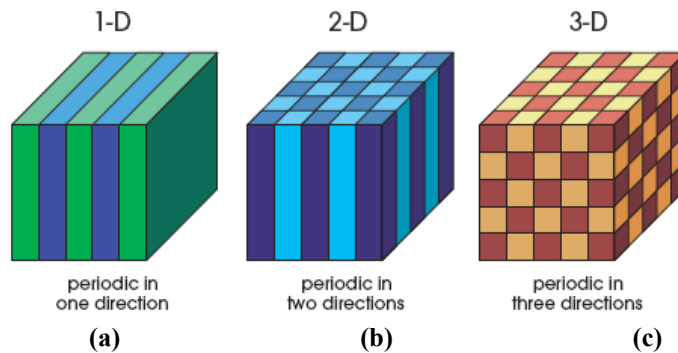


**Figure 1.1: Schematic depiction of three types of photonic crystals (a) 1-D, (b) 2-D and (c) 3-D. The different colours represent materials with different dielectric constants [1]**

Theoretically a PC can be considered as an optical analogue to the semiconductor crystal lattice which provides a periodic potential to an electron propagating through it. Hence Bragg like diffraction energy bandgaps is introduced to explain the electrons forbidden

phenomenon. The electron bandgap (Figure 1.2(a)) is an energy range where there are no electrons stable. The electron bandgap is due to the periodic lattice of the atoms in semiconductor. Similarly in a PC, if the dielectric constant of the materials forming the crystal is varied periodically, the scattering at the interface can produce photonic bandgaps, thus preventing light from propagating in certain directions with specific energies (Figure 1.2(b)) [3]. Photonic bandgap is a frequency gap where there is no photons existing in this range in the PC structures. This is due to the destructive interference of the light in the periodic structure.

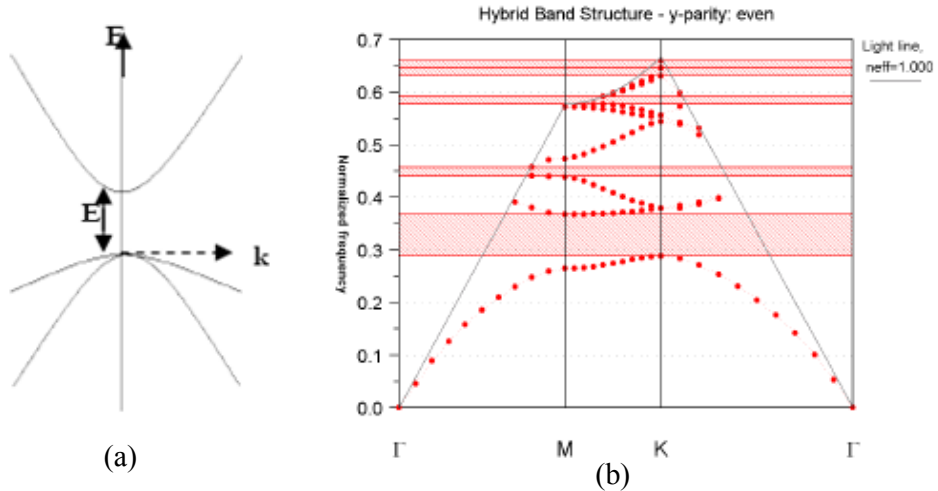


**Figure 1.2: (a) Electronic bandgap [3]; (b) Photonic bandgap**

The underlying concept behind these materials stems from the pioneering work of Yablonovitch [3] and John [4]. Yablonovitch demonstrated the existence of a PBG through simulations, where modes were missing in all the directions (i.e. entire  $K$ -space) and hence spontaneous emission corresponding to the gap energy is inhibited inside a 3-D PC. John similarly pointed out that new phenomenon can be observed using a PC, including the localization of light. 3-D PCs offer complete photonic bandgap through which light can be controlled in all directions in space, how ever it is limited by the fabrication techniques and are more difficult to realize compared to 1-D and 2-D PCs.

Meanwhile, 2-D planar PCs are much easier to fabricate and integrated with planar chips. They offer most of the desirable qualities of 3-D PCs. However, they exhibit quasi 3-D confinement resulting from in-plane periodicity in the horizontal direction and total internal reflection in the perpendicular plane.

## 1.2 Overview of Photonic Crystal Splitter

The optical power splitter or divider is an indispensable component in photonic integrated circuits which is used in fiber optic networks. Basic structure of the splitter is divided into two parts, an input and an output port. Ideally, input power is equally divided into the output ports without any significant reflection and radiation loss. To our knowledge the most straightforward power splitter is the Y-junction structure. The structure of this Y-junction is formed by the intersection of three photonic crystal waveguides (PCWs) at  $120^\circ$ . The output channels have an additional  $60^\circ$  bend which is parallel to the input channel as shown in Figure 1.3. Due to Y-junction and  $60^\circ$  bend single mode operation might suffer which causing the reflection and large transmission loss.

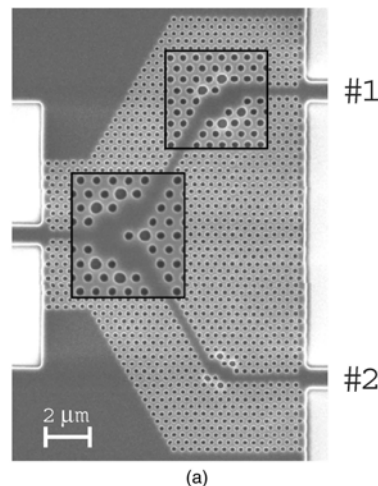
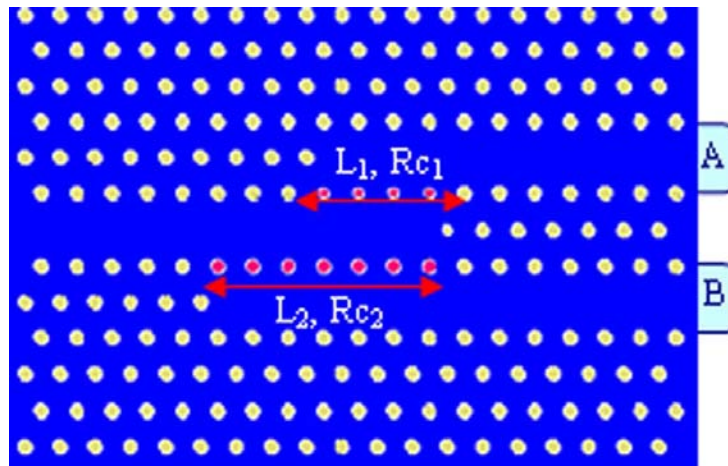


Figure 1.3: Schematic Y-junction power splitter based on photonic crystal [5]

To overcome these difficulties the junction and bend must be carefully designed. Even after that there are some difficulties (mode mismatch and bending loss) which are not easily addressed for practical applications [5, 6]. To minimize the multimode problem and bending loss, many researchers investigated theoretically an array of dielectric rods in air. The advantage of this structure is the waveguide created by removing a single line of rods which is single mode and light travels around the sharp bends with high transmission is relatively straight forward. Based on this concept the T-junction, Y-junction and multiple coupled photonic crystal waveguides have already been investigated [6, 7]. Unfortunately the rod in air approach does not provide enough vertical confinement and it is very difficult to implement as a practical device implementation in optical regime. After that Afsin Ghaffari et al. proposed a PC power splitter design where working principal depends on directional coupling as shown in Figure 1.4.



**Figure 1.4: Schematic diagram of power splitter based on directional coupling with two branches [8]**

In the above design two, parallel waveguides are replaced with a single line defect waveguide W1 (One missing row of holes). These waveguides are preferred over two

parallel waveguides due to their single mode of operation and low loss activity and nearly 50% transmission is achieved at each of the output channel. The transmission depends on the coupling coefficient ( $\kappa$ ) which is again related to the radius of the coupling rod and the coupling length. So the key parameters for high transmission efficiency are coupling length and radius of coupling rod. As a result the device design is more complicated and it is very cumbersome to consider it as a whole device on 2D slab PC configuration.

### **1.3 Overview of Multi Mode Interference Splitter**

The optical waveguide splitter is an important device in integrated optical interconnect systems. Standard splitters based on X and Y junction designs have reflection and radiation loss due to their mode complexity. To avoid this problem MMI inclusion in the splitter series is growing research interest. It has many advantages such as low loss, good uniformity, insensitive to operation wavelength, polarization, large bandwidth, simple fabrication technique, larger tolerance, minimized structure, temperature and other environmental factors. MMI splitters work on the principle of the self-imaging effect, a property of multimode waveguides by which an input field is reproduced in single or multiple images at periodic intervals along the propagation direction of the guide [9]. MMI structure consists of single mode input waveguides, a multimode section and single mode output waveguides as shown in Figure 1.5, where  $W_{\text{mmi}}$  is the width of the multimode waveguide and  $L_{\text{mmi}}$  is the length of the multimode waveguide. Due to the principle of self-imaging, the optical field generates one or several images of the input field periodically in the direction of transmission. Therefore effective width ( $W_e$ ) and beat length ( $L_\pi$ ) of the two lowest order modes are defined as:

$$L_{\pi} = \frac{\pi}{\beta_0 - \beta_1} \cong \frac{4n_r W_e^2}{3\lambda_0} \quad (1)$$

$\beta_0$  and  $\beta_1$  are the propagation constant of the fundamental mode,  $\lambda_0$  is the wavelength in free space and  $n_r$  is the effective refractive index of the core layer of the planar waveguide.

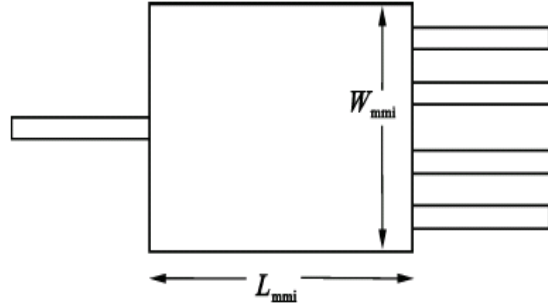


**Figure 1.5 Illustration of a 1×4 MMI splitter [9]**

The effective width of the multimode waveguide is little larger than the geometrical width ( $W_{\text{mmi}}$ ) of the waveguide. In order to reduce the influence of the higher order mode in MMI splitter, the input and output waveguide shape in the form of ridge so it maintain the uniform single mode operation at the output end.  $L_{\text{mmi}}$  plays an important role to locate the output port at the multi mode waveguide.

## 1.4 Motivation

Equal amount of power distribution in each branch is the fundamental function in electronics. Chip designs more complex the latency of the power distribution is increasing, leading to increased skew and jitter. Moreover as chips become faster, the accuracy of electrical distribution networks is declining [10, 11]. Some of these limitations can be addressed by optical power distribution, which refers to the use of

optical signals to provide the timing boundaries and keep data paths synchronous in digital systems.

Many approaches of optical power distribution are being researched using conventional dielectric waveguides [11, 12], free space optics [13] and PC based virtual waveguides [14]. Its implementation on a chip requires a light source, a distribution layer consisting of optical interconnects and an active optoelectronic device layer providing the conversion of an optical signal into corresponding electrical signal. The power distribution is essentially carried out through a series of optical waveguides acting as interconnects. The main advantages of using an optical interconnect layer over electrical ones include better immunity to electromagnetic noise and temperature variations, reduce skew and jitter at higher frequencies, lower power consumption, design simplification and possibility to make crosstalk free crossings which would simplify the interconnect problem considerably. On the other hand, on-chip optical interconnects have to face several challenges like the compatibility with the mainstream silicon technology and the reduced physical size of all optical devices for both integration and high-frequency operation. Therefore optical interconnects needs high-index contrast platforms where the optical field intensity is strongly confined with the sharp bends without significant bending loss.

In this thesis, we propose a novel schemes of implementing an equal amount of power distribution through photonic crystal based waveguides. The research work in this proposal is mainly motivated by the following aspects:

- PC line defect waveguides (LDWs) integrated with MMI block for power splitting has potential to transmit power from input to the output without any changes of



the PC dielectric hole size. It has large optical bandwidth as compare to existing power splitter. In proposed design there are no  $120^{\circ}$  junctions or  $60^{\circ}$  bends. As a consequence the single mode operation will not be suffered. The entire structure will be formed by triangular lattice of dielectric holes so the vertical confinement will be better as compared to the triangular lattice of dielectric rod structure. In account of having all this advantages the entire structure can be considered as a 2-D slab PC configuration. Therefore, the application of power splitter by using PC LDWs integrated with MMI is attractive.

- It is known that the typical Y-junction structure has poor transmission without any structural tuning at the bends and input and output ports. In addition to that the performance of the Y-junction can be improved by tuning and displacing the holes at  $120^{\circ}$  junction and also by bending the output ports but still difficulties exist which can not be easily addressed for practical application. These difficulties arise from the mode-mismatch at  $120^{\circ}$  junction and the bending loss from the output ports. It is conspicuous from a number of researcher's work that Y-junction based power splitter itself identifies some problems in its own design. Here a unique design is proposed which will not be having any disturbances like  $120^{\circ}$  junction and bending loss. 2-D PC multiple line defect waveguides based power splitter is that proposed design which will be capable of addressing the issues of Y-junction based power splitter as mention before.
- For having the identical hole size of both of the 2-D multiple line defect waveguides as well as PC line defect waveguides integrated with MMI block, it is feasible to transfer these two structures to 2-D slab PC configuration. In existing

scheme, only Y-junction based  $1 \times 2$  power splitter has been investigated on 2-D PC slab. So there are immense prospect to study the proposed designs on 2-D slab PC configuration for practical device aspect.

- PC multiple line defect waveguides power splitter minimizes the multimode mode problem occurred in the existing design. Therefore, this proposed scheme transmits more power as compared to the existing design. So, PC multiple line defect waveguides based power splitter should be investigated.

The real motivation behind using PC waveguides over conventional dielectric waveguides for optical interconnects includes better routing capabilities with lower transmission, bending loss, coupling loss, reduced cross talk and larger design flexibility provided with the PC environment, monolithic integration with other on-chip photonic component like a PC based laser or photodetector. A schematic representation of an optical signal distribution layer using PC based waveguides (Line defect waveguides) integrated with MMI block is shown in Figure 1.6. The architecture of output optical signal consists of four PC line defect waveguides (LDWs) which is integrated with MMI block. Optical signal is equally divided at the each output channel.

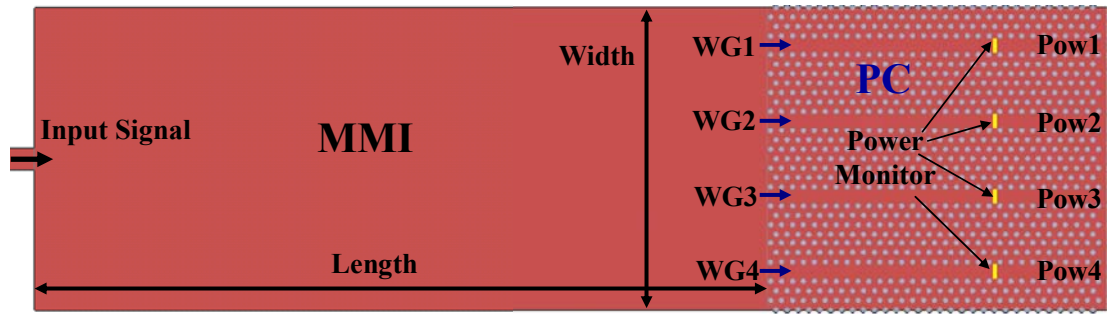


**Figure 1.6 Optical signal distribution using PC line defect waveguides integrated with MMI block**

## 1.5 Challenges

PC based LDW has been attracting researchers for the last two decades for their stimulating possibilities for novel devices. PCs and their devices have been theoretically investigated and experimentally realized. However, many challenges lie in the practical implementation.

One of the main concerns being faced by PCs is its fabrication. Patterning such small features in high-volume production lines is a challenge for commercial lithography systems [15]. Fabrication of 1-D and 2-D PCs has been improved. However, 3-D PC manufacturing is still a challenge. Small imperfections in feature sizes, configurations, defect placements and surface conditions severely affect the dispersion and scattering in PCs. In the laboratory the electron beam writing can provide as good as 10-20nm accuracy in the feature size [16, 17].

Second issue remaining is to develop suitable structures for novel device applications and systems that are economically feasible. This difficulty arises from the challenging aspects of PCs fabrication for the shallow etch height on Silicon-on-insulator (SOI) platform, which requires high-resolution lithography and high aspect ratio etching [15].

Third issue is developing in the device measurement area. Coupling light into the conventional waveguide (CWG) with less loss is major challenging task. To minimize this loss several researcher proposed different methods but there results was not very optimistic. Therefore new techniques of measurements of PC based devices need to be developed to specific power measurement.

## **1.6 Organization of Thesis**

In this thesis 2-D and 2-D slab PC based power splitting techniques have been investigated to improve spectrum, output and equal power splitting characteristics. These splitters are based on PC LDWs and designed to be able to divide the power equally at each output channel and transmit the maximum output power. We first demonstrated the Y-junction based power splitting scheme. This scheme is good for  $1 \times 2$  purpose but it has some drawbacks in  $1 \times 4$  splitting scheme (detail in chapter 3). So in order to overcome these drawbacks, we have demonstrated a new scheme of generating equal amount of power at each output channel with broad spectrum using PC LDWs integrated with MMI block. Such power splitters are useful and necessary for applications such as on-chip optical interconnects and optical clocking applications.

In Chapter 2, an overview of 2-D slab PC is provided and several application examples using PCs are presented to show the potential of PCs as optical power splitter.

Chapter 3 provides a comprehensive review of the Y-junction based power splitter. Here is presented a new structure of 2-D slab PC Y-junction based  $1 \times 2$  and  $1 \times 4$  power splitter. The final optimized has been fabricated and its optical properties will be analyzed to show the advantages, disadvantages and potential application.

In Chapter 4 focuses on a novel power splitting technique which is based on 2-D and 2-D slab PC LDWs integrated with MMI block. The full structure investigated with 2-D and 3-D finite difference time domain (FDTD) method and their optical properties are analyzed.

In Chapter 5 we investigate the PC based multiple line defect waveguides for  $1\times 4$  and  $1\times 3$  power splitting applications. The structure is examined using FDTD. Equal power distribution is dependant on the length of the waveguides. Optical properties are analyzed to show the advantages and disadvantages of this power splitter structure for practical applications.

In Chapter 6, we provide a comparison of the results of all investigated power splitter techniques which were described in chapter 3-5.

Chapter 7 includes a summary and conclusion of the work and introduces the prospects for future work that can be pursued.

# Chapter 2

## 2-D Slab Photonic Crystal Based Power Splitter

### 2.1 2D Slab Photonic Crystal

One of the most promising and interesting classes of PC structure is the photonic crystal slab (PCS), which has two dimensional (in-plane) periodicity, finite height and comparable with the wavelength of light. The PCS is attractive because it is relatively easy to fabricate when compared with 3-D PCs and also easy to chip-level integration [18]. PC slab consists of two dimensional periodic dielectric materials as core, surrounded by lower refractive index cladding either of air or of a low index material. This provides light confinement in the z-direction by index guiding as shown in Figure 2.1. PC slabs share a few similar properties with true 2-D PCs (infinite height), and at the same time they are easy to be realized at sub micron scales and become quite popular for PC application.

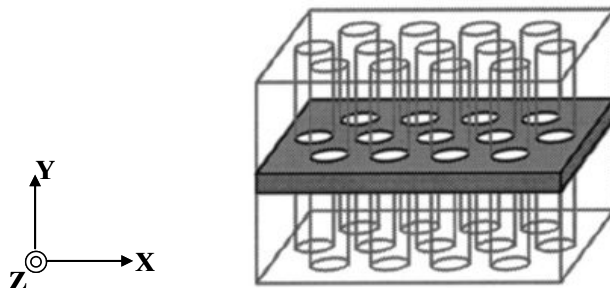


**Figure 2.1 2-D PCS with finite-height high-index slab surrounded by low index dielectric region [19]**

As the finite height property is associated with 2-D PCS, eigenmodes are no longer into pure TE and pure TM modes where as they are in the true 2-D PC's. However, the eigenmodes of the slab can be classified into even and odd modes when both the claddings are identical and the middle of the slab offers symmetry. Field distribution pattern of  $H_z$  component is symmetrical for even modes and anti-symmetrical for odd modes. Polarization mixing is very small in the case of first order modes and can be assumed as even TE-like polarized and odd TM-like polarized. Apart from the polarization mixing effect, another important difference between infinite height 2-D PC and PC slabs is the role of the light line which consists of states or radiation modes extending infinitely in the region outside the slab. Guided modes that are localized to the slab can only exist in the regions of the band diagram which are out of the light cone. Above the light line of the cladding material the modes lie within the continuum of leaky modes of the planar waveguide. These modes are quasi-guided because they have intrinsic radiation losses related to out-of-plane diffraction. The discrete bands below the light cone are therefore guided modes. These states are infinitely extended within the plane of the slab, but decay exponentially in the background region, shown in figure 2.2 [19].

Hence a bandgap, in 2-D slab with finite height, is defined by the range of frequencies in which no “guided mode” exists. It is not a true bandgap since there are radiation modes at those frequencies. Still the lack of guided modes is analogous to the bandgap in infinite 2-D PC. Though in many cases PC slab is analogous to infinite 2D PC, the restriction of a slab to finite height gives rise to issues such as slab thickness,

index contrast with the substrate and mirror symmetry, which play an important role in determining the properties of PC slabs.

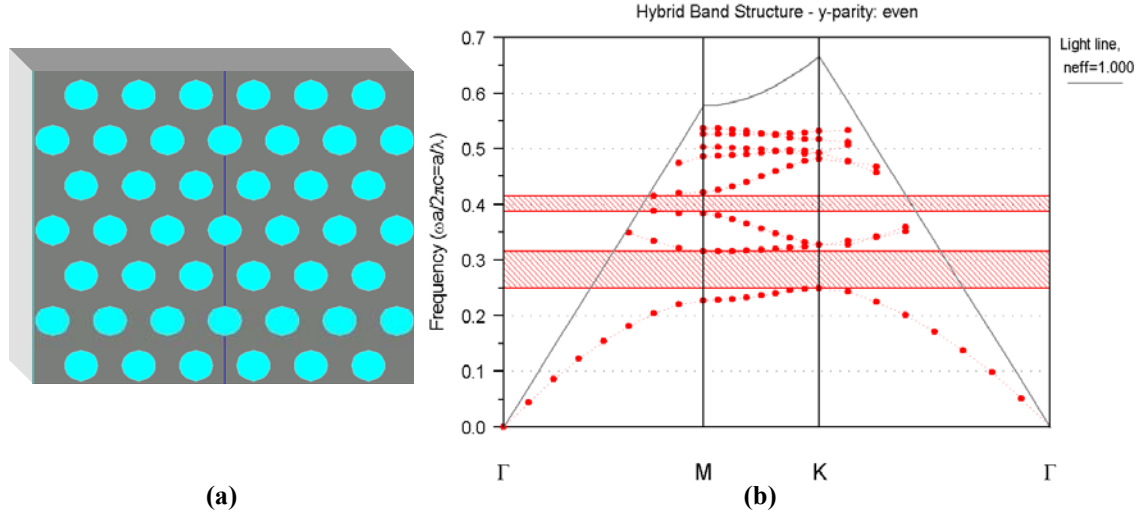


**Figure 2.2 Simulated photonic band structures for bulk PC with finite height (a) Schematic of 2-D PCS triangular lattice structure; (b) Simulated photonic band structure of 2-D triangular lattice PCS, the shadow region marked the PBG**

The 2-D PCS structure can be simulated by two ways. The first way is by performing 2-D calculations using the effective index of the slab at the operating wavelength. This requires less computation resources but the scattering in the vertical direction cannot be accounted for. The second way is by performing a complete 3-D analysis by taking the height of the PC slab into consideration. This method can predict the scattering in the vertical direction but requires very high computational resources.

## 2.2 Defects in PC

The most important property of PCs is their ability to localize the light. This is achieved by introducing defects which breaks the periodic structure locally. The proper introduction of single or line defect into perfect PCs can create resonant states within the



bandgap. A defect design in the PC could be of any size, shape or form and it could be chosen from any of wide varieties of dielectric constants. Therefore, defects states in the gap could be tuned in frequency and spatial extent of design interest [1, 15]. In addition to tuning the frequency, it should be controlled over the symmetry of the localizing photonic state. All of these capabilities provide a new “dimension” in the ability to control or mold the properties of light. In the following section we look into the different types of defects that can be formed in PC and their properties.

## **2.2.1 Line defect waveguides**

Waveguides are the important element of photonic integrated circuits (PIC). It is connected with the various functional elements like multiplier, detector, source and modulator. In a PC, a simple LDW is created by removing a row of holes along one of its main crystalline directions as shown in figure 2.3. Due to this defect single or multiple modes is appeared. These modes can be classified into evanescent, standing or traveling modes. The traveling modes can be used to carry optical signals between components in an integrated system, which thereby turns linear defects into bona fide waveguides.

The line defect traps light of specific range of wavelength within the waveguide with minimal losses even around the tight bends. LDW has the feasibility of ultra compact waveguide elements such as sharp bends, small branches and short directional couplers for dense all-optical integrated circuits [20]. High transmittance for the guided modes through sharp bend has been theoretically and experimentally reported [21] in figure 2.4. The wave confinement in the waveguide is achieved by Bragg reflection in the transverse directions. The field associated with the mode is strongly confined in the vicinity of the defect and decays exponentially in the bulk crystal regions. A dispersion property of the

PC LDW is calculated by plane wave expansion method (PWEM), which solves Maxwell's equations in the frequency domain for a given PC configuration. PWEM also helps to find out how many modes are supported by the PC LDWs. In other words, the band structure, which describes the functional dependence of frequency  $\omega$  on the wave vector  $K$ , can be calculated.

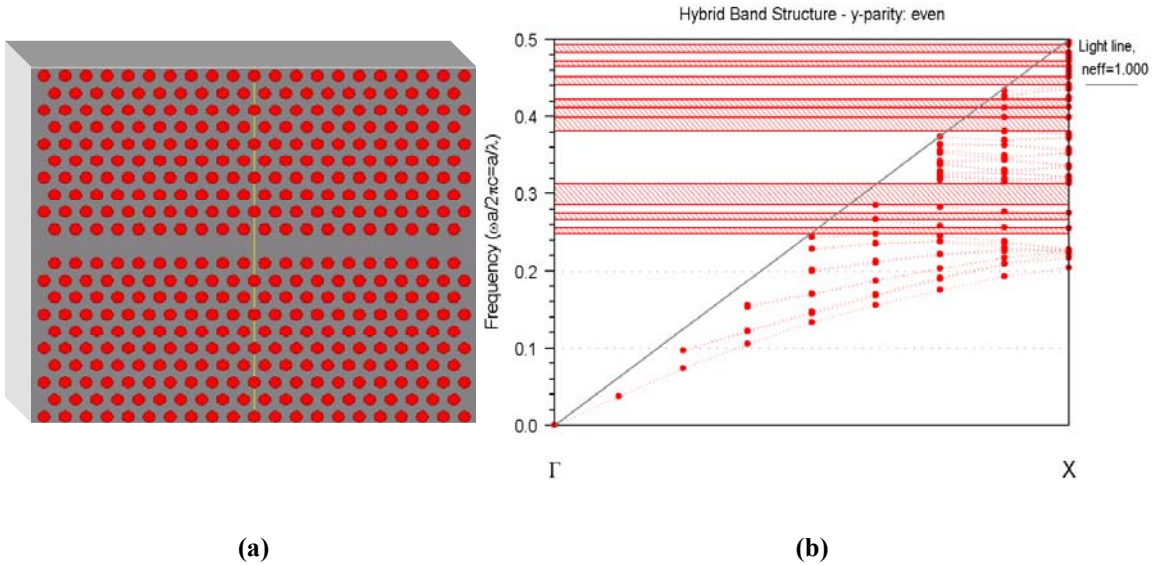


Figure 2.3 LDWG formed by (a) introducing a single defect inside a regular PC lattice breaks its periodicity and (b) band structure of corresponding PC LDW

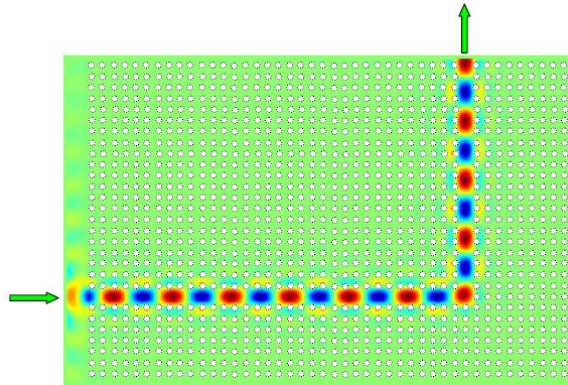


Figure 2.4 Light transmissions in 90-degree waveguide [21]

## 2.2.2 PC microcavity

Microcavity in a PC can be realized by introducing a point defect or group of point defects [21-24] as shown in Figure 2.5. The defect is obtained by locally modifying the shape, size or dielectric constant of the PC features. By varying these parameters, the number of modes supported by the cavity and their resonant frequencies can be tuned. These point defects trap electromagnetic modes and, hence form optical cavities. The light-trapping efficiency of an optical cavity is characterized by the quality factor  $Q$  which is a measure to know the length of the time an electro-magnetic wave stays inside the cavity and it is defined by the following formula [26]:

$$Q = \frac{\omega E}{P} \quad (1)$$

where  $E$  is the energy stored inside the cavity,  $\omega$  is the resonant frequency, and  $P = -dE/dt$  is the power dissipated outside the cavity [27, 28]. In the other words, the quality factor is, up to a factor of  $2\pi$ , which is the inverse of the fraction of energy lost in a single period of the oscillating electromagnetic field. The quality factor of a cavity plays a major role in designing high-density wavelength filtering and multiplexing systems. Microcavities high  $Q$  factor depends on the depth of the holes and on the refractive index of the materials. The combination of high quality factor and extremely low mode volume make PC microcavities especially attractive for experiments in cavity quantum electrodynamics. The compact size and high spontaneous emission-coupling factor of the defect microcavity also make it interesting for low-threshold light sources [29, 30]. Many results have been reported both by theoretically and experimentally since then. Most works require specific working wavelength, therefore effort has been put into finding easy and practical methods of tuning the resonant wavelength. It was found that the

resonant wavelength of PC microcavities are extremely sensitive to the fill factor, the dielectric constant, cavity size, properties of objects in the cavity and the slab thickness on the case of planar structure. The mode volume  $V$  and the quality factor are two critical properties of microcavities. These properties of PC microcavities have been extensively studied [31].

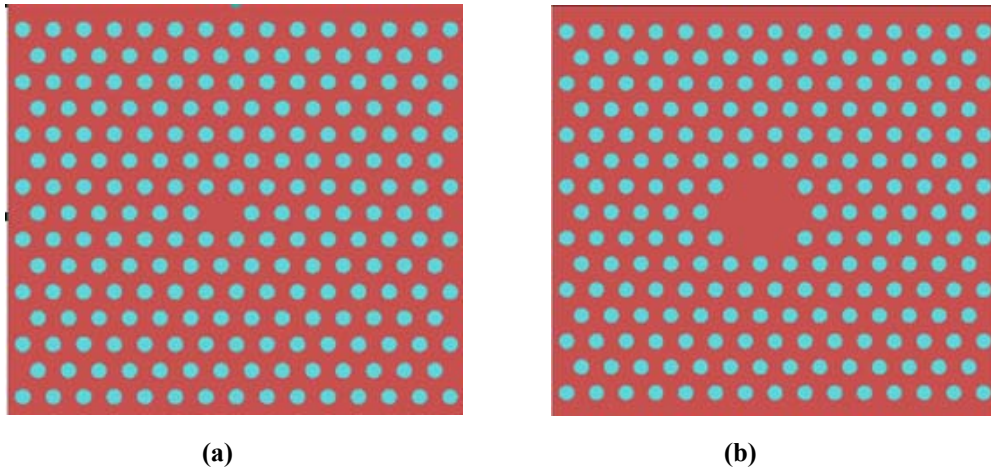


**Figure 2.5** Schematic of (a) microcavity formed by removing a single air hole and (b) microcavity formed by removing 7 air holes at the center of PC

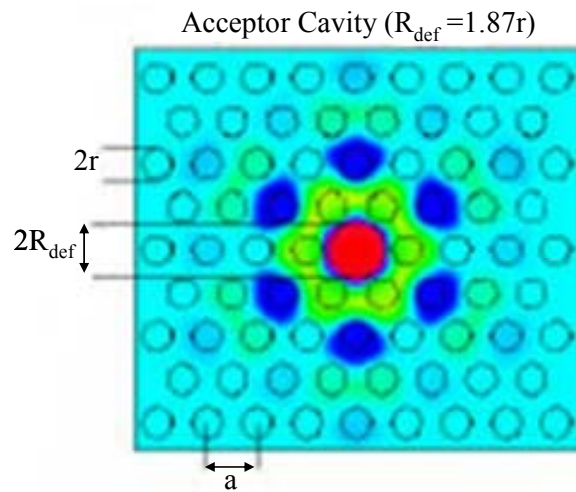


**Figure 2.6** Structure and the TM field profile of an acceptor type point defect made by increasing the radius of the central hole [32]

Figure 2.6 shows a point defect in a triangular PC lattice of air columns in dielectric host. By increasing the radius of the air hole, a cavity known as an acceptor type is created. It can be seen clearly that the energy is confined around the cavity [32].

## **2.3 2D Photonic Crystal in Splitter Application**

After the introduction of PC and its defects, their different applications as splitters are described in this section. Optical component based on planar PC structures can substitute the total internal reflection (TIR) by using the unique properties of PBG effect. The PBG effect allows the interaction between light and the PC structure which takes place into a wavelength scale. This can minimize the size of the individual components and increase the device-packing density (up to  $10^6$  times compared with conventional TIR) [33]. The devices on the 2D PC slab have many advantages such as relatively easy fabrication and convenient integration into conventional devices. Power splitter is one of the most indispensable components, however the power-splitting functions on PCs have been demonstrated by many researchers and some of these are described below.

### **2.3.1 2-D slab PC based Y-Junction Splitter**

An example of an ultralow-loss 3-dB PC Y-junction based power splitter is shown in figure 2.7 (a), (b) [33]. The planar PC structure is fabricated on a silicon-on-insulator substrate with a Si slab of thickness  $t = 220\text{nm}$  separated from the Si substrate by  $1\mu\text{m}$  silica layer. The holes are placed in a triangular lattice and have a diameter  $d = 0.57a$ , where 'a' is the lattice constant i.e.  $435\text{nm}$  [33]. The structure of this Y-junction is formed by the intersection of three PCW at  $120^\circ$ . The output channels have an additional  $60^\circ$  bend which is parallel to the input channel as shown in figure 2.7 (a). Due to  $120^\circ$

junction and  $60^\circ$  bend; single mode operation might suffer which can cause the reflection and large transmission loss. To overcome these difficulties the junction and bend must be carefully designed.

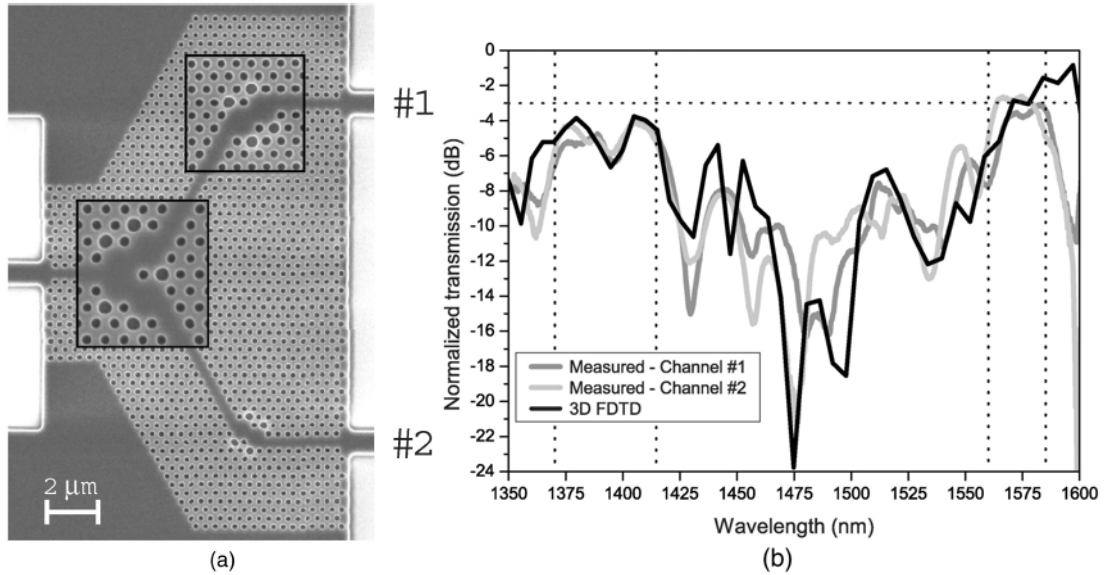


**Figure 2.7 (a) Schematic of Y-junction power splitter based on 2-D slab PC; (b) Normalized transmission spectra (Measured and Simulation) of channel 1 and 2 between 1350nm-1600nm wavelengths [33]**

The measured and calculated losses per bend are shown in figure 2.7 (b). Bending losses are found between the two wavelength ranges i.e. 1555-1585nm and 1370-1410nm. In these wavelength bending loss are  $0.25 \pm 0.58\text{dB}$  and  $0.70 \pm 0.35\text{dB}$  respectively. The zero-loss 3-dB output is obtained at each output channel in the range of 1560-1585nm wavelength. The low-loss bandwidth can be achieved by further optimization of the Y-junction and  $60^\circ$  bend of the splitter.

## 2.3.2 Ultracompact multiway beam splitter using photonic crystal dielectric rod

Tianbao Yu, et al has demonstrated 1 to 3 and 1 to 4 ultracompact power splitter using coupled PCWs (CPCWs) as shown in figure 2.8 (a) and (b) [6]. The operation principal based on self-imaging phenomenon and entire structure is based on 2-D PCs consisting of an array of dielectric rods in air with a triangular lattice of  $r = 0.18*a$ , where ‘a’ is the lattice constant.

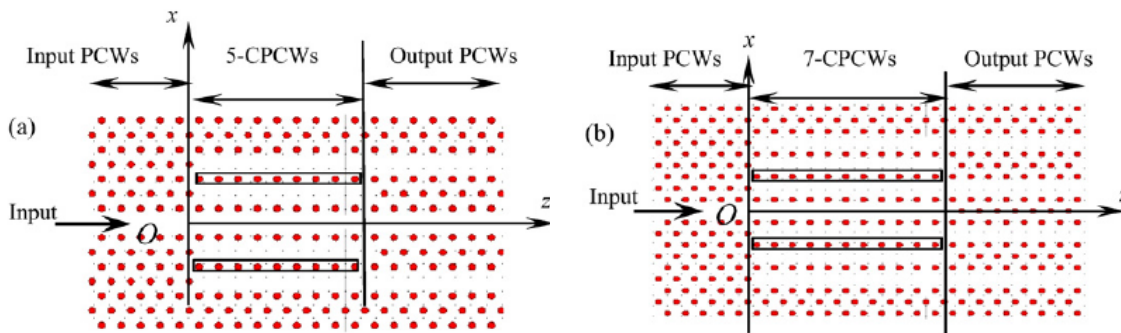


**Figure 2.8 (a) Schematic diagram of beam splitters consist of the input PCWs (a) 5-CPCWs; (b) 7- CPCWs and output PCWs. Modified rods are enclosed by rectangle [6]**

This splitter consists of three parts: a single-mode input PCW, a multimode region with a length  $L_M$  and  $N$  single mode output PCWs which is shown in figure 2.8 (a) and (b). The interaction between adjacent output PCW is negligible at a short propagation distance because the beating length of the adjacent PCWs separated by three rows of rods. Therefore the device length is totally depends on the number of output channel. However multimode region length is also depending on the number of output channel. When the input beam is splitt into 3 output channels, the length ( $L_M$ ) of the multimode region is  $5.58\mu\text{m}$ ; where as for 4 output channel this length ( $L_M$ ) is  $6.82\mu\text{m}$ . The CPCW based splitter length is smaller due to weak interaction of the neighboring output PCWs while conventional MMI splitter is set wide and long so as to minimize the coupling of the

adjacent output ports. Therefore, the CPCW based splitter is much more compact compared to conventional MMI splitter. The entire structure is simulated by 2-D FDTD method. The intensity and phase of propagation field in the CPCWs are distributed symmetrically for the symmetrical nature of the structure and the input position. For equal splitting at each output channel the radius of rods in CPCWs plays an important role. When the radius of 5-CPCWs rods are  $0.208*a$  and  $0.232*a$ , output transmitted power is equally distributed and is also maximized which is shown in figure 2.9 (a). Similar result is also achieved for 7-CPCWs when the radius of the hole  $0.143*a$  as shown in figure 2.9 (b).

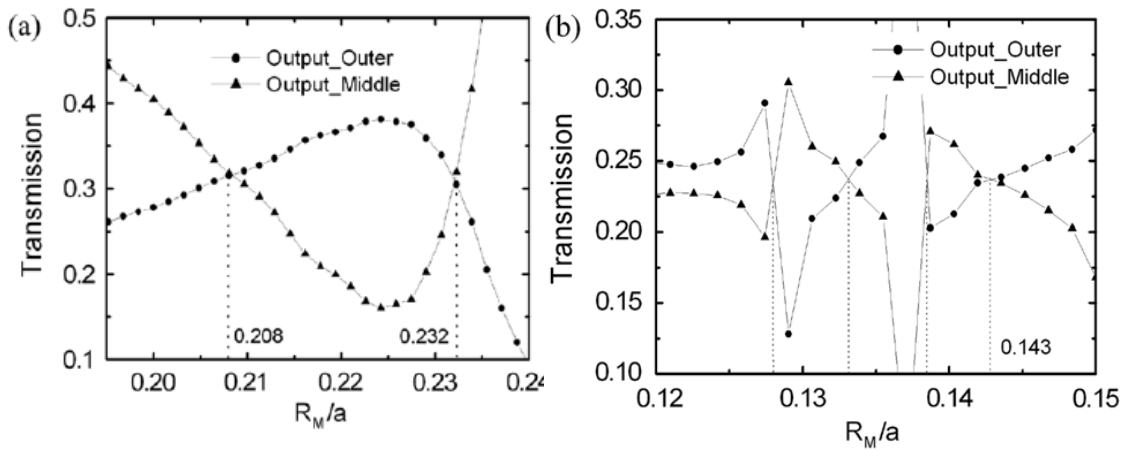


**Figure 2.9 Output transmitted power is a function of the variable of CPCWs rods (a) in the  $1 \times 3$  splitter and (b) in the  $1 \times 4$  splitter [6]**

The above analysis shown that input field is divided on average into multiple parts by tuning the radius of the designated rods due to the fact that transverse redistribution may be achieved. The analysis shows output transmission for three and four ports are 96% and 94.8% with propagation length of  $5.58\mu\text{m}$  and  $6.82\mu\text{m}$  respectively.



### 2.3.3 Photonic Crystal power-splitter based on directional coupling

Focusing on a practical design for integrated photonic circuits and avoiding the circumventing complex problem involved other power splitter design, EI-Hang Lee et al have proposed new power-splitting scheme which is based on the coupling between guided modes supported by the PCLDWs [34]. Due to the efficient power splitting scheme the entire structure is symmetrical with respect to the input waveguide which leads to a three waveguide structure with the central waveguide used as an input port as shown in figure 2.10.

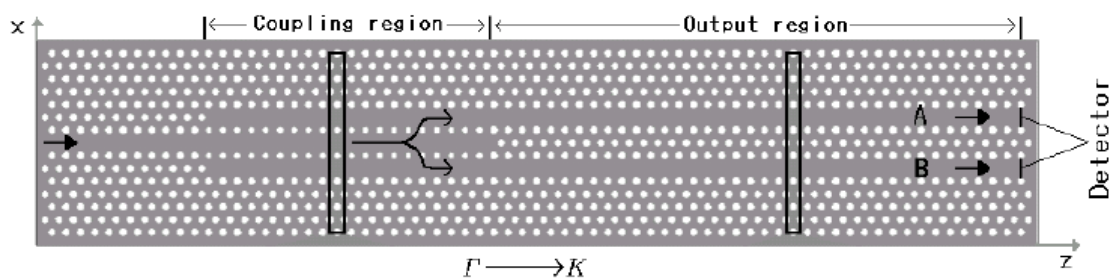
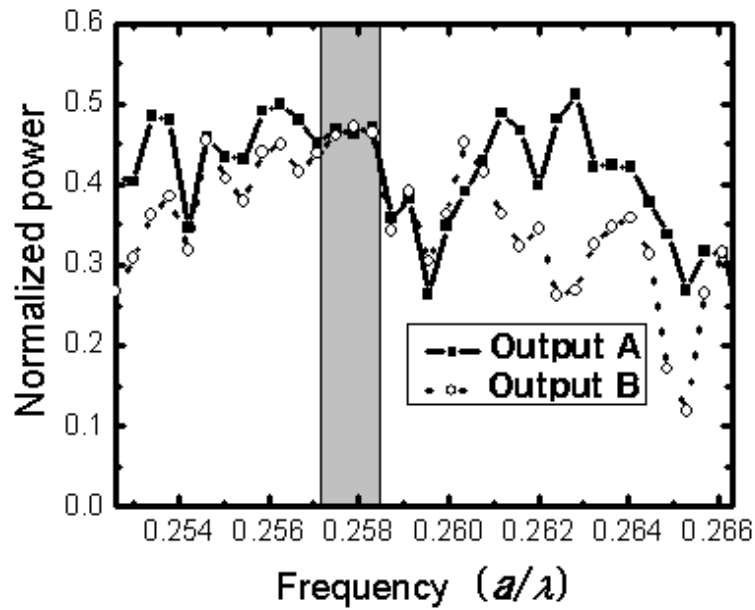


**Figure 2.10** Schematic diagram of photonic crystal power splitter. The device is divided into two regions, as labeled on top. Black boxed area indicates super-cells. White holes represent air-holes [34]

The PCLDWs are formed in  $\Gamma$ -K direction by removing one row of air holes. The structure of power splitter is divided into two regions, one is coupling region and other one is output region as shown in figure 2.10. In the coupling region, the input field propagates through the middle of PCLDW and then is coupled into top and bottom PCLDW. Subsequently the coupled power is transferred to the output waveguide A and B without coupling from one waveguide into another with a target wavelength of  $1.55\mu\text{m}$ .

To work on a large spectral range, this splitter has two requirements: a) the coupling region where the wavelength-insensitive coupling should be supported without change in

the coupling length, ii) the output region where the coupling between the two output waveguide is prevented for balanced the output power. The calculated length of the coupling region is  $20 \cdot a$ . To verify this, the whole structure is examined by FDTD method. As being considered a finite structure the whole computational domain is surrounded by perfectly matched layers to absorb the outgoing waves. The simulation result is shown that each channel transmit 47.6% of the input power (Figure 2.11).



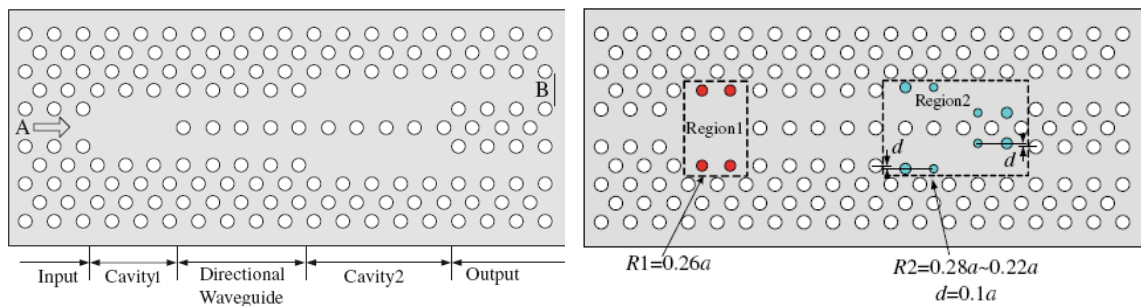
**Figure 2.11 Normalized output power after FDTD computation, Grey area indicated spectrally flat coupling range [34]**

Figure 2.11 shows that calculated output power is normalized to the input power. The flat transmission (46-47.6%) is achieved around  $a/\lambda = 0.258$  (grey area depicted in Figure 2.11). An abrupt dip between 0.259 and 0.260 is due to anti-crossing of different order modes.

## 2.3.4 Power splitter based on cascaded multimode photonic crystal waveguides

In order to achieve a wide bandwidth and compact size of a high transmittance power splitter, Zetao Ma et al have proposed a power splitter based on two-dimensional PC with triangular lattice of air holes (Figure 2.12) [35]. The operational principle of the splitter can be described as the input field divided into two fold pattern with a small distance in the first area-defect and then shifted by the secondary area-defect regions to output port.

The entire structure is simulated by 2-D FDTD method with uniaxial perfectly matched layers (UPML) absorbing boundary conditions. A continuous wave with a normalized frequency of 0.255 ( $a/\lambda$ ) is launched into input port A and propagating through line detector B to measure the output power.



**Figure 2.12 (a) Configuration of PC power splitter with cascade area-defect structure. (b) Optimized structure with radius of air holes in region 1 is set to  $R_1 = 0.26a$ , the radius of air holes in region 2 is designed with a taper structure that  $R_2$  decreases from  $0.28a$  to  $0.22a$  in contra-direction, and with the same displacement  $d = 0.1a$  [35]**

To achieve the broad band width and high transmission, the previous structures is optimized which is shown in figure 2.12 (b). According to optimized structure, there are two regions and one directional waveguide. The function of the directional waveguide is to transfer the power from first region to second region. The performance of the power transmission is slightly affected due to the defect area in region 2. So to overcome the

obstacle of power transformation at the output, the length of the directional waveguide is optimally set to  $5a$ . Therefore more than 45% output power achieved at each output channel with a frequency range of  $0.2525 - 0.2580$  as shown in figure 2.13. The power is flown along the  $\Gamma$ -K direction inside the device structure. The simulated power flow is in good agreement with the function of 3 dB power splitter. The total length of region 1, directional waveguide and region 2 is about  $17a$  which is very compact. Therefore the area defects find its applications as a platform for broadband and compact passive devices.

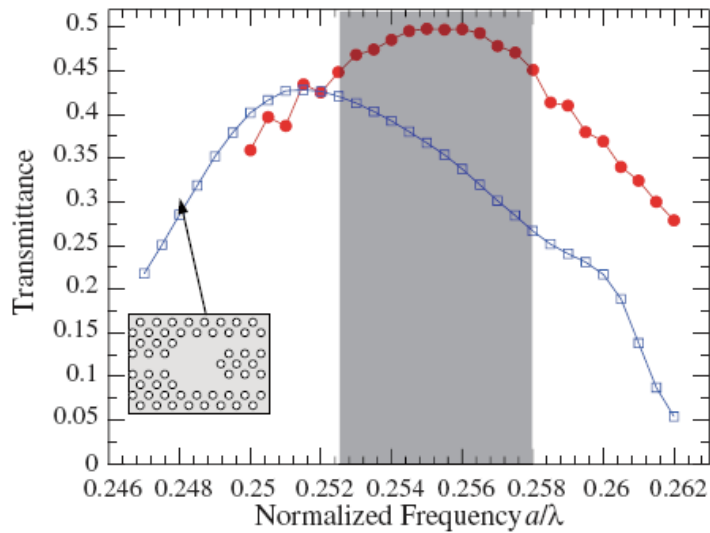


**Figure 2.13** Normalized output power transmission is indicated by solid-circle red line for proposed structure whereas square-blue line indicated the power transmission of the simple structure. Grey line indicates over 45% power is transmitted [35]

## 2.4 Summary

To summarize this chapter, the principle of the PC power splitter is introduced with the explanation of the 2-D and 2-D slab and splitting components PC waveguide and PC microcavity. Several examples are offered to give a quick review on how PCs are applied in the splitting applications. Those splitters presented above have some common features,

small in size and minute changes in the design bring in maximum power transmission. The ultracompact power splitter is shown in figure 2.8 (a) and (b) which show the technique for achieving  $1 \times 3$  and  $1 \times 4$  power splitters. However, there are some problems that need to be resolved before it is used in practical situation, such as transfer into the 2-D slab and minimizes the vertical loss. We will explore different way of power splitting techniques through out the thesis. Chapter 3 focuses on Y-junction based power splitter.

# Chapter 3

## **2-D slab photonic crystal based Y-junction 1×2 and 1×4 power splitter**

Since, the implementation of photonic crystal by John and Yablonovitch in 1987 there have been increasing attention paid to develop the nanostructure in microscale device in various applications [4, 36]. PCs have the potential to provide ultracompact photonic component that will enable the miniaturization of optical circuits and promise to revolutionize integrated optics. These photonic components are based on the planar PC structure and operate in the PBG of the periodic dielectric structures which allow control of the light propagation on the wavelength scale. Photonic crystal waveguides (PCWs) are formed by line defects in PC. Thereby light is confined horizontally by an in-plane PBG and vertically by TIR. Because of the PBG effect in a PCW, light can be routed around sharp corners with bending radii of the order of the wavelength. Due to the sharp bend higher-order modes are generated that affect the single mode operation in the PCW [37].

Researchers have theoretically investigated photonic crystal with array of dielectric rods in air. Based on this concept the T-junction, Y-junction and MMI effects have already been extensively studied [38, 6-7]. Unfortunately, the ‘rod in air’ approach does not provide sufficient vertical confinement and is difficult to implement for most practically useful device implementations in the optical regime. A slab waveguide structure consists of air holes etched into a dielectric medium such as silicon [32],

GaAs/AlGaAs hetrostructure [39] or a semiconductor membrane [40-42] which remedies this problem and allows waveguides with tolerable losses. The problem encountered for the ‘holes in dielectric’ approach is that the single-defect PCW becomes multi-moded, which makes it difficult to get light to flow efficiently around the circuit because higher-order modes are easily excited at discontinuities [42-43, 14]. This multimode leads to mode-mixing problem at intersection of the PCW which creates a mismatch between input and output fields and introduces large reflections at the interface. Whereas straight waveguides and bends have been studied by many groups, the very important problem of junctions based complex circuits operation has only recently received attention [33, 44-46]. The most straightforward Y-splitter design consists of three single-defect (‘W1’) waveguides joined together at  $120^{\circ}$  which leads to strong reflections and narrow-bandwidth operation. Due to strong reflection only 20% of the input power is transmitted at the output ports [47]. After that L.H.Frandsen et al. [33] proposed an alternate design which was based on a triple line defect waveguide. In their design the bandwidth and power transmission were improved by 25nm and 45% of input power by adding an additional hole at  $120^{\circ}$  junction and modified  $60^{\circ}$  bend.

In this chapter, we investigated the PCW based Y-junction splitter through 3-D FDTD simulation method to overcome some of the above difficulties (i.e. mode mismatch, bandwidth and bending region transmission) and challenges. The structure can be applied to communication systems and also be integrated with other PC based devices. Before starting investigation of the Y-junction structure, we first demonstrate the 3-D FDTD computational method.

## 3.1 FDTD Simulation

FDTD is a time domain simulation method for solving Maxwell's equations in arbitrary materials and geometrics. The basic principle is to substitute the curl equations and partial time differential with finite central differences in spatial domain and time domain respectively [48].

### 3.1.1 Basic aspect of 3-D FDTD

The computational domain is meshed as shown in figure 4.1, where different field component are located at different computational nodes. This typical configuration is referred to as Yee's cell.

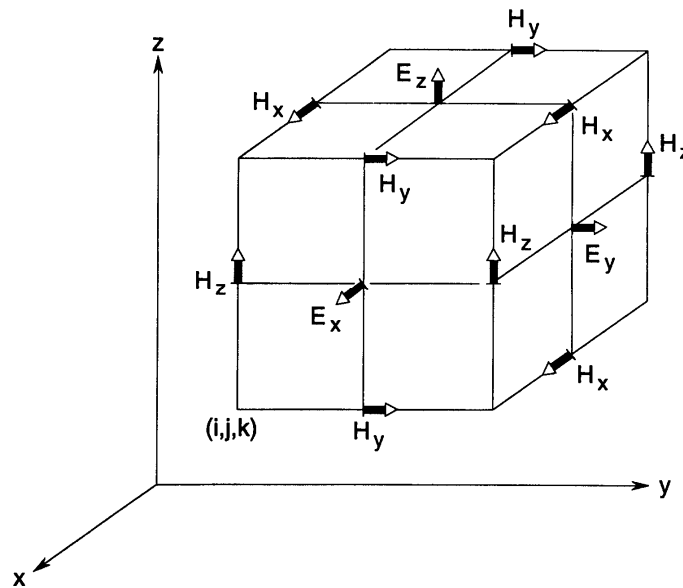


**Figure 3.1 Yee's cell used in 3-D FDTD simulation [48]**

By substituting partial differentials in Maxwell's equations (3.1-3.4) with central finite difference, the electromagnetic field at each time step is calculated by iteration of algebraic equation. FDTD simulation can provide complete information on the



propagation of electromagnetic waves in dielectric structures with any arbitrary geometry.

$$\nabla \cdot \vec{H}(\vec{r}) = 0 \quad (3.1)$$

$$\nabla \cdot [\varepsilon(\vec{r})\vec{E}(\vec{r})] = 0 \quad (3.2)$$

$$\nabla \times \vec{H}(\vec{r}) = -j\omega\varepsilon(\vec{r})\varepsilon_0\vec{E}(\vec{r}) \quad (3.3)$$

$$\nabla \times \vec{E}(\vec{r}) = j\omega\mu_0\vec{H}(\vec{r}) \quad (3.4)$$

In order to obtain convergent simulation results and to reduce the numerical dispersion, a fine mesh is critical. In our study, the grid size  $d$  is chosen that is  $d < \lambda/20n$ , where  $\lambda$  is the minimum wavelength of the source spectrum and  $n$  is the refractive index of the slab. This mesh configuration ensures the convergence and high accuracy of the simulations. The stability factor  $S$  is defined as  $S = \frac{c\Delta t}{d}$ , where  $c$  is the speed of light in vacuum and  $\Delta t$  is the time step. In Y-junction base splitter simulation file  $S$  is set to 0.99 for satisfying the stability condition of 3-D FDTD simulations.

### 3.1.2 Simulation boundaries in 3-D FDTD

Since any computational resource can only deal with finite size of the matrix, the simulation region has to be terminated boundaries, which must have very low reflection otherwise the waves will be reflected back from the boundaries into the simulation region to affect the results. In Y-junction based structure analysis, perfect matched layer (PML) is used in the 3-D FDTD simulations.

Instead of PML boundary other two types of boundaries are also frequently used in 3-D FDTD. These are symmetric/anti-symmetric boundaries and Bloch boundaries.

## 3.2 Description of Y-Junction Structure

The planar PC Y-junction based structure is defined by an array of air holes in a 300nm thick dielectric substrate with refractive index of 3.47 (silicon). The regular holes are placed in a triangular lattice and have a radius  $r = 0.25a$ , where lattice constant 'a' = 400nm. The PC Y-junction base structure is formed by the intersection of three PCWs at  $120^\circ$  as shown in figure 3.2. The output channels of Y splitter are parallel to the input channel and have a  $60^\circ$  bend and seven periods spaced from the Y junction. The  $120^\circ$  junction and  $60^\circ$  bend represent severe discontinuities in the PCWs and are potential regions in which the single-mode operation might suffer from large transmission losses. Therefore the discontinuities in these regions are carefully designed.

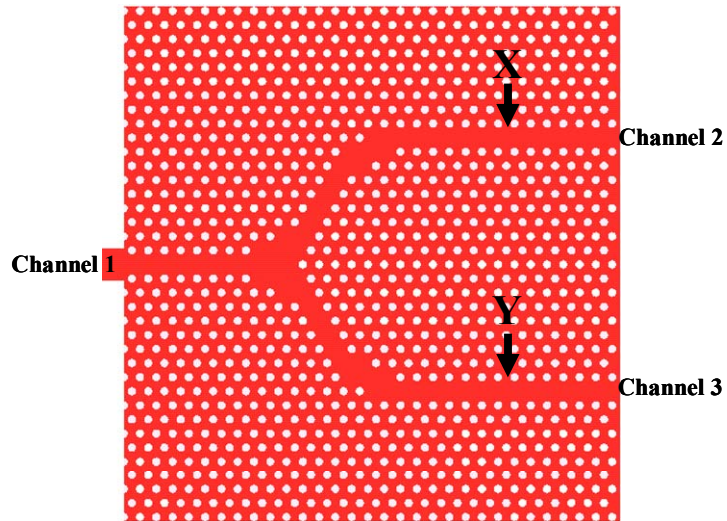


Figure 3.2 Preliminary Y branch structure

## 3.3 Characterization of Y-Junction in 3-D FDTD

From 3-D FDTD simulation time domain electromagnetic field is obtained. The Y-junction structure is simulated by a mode source located on the conventional waveguide

which is attached with the Y-junction structure. This technique is very powerful and versatile and is useful for this type of waveguide [47, 49].

### 3.3.1 Simulation setup

The 3-D FDTD simulation for the designed of Y-junction in slab is shown in figure 3.3.

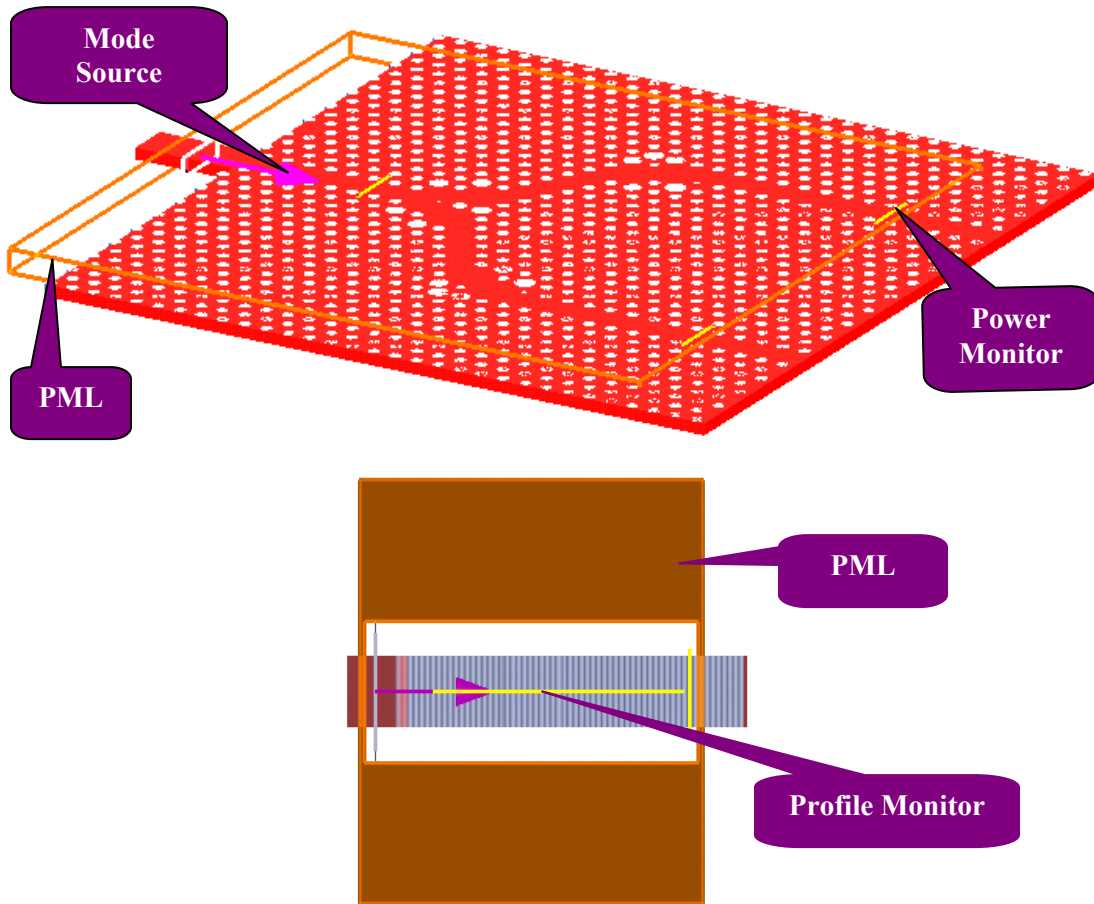


**Figure 3.3 3-D FDTD simulation setup for the designed Y-junction**

The design of Y-junction in silicon slab is created in the simulation region. In order to excite the mode, PML boundary is used. This boundary absorbs the outgoing wave. A 3-D profile monitor is located on the Y-junction structure to record the electric field distribution at  $120^\circ$  junction,  $60^\circ$  bend and output channels. Two power monitors are

placed at the output channel in order to record the power transmission from input to output. The output power is calculated at each port by integrating the Poynting vector over the cells of the output ports. The spectrum of the power transmission is calculated by using FDTD method over a time period of 800fs. The FDTD mesh size and time step are  $0.0142\mu\text{m}\times 0.0142\mu\text{m}\times 0.0349\mu\text{m}$  and  $\Delta t = \Delta x * S / c$  (c is speed of light in free space,  $\Delta x$  is distance between two mesh point, S is stability factor and  $\Delta t$  is time interval of the time step) respectively.

### **3.3.2 Power transmission of unmodified structure**

Figure 3.2 shows the basic structure of Y junction base splitter. First we have investigated the transmission of this structure using 3D FDTD method with perfectly matched layer (PML) boundary condition. The output transmitted power is monitored at two points on the  $60^\circ$  bend output waveguides; one at the output of channel 1 (Point X) and the other at the output of channel 2 (Point Y) is indicated in Figure 3.2. The optical pulses are injected on the waveguide and each pulse covers the same range of wavelength which is  $1.5\mu\text{m}$ - $1.588\mu\text{m}$ . The numerical transmission spectrum of unmodified Y-junction structured is shown in figure 3.4. The spectrum indicates that a maximum of 20% of the input power is transmitted through each channel that is quite low. The discontinuities at the Y-junction and the subsequent  $60^\circ$  bend are said to be responsible for this low transmission.

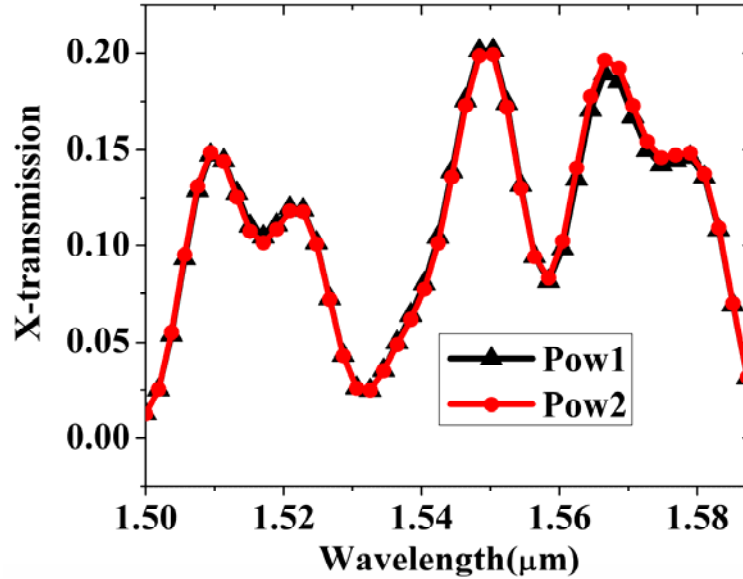


**Figure 3.4 3-D FDTD calculation of normalized output power transmission of an unmodified Y-junction structure**

### **3.3.3 Modification of the design**

In order to maintain the single mode operation and achieve the better transmission we modified the Y branch structure. The  $60^\circ$  bends are modified by displacing one hole and removing two holes in the bend. Moreover, four border holes (denoted by ‘A’, ‘F’, ‘G’; as shown in Figure 3.5) and one top corner holes (denoted by ‘D’) are placed with larger holes with radius ‘A’= 160nm, ‘F’= 180nm, ‘G’=150nm and ‘D’= 170nm respectively. However, one border hole (denoted by ‘E’) in the  $60^\circ$  bending region and displaced hole also in the  $60^\circ$  bending region (denoted by ‘C’) are replaced with smaller holes with radius 50nm and 80nm respectively. The Y junction is altered in a similar way by removing three holes on both sides of the junction and replacing five border holes with larger holes. However, this could transform the Y junction into a multimode optical cavity which could decrease the performance of the splitter because the cavity modes might not be supported by the PCWs. Therefore two additional holes are added in the

splitting region, whereby the size of the junction cavity is reduced. In the splitting region i.e. at  $120^\circ$  junction the smaller hole followed by a line of holes gradually increasing in size which minimizes the mode mismatch problem between the  $120^\circ$  junction and  $60^\circ$  bending waveguide. The radius of the initial hole is designed to be 40nm and the second to be 120nm. The design of the modified Y-junction based power splitter is shown in figure 3.5.

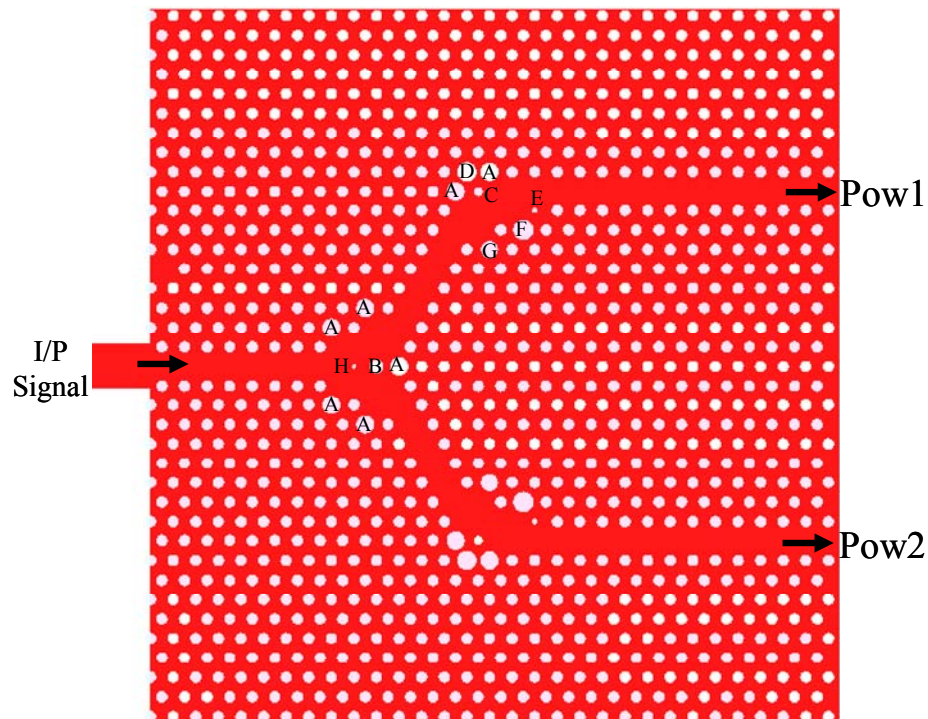


**Figure 3.5 Modified Y branch structure**

### **3.3.4 Analysis of modified Y-junction**

To improve the power transmission at the output channels we have modified the Y-junction and adjacent  $60^\circ$  bend. While doing so we have changed the radius of the holes at Y-junction (denoted by 'A') and  $60^\circ$  bend (denoted by 'A', 'C', 'D', 'E', 'F' and 'G') which is depicted at figure 3.5. Figure 3.6 displays the improved power transmission of modified Y-junction based power splitter based on these modifications. Due to this

modification the single mode operation is not disrupted. Therefore more power is transmitted from input to output channels.

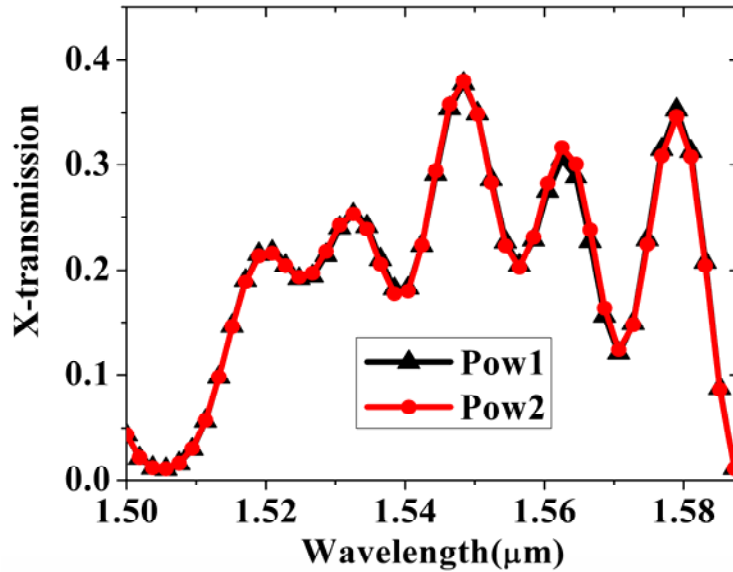


**Figure 3.6 Normalized transmission of output power spectrum of modified Y-junction based power splitter**

The performance of the transmitted power is improved by 18% at each output channel which means 38% power is transmitted at both of the output channels. The improved transmission which has been received by optimizing of Y-junction based power splitter structure is still lower than the existing Y-junction based design [46]. As a result, a better improvement is inevitable. So we have introduced additional two holes at the  $120^\circ$  junction denoted by ‘H’ and ‘B’. Due to this modification the performance of transmitted output power of Y-junction splitter is improved. Figure 3.7 shows the improved version of transmitted output power of the second set of modification of the Y-junction based power splitter. In this modified version of the structure the higher transmitted power is achieved which is 84.4% with each channel equally transmits 42.2% of input power. Where as more than 22% power is achieved at each output channel in the

frequency range of 1540nm-1567nm (with bandwidth about 27nm) and 20% power is achieved at each output channel in the frequency range of 1526nm-1568nm (with bandwidth about 42nm), indicated by blue dash line with highest pick value of 42.2% power for channel 1 and 2. This maximized transmitted power is well comparable with the published results [33, 46].

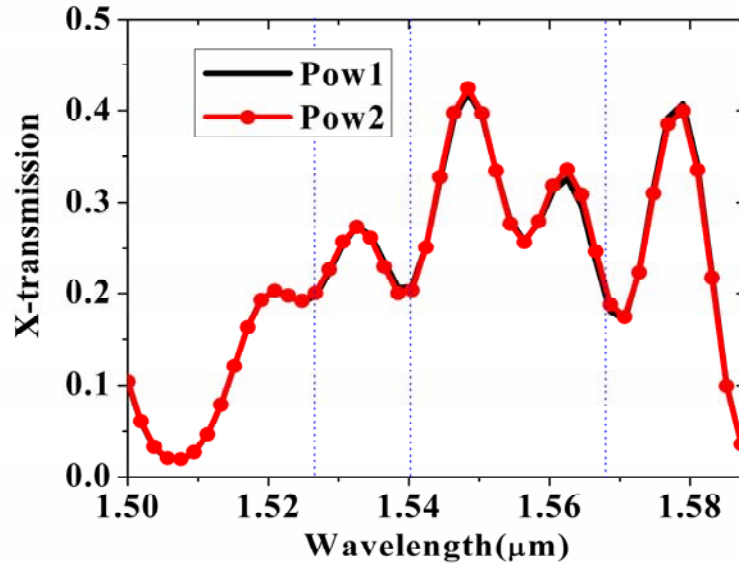


**Figure 3.7 Normalized maximum transmitted output power of Y-junction based power splitter**

The unmodified structure of the Y-junction which is shown in figure 3.2, transmits only 20% of input power to each channel. This is due to mode mismatch of input PCW and 60° bend output PCWs. To overcome this large transmission loss holes are resized at the splitting region i.e. the 120° junction and the 60° bending regions. As a subsequent result of resizing the holes size, the bending loss gets minimized and it has an impact on the transmitted output power. For further improvement two additional holes are placed at the junction. The effect of introducing additional holes at the junction is the decrease in volume of the intersection which prevents the expansion of the higher-order mode. Boscolo et al [5] showed that poor transmission can originate from modal mismatch at



the junction. If the incoming mode has space to expand in the junction area, it excites the higher order modes which are either lossy or cannot able to propagate through  $60^\circ$  bend output waveguides. So, most of the incoming light is reflected and the transmission is poor. By placing the two additional holes at the junction, the incident wave is divided into two parts and propagated through the each output channels. Here, the dimension of the additional holes play an important role which distributes the single mode incident wave in two single mode waves crossing the two output channels as illustrated in figure 3.8.

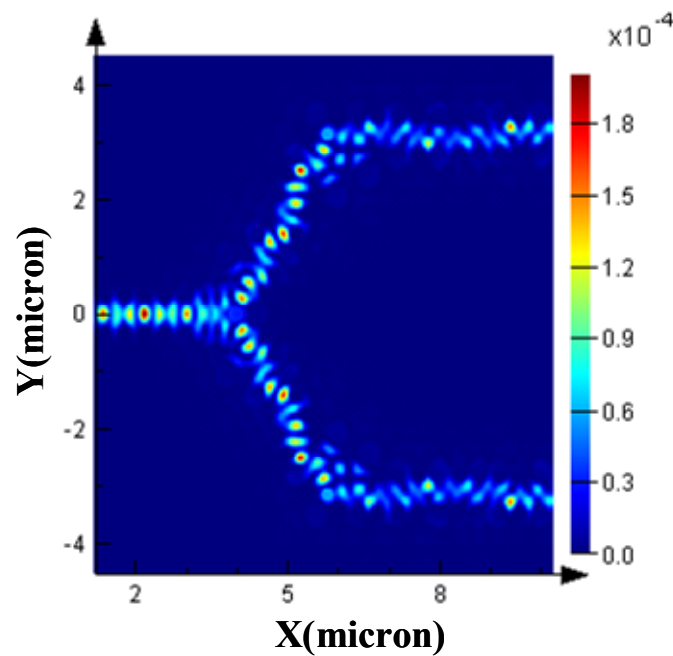


**Figure 3.8 FDTD simulation of the electric field distribution in the optimized Y-junction base power splitter when the incident wave arrives at the level of the additional holes**

According to modification, the Y-junction based power splitter transmits 84.4% of input power on both output channels. Due to the higher transmission of power at each channel, the  $1 \times 2$  splitting topology is divided into  $1 \times 4$ . In the next section, we will elaborate.

### 3.3.5 Design of 1×4 power splitter based on Y-junction

Based on the FDTD analyzed result of unmodified and modified Y-junction in previous section we want to investigate 1×4 power splitter which is based on Y-junction. The schematic diagram of 1×4 power splitter is shown in figure 3.9.

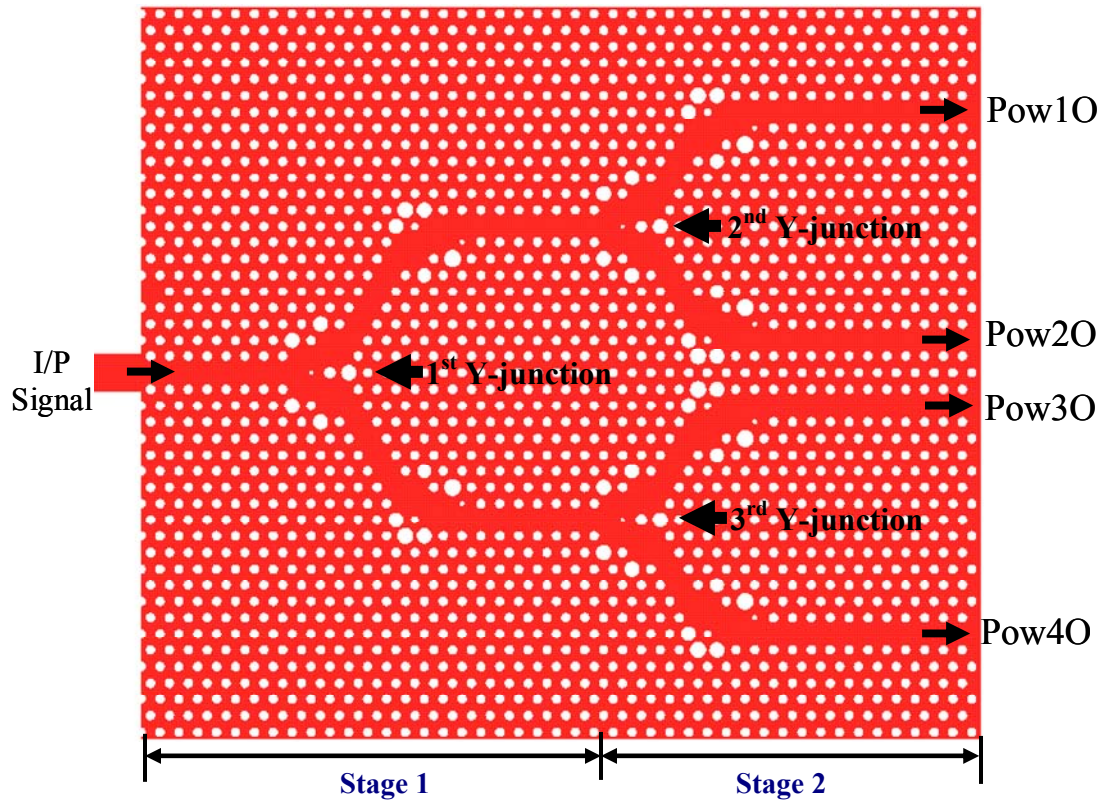
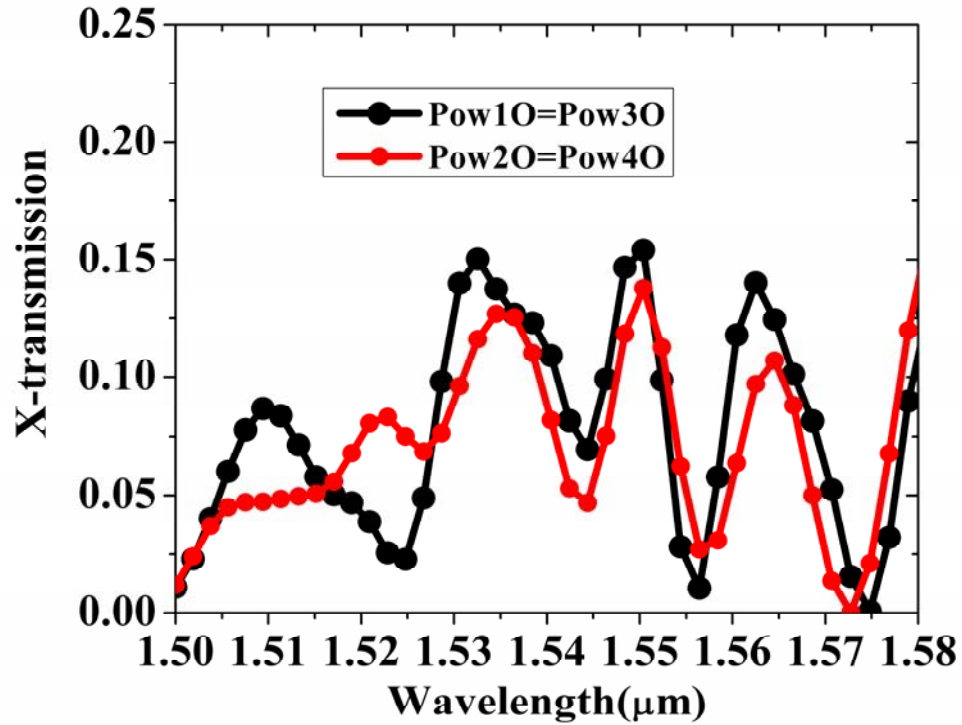


Figure 3.9 Architecture of 1 to 4 power splitter using Y-junction

Basically the whole structure is divided into two stages. First stage consists of one Y-junction and second stage consists of two Y-junctions. The two stages cascade each other. The configurations of holes size of 2<sup>nd</sup> and 3<sup>rd</sup> Y-junction are same as 1<sup>st</sup> Y-junction. The entire structure is surrounded by twelve PML layers to absorb the outgoing waves. A continuous optical pulse is injected into the first Y-junction PCW (Figure 3.9) and then after propagation of the certain distance this pulses are divided into two channel

and coupled into the next stage i.e. stage 2. In the second stage the signal is divided into four channels which are shown in figure 3.9. The whole structure is partially optimized and 58.3% of input power is achieved at four channels as shown in figure 3.10.



**Figure 3.10 Normalized transmitted output power of Y-junction based 1×4 power splitter**

The output transmitted power is quite low and is not equally distributed. In order to maintain single mode operation at each channel the design should be further modified to transmit equal and maximum power at each output channel. Modification of smaller Y-junction which in turn increase spacing between channel 2 and 3 at the output, which may improve the equal power distribution and also maximize the power at each output channel.

The high power transmission and broad bandwidth of Y-junction based 1×2 power splitter is achieved through 3-D FDTD simulation analysis. This simulation is well

comparable with the published result [33, 46]. So, we have decided to fabricate the Y-junction  $1 \times 2$  structure in silicon on insulator (SOI) platform. In order to do that 250nm SOI substrate is available so we have configured our structure on the basis of 250nm slab thickness.

### 3.3.6 Improve transmission by changing slab thickness

In order to fabricate Y-junction structure for  $1 \times 2$  power splitter application, the entire structure is simulated with 250nm slab height. The simulation parameter and hole size are similar as before but slab height is changed only.

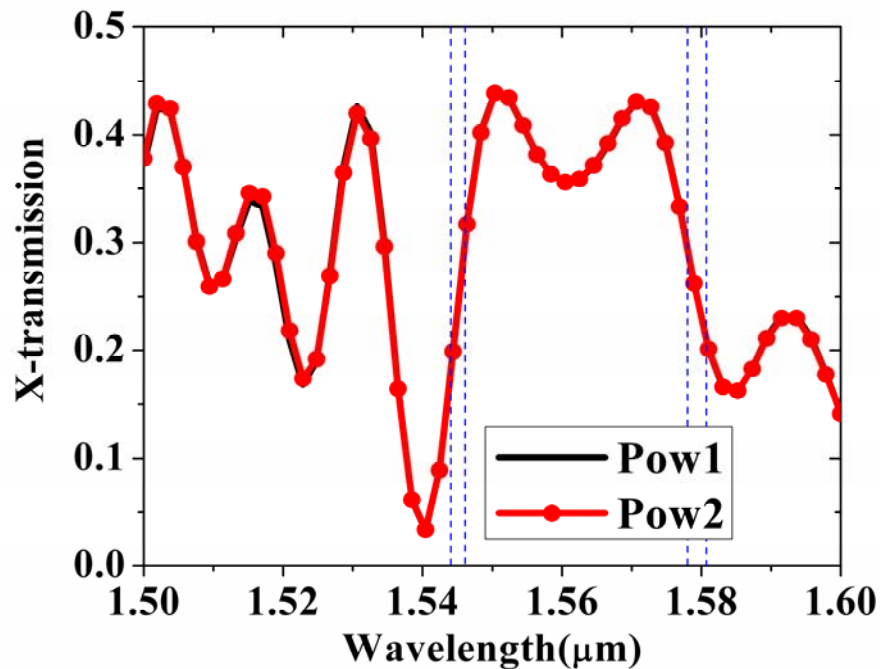
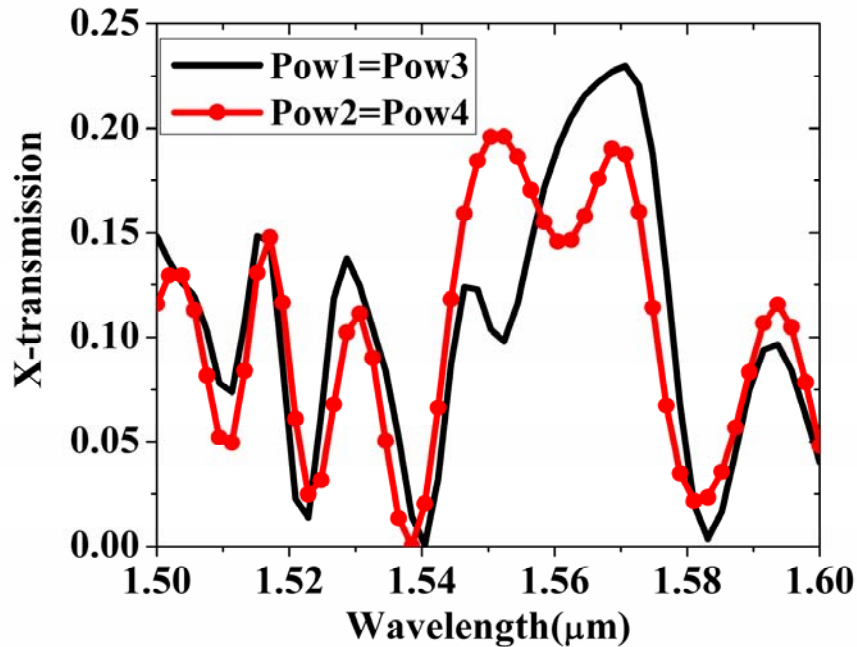


Figure 3:11 Normalized transmission of output power spectrum of modified Y-junction with 250nm slab thickness

The whole structure is investigated with 3-D FDTD simulation method. Figure 3.11 shows the each channel transmits 43.9% of input power which is higher than the 300nm slab height of Y-junction structure. As a result overall power transmission is also

improved. The power transmission of the new Y-junction based power splitter is 87.5%. At each output channel more than 30% power is achieved in the frequency range of 1546nm-1577nm (with bandwidth about 31nm) and 34% power is achieved at each output channel in the frequency range of 1547nm-1576nm (with bandwidth about 29nm), indicated by blue dash line (Figure 3.11) with highest pick value of 43.9% power for channel1 and 2. This maximized transmitted power is well comparable with the published results [33, 46]. The output transmitted power is maximized due to less amount of vertical loss. In 2-D slab PC the vertical loss is depend on the slab thickness. If the slab thickness is more then the vertical loss will be more and vice versa. In order to achieve a high transmission at 1×2 Y-junction structure, we have also partially investigated 1×4 splitter based on Y-junction structure. In this investigation the power transmission is improved by only 1.6% which is not a considerable increment. The output transmission of 1×4 power splitter is shown in figure 3.12.



**Figure 3.12** Transmitted output power of Y-junction base 1×4 power splitter with 250nm slab thickness

This power transmission is not high enough and also it is not equally distributed into each channel which is shown in Figure 3.12. 10.3% of the input power is transmitted through channel 1 and channel 3 and the 19.5% of input power is transmitted through channel 1 and channel 4. From the simulated result it is quite clear that Y-junction is better for 1×2 splitting technique not for 1×4. Based on 1×2 Y-junction power splitter simulation result, we have fabricated this structure on 250nm thick SOI platform. In the next section we will discuss the fabrication step of 1×2 Y-junction base power splitter.

### **3.4 Fabrication of 2-D Slab 1×2 Y-Junction Base Power Splitter**

This section deals with nanofabrication steps of 1×2 Y-junction base power splitter. Electron beam lithography (EBL) is used to transfer the pattern and etched on the top silicon layer. Bosch process is used to develop the pattern. Proper steps have been developed to make a Y-junction base 1×2 power splitter.

The parameter of the fabricated device are lattice constant ( $a$ ) of 400nm and radius of dielectric hole with 100nm. The device is fabricated on 4'' SOI wafer purchased from SOITEC. The wafer consists of 500 $\mu$ m thick silicon handle with a layer of buried oxide followed by a device layer of crystalline silicon. The thickness of the buried oxide is 1 $\mu$ m and thickness of device layer is 0.25 $\mu$ m. The 1 $\mu$ m silicon oxide is selected to prevent the substrate from affecting the transmission characteristics of the PC waveguide. PC Y-junction structure with air above and 1 micron oxide below is fabricated on SOI wafer. For good coupling, the PC Y-unction structure is connected with a 0.8 $\mu$ m dielectric waveguide. The recipe developed for conventional waveguide and alignment mark is

presented in Appendix A and Appendix B. The process flow of PC Y-junction structure is shown in figure 3.13.

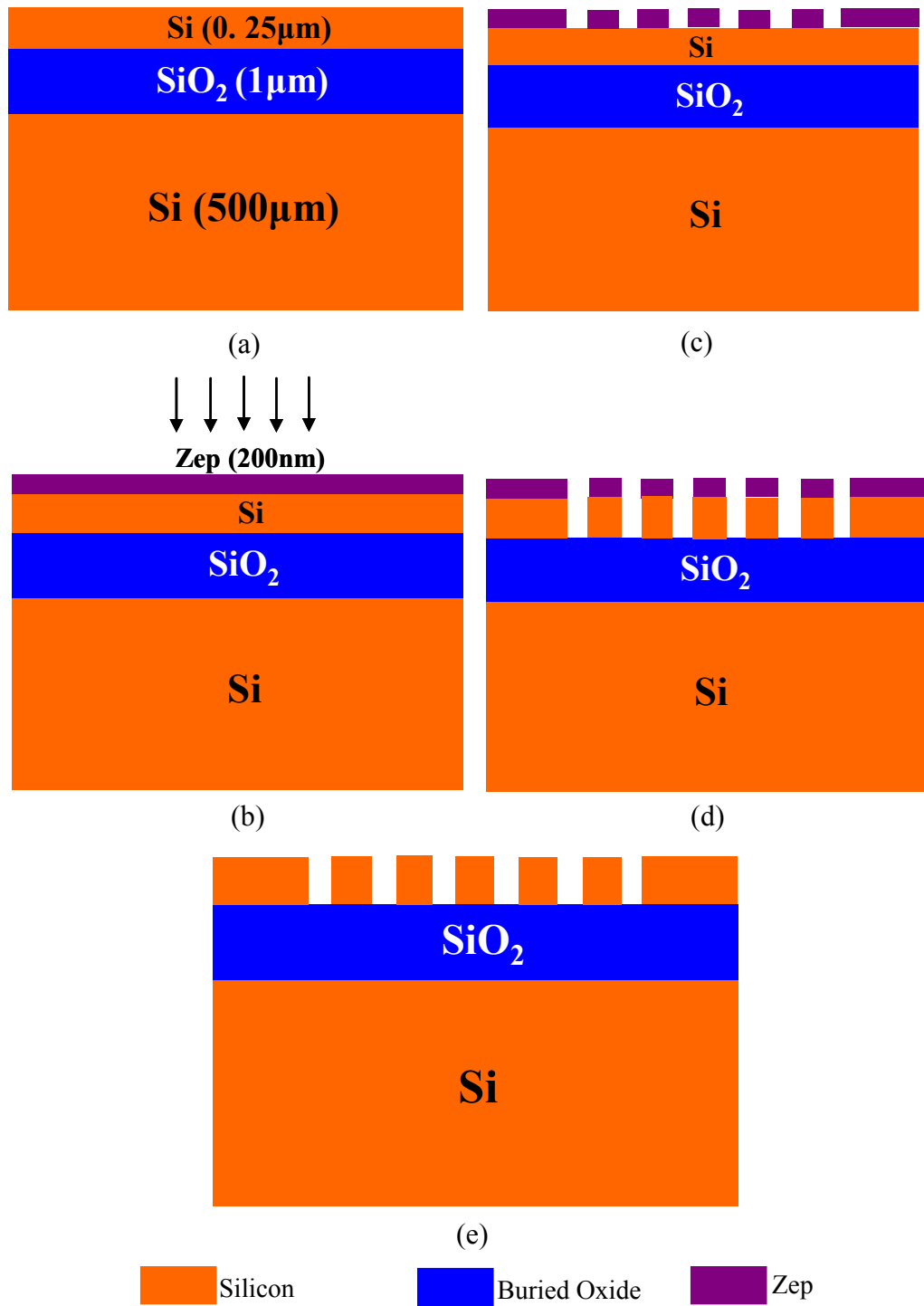


Figure 3.13 Schematic diagram of a PC base 1×2 Y-junction power splitter fabrication on SOI platform

For electron-beam (e-beam) lithography, the sample is coated with Zep photoresist which is an electron-beam sensitive resist. The resist has to be thin to allow for the fine features of the photonic crystal. The detail process is in Appendix C. It is worth mentioning that when an electron beam is incident on a material, the electrons are not destroyed but are scattered both elastically (with an angle changes but without energy loss) and inelastically (with energy loss). Back-scattered electrons often cause features written by e-beam lithography to be wider in densely patterned areas. Due this proximity effect, the hole size on the PC is not exactly the same as what is written on the sample. For good accuracy, a dose test helps to determine the proper hole diameter written and beam current so that the developed hole radius equals the expected value.

To pattern the PC Y-junction base splitter (Figure 3.13c), e-beam lithography is employed. After exposure of e-beam, the sample is subject to develop in Zep developer then the pattern is ready to be etched into the silicon. Dry etching method selectively removes away the exposed part which is not protected by photoresist. There are two leading technique of dry etching for etching deep into silicon which are “Bosch” process and a cryogenically cooled process.

After the e-beam exposure, the silicon etch process is accomplished with an Inductive Coupled Plasma set up (Alcatel 601E). Anisotropic etching in SF<sub>6</sub> inductively coupled plasma has become standard for silicon etching. The PC base Y-junction design, written by using e-beam lithography, is transferred to 250nm thick device layer silicon by inductively coupled plasma (ICP) etched in the Alcatel operating at 2.45GHz. with He (Helium) gas flowing at the back of the substrate for temperature control. The substrate is RF (Radio Frequency) driven for independent ion energy control towards the sample.



Bosch process is used to achieve vertical deep plasma etching. Thin fluoro-carbon polymer film is used for side wall protection. The recipe developed is presented in Appendix D.

After dry etch the Zep layer is stripped by using Deep UV (ultraviolet) exposure and sample is cleaned in PG remover. The cleaning process terminated by using Acetone followed by Iso-Propyl-Alcohol (IPA) and blow drying. The result of this process is a planar PC Y-junction base splitter made of a perforated silicon membrane lying on the buried oxide is shown in figure 3.14e. The SEM (Scanning Electron Microscope) image of fabricated Y-junction is shown in figure 3.14.

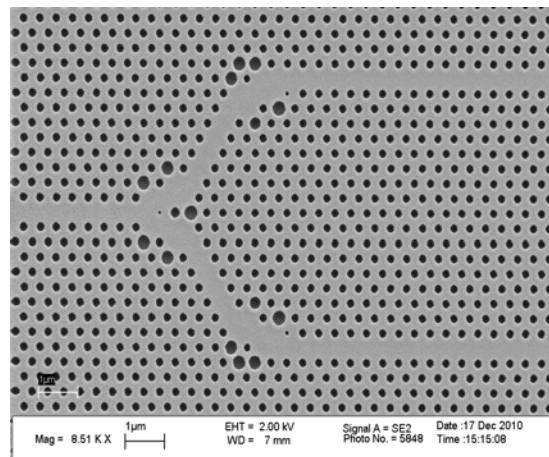


**Figure 3.14 SEM image of Y-junction structure**

## Summary

Y-junction is convenient for  $1 \times 2$  power splitter application. It has less mode mismatch and bending loss problems. It is also the most compact design. On the other hand, cascaded Y-junction based  $1 \times 4$  power splitter is not suitable for equal power splitting, as it has problem of junction and bending loss. Tuning the entire device would be very challenging. Therefore we have chosen a different design technique which does not contain junction and bending waveguide. So in next chapter we will discuss that new technique.

# Chapter 4

## **Photonic Crystal Line Defect Waveguides Integrated with Multimode Interference Block based Power Splitter**

In this chapter we have discussed a novel idea of a power splitter based on 2-D and 2-D slab PC LDWs with multimode interference block. The entire structure is divided into three parts i.e. conventional waveguides, multimode interference block, and PC LDWs. The operational principle of the device is based on the self imaging phenomena in the multimode interference region and then coupled into the PC LDWs which are integrated with MMI block.

Recently PC based power splitter has been attracted by many researchers for their vast application in multi/demultiplexers and optical communication area due to their unique characteristics and ability to control the behavior of light by introducing defects into them. Power splitters are indispensable components in optoelectronic circuits which are implemented with PC-based Y-junction, multimode interference effect and directional coupling effects [33, 6, 8, 50-51]. The PC-based Y-junction power splitter has problems with mode mismatch and bending loss which excites the higher order modes. So in order to obtain an acceptable output transmission, the bending region needs to be carefully optimized which adds difficulties in design and fabrication. To minimize mode mismatch and bending loss, many researchers have investigated theoretically on array of dielectric rods in air. The advantage of this structure is obtaining a waveguide by removing a single

line of rods so that light can travel around the sharp bends with high transmission of power. Based on this concept the T-junction and MMI effects have been a matter of interest for many investigators [50-51, 7]. Unfortunately the rod in air approach does not provide enough vertical confinement and it is very difficult to implement as a practical device. After that directional coupling structure which was proposed by Afshin Ghaffari et al. 2009 [8] has replaced two parallel waveguides with one single line defect waveguide W1 (one missing row of holes). These waveguides are preferred compared to two parallel waveguides due to their single mode operation and low loss activity and nearly 50% transmission is achieved at each of the output channel. The output transmission depends on coupling coefficient ( $\kappa$ ) which is again related to radius of the coupling rod and coupling length. So the key parameters for high transmission efficiency are coupling length and radius of the coupling rod.

To avoid some of the above difficulties and challenges, in this thesis we have investigated a novel idea for a 1×4 power splitting technique which is a 2D photonic crystal triangular lattice of dielectric air holes line defect waveguides integrated with an MMI block. Moreover, the proposed power splitter structure overcomes the mode matching phenomena, poor transmittance of Y-junction structure and the limited bandwidth and is easier to fabricate as compared to a Y-junction structure and MMI effect dielectric rod structure. The structure can be applied to optical communication systems and also be integrated with other PC-based devices.

## 4.1 Design of 2-D Photonic Crystal Crystal Line Defect Waveguides Integrated with MMI for Power Splitter Application

In most of the references the MMI block has been simulated by using Beam propagation method (BPM). However, this is not a proper method for PC structures. 2-D FDTD method is ideally suited for the purpose of simulation of the entire structure i.e. PC line defect waveguides integrated with MMI block.

### 4.1.1 Basic structure of MMI

MMI block is basically a waveguide which can support a large number of modes (typically  $\geq 3$ ). The typical structure of MMI consists of three sections i.e. single mode input and output waveguides and a multimode waveguide in the middle as shown in figure 4.1 where  $W_e$  is the effective width of the multimode waveguide and  $L_{\min}$  is the length of the multimode waveguide. The working principal of MMI is based on self-imaging effect [52].

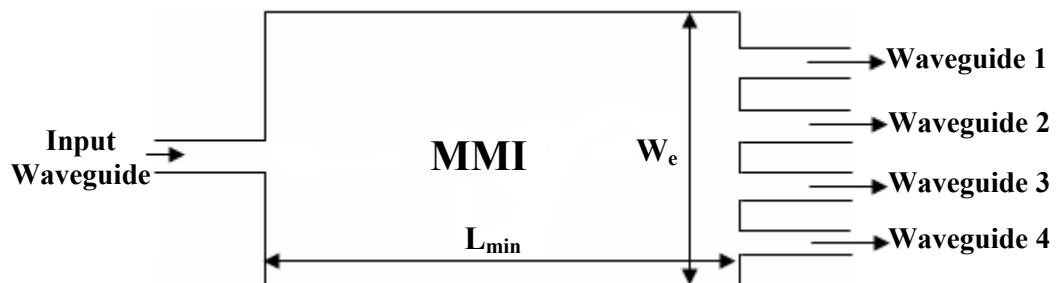


Figure 4.1 Schematic diagram of MMI power splitter

The minimum length ( $L_{\min}$ ) and the effective width ( $W_e$ ) of the multimode waveguide are determined by [53]

$$L_{\min} = \frac{p}{N} \left( \frac{3L_{\pi}}{4} \right) \quad \text{with } p = 1, 2, \dots \quad (4.1)$$

where factor  $p$  denotes the periodic nature of the images along the multimode region,  $N$  is the number of folded images which is obtained at distances and  $L_{\pi}$  is the beat length and is defined by [53]

$$L_{\pi} = \frac{\pi}{\beta_0 - \beta_1} \approx \frac{4nW_e^2}{3\lambda_0} \quad (4.2)$$

where  $\beta_0$  and  $\beta_1$  are the propagation constants of the fundamental mode and the first mode of the multimode waveguide respectively,  $n$  is an effective refractive index,  $\lambda_0$  is the free space wavelength and  $W_e$  is the effective width of the multimode region. The above formula is used to determine the output port location in the multimode.

#### **4.1.2 Integration of MMI and photonic crystal line defect waveguides**

The proposed 2D PC power splitter consisting of a triangular lattice of air holes with its radius  $r = 0.25a$ , where  $a = 0.410\mu\text{m}$  is the lattice constant. This triangular lattice consists of air holes etched into the dielectric substrate with an index of refraction  $n = 3.01$  which is compatible with silicon micro-fabrication technology. In this power splitter, the key element is an MMI block which is placed in the middle part of the power splitting device as shown in figure 4.2.

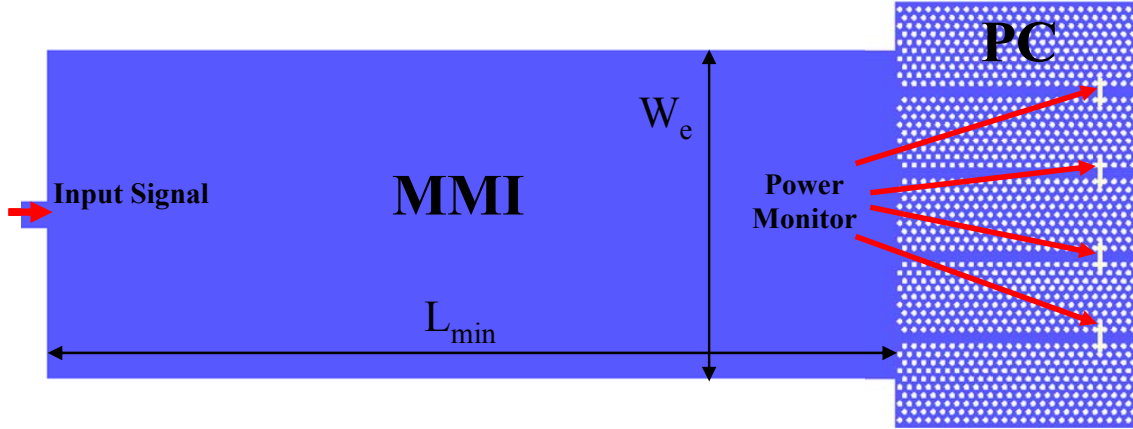


**Figure 4.2 Basic structure of proposed power splitter, consist of input conventional waveguide, multimode interference region and PC line defect waveguides**

The length and width of the MMI block is determined by using equation (4.1) and (4.2). According to working principle of MMI, the folded images of the multimode region depends on its length i.e.  $L_{min}$ . On the other hand, the location of the output channels depends on the  $L_{min}$  and PC line defect waveguides integrated correctly to those locations. The calculated value of  $L_{min}$  is  $97.56\mu\text{m}$  which is shown in figure 4.3 (a).

### **4.1.3 FDTD simulation parameter for entire structure**

The mode propagation inside the MMI block is analyzed and the position where the mode pattern splits is estimated. The simulation regions are reduced to half of the original size of the entire structure by using the symmetry boundary. The whole configuration of proposed structure (Figure 4.2) is then examined by 2-D FDTD computational domain with PML absorbing boundary condition with high mesh resolution for investigating the transmitted output power. The mesh size of this simulation is  $0.01\mu\text{m}$  (dx)  $\times$   $0.01\mu\text{m}$  (dy). A 2-D profile monitor is located at the output edge of the MMI to record 2-D mode profile assisting in the integration of PC LDWs with MMI for splitting application.

#### 4.1.4 Mode profile analysis

A mode source is chosen to excite the input field on the conventional waveguide and to generate the multiple modes inside the MMI region. A continuous wave at  $1.55\mu\text{m}$  wavelength is launched into the input conventional waveguide that propagates through the multimode waveguide. During the propagation through the MMI region, the multiple modes interfere with each other and produce four spots at the output edge of the MMI block. These spots are well separated from each other and smoothly coupled into the PC line defect waveguides. The distribution of the mode is captured by the profile monitor whose result is illustrated in figure 4.3 (b). The splitting of the mode is clearly observed in figure 4.3 (b). And we have integrated the PC line defect waveguides with the region where the mode is divided and calculated the output power at each output channel of PC line defect waveguides.

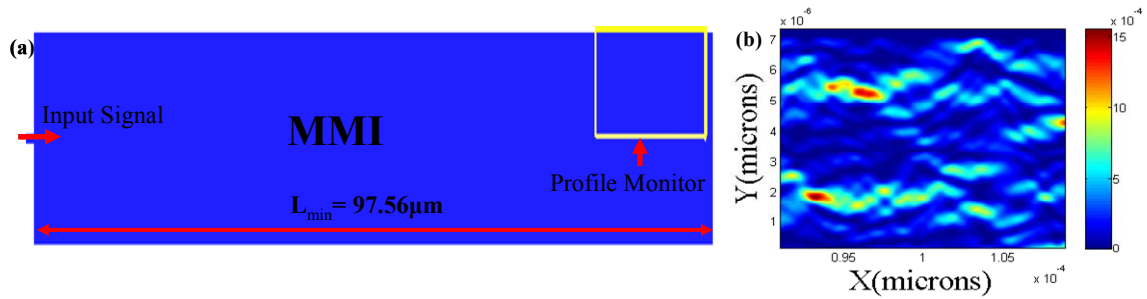


**Figure 4.3 (a) Initial structure of MMI block integrated with conventional waveguide (b) FDTD simulation of electric field profiles at the output edge of MMI. The operating wavelength of this excitation is  $1.55\mu\text{m}$**

## 4.2 Optimization Process

In order to achieve maximum power as well as equal power splitting at each output channel the design of the proposed power splitter has been optimized. In the process of optimization, to obtain the maximum power we first simulated the output transmitted

power with respect to varying length of the MMI. Secondly, the power flow propagating through the PC line defect waveguide is optimized with respect to varying width of the input conventional waveguide in order to get equal power at each output channel. The power transmission is calculated as the ratio of the output power to incident power.

#### 4.2.1 Optimization of MMI length

Figure 4.2 shows the optimized device structure after modifying the original power splitter. The method of optimization is done in two stages. First transmitted output power is maximized with respect to multimode region length and second equal amount of power at each output channel is achieved after optimization of the structure with respect to width of the input conventional waveguide. Here we consider the power splitter structure which is shown in figure 4.4. According to numerical consideration, the length of the multimode region is optimally set to  $93.5\mu\text{m}$  (the result is shown in figure 4.5).

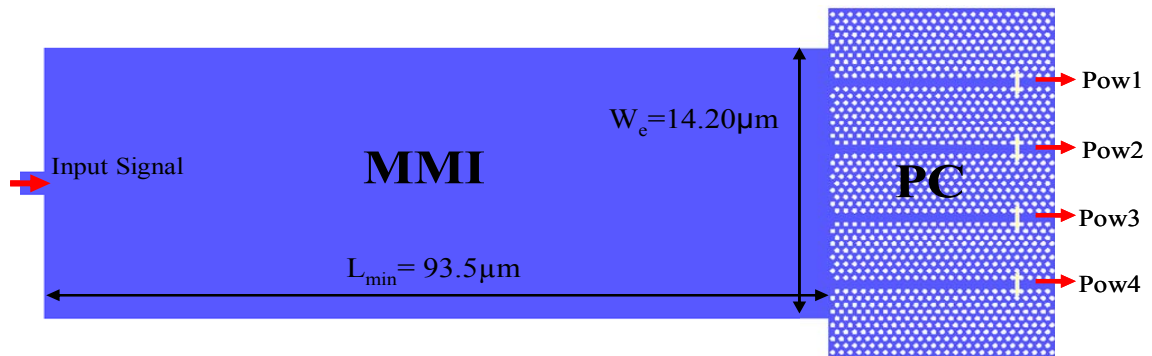


**Figure 4.4 Optimized structure of 1 to 4 power splitter with length of multimode region is  $93.5\mu\text{m}$ . The width of the MMI region is  $14.20\mu\text{m}$**

Therefore energy is perfectly transferred from the multimode region to the single mode defect region based on PC line defect waveguides. In this first stage result the energy is not equally divided at each output channel ( $\text{Pow1}=\text{Pow4}=15.9\%$  and



Pow2=Pow3=19.3%) as shown in figure 4.5. In this case the transfer of energy from multimode region to PC line defect waveguide is a function of multimode region length.

#### 4.2.2 Improvement of output power

In order to achieve equal amount of power at each output channel we have simulated the entire structure (Figure 4.4) with variable conventional input waveguide width.

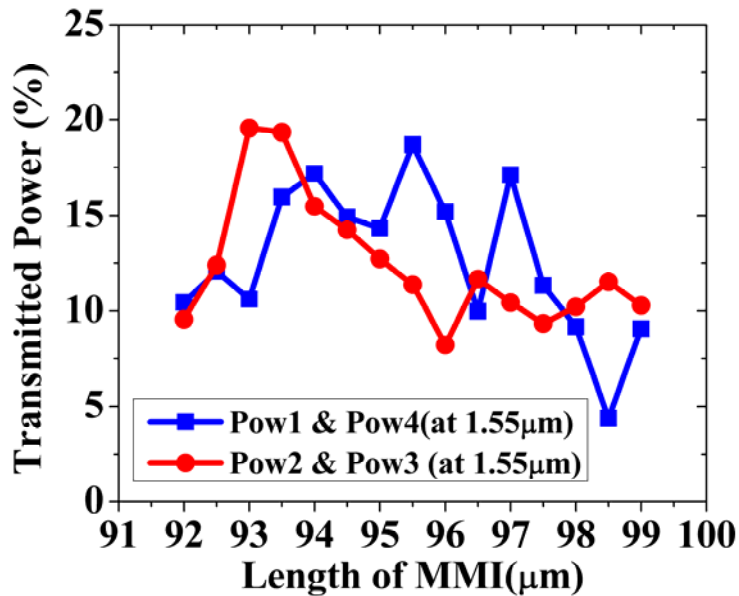


Figure 4.5 Normalized output transmission spectra at four channels with different  $L_{min}$  values and maximum energy transfer when  $L_{min} = 93.5\mu\text{m}$

The entire simulated result is shown in figure 4.6 and it is indicated that when conventional waveguide width is  $1.15\mu\text{m}$ , the input energy is equally divided at each output channel i.e.  $\text{Pow1}=\text{Pow4}=19.2\%$  and  $\text{Pow2}=\text{Pow3}=19.3\%$ . Based on this result, it has been possible to achieve  $1\times 4$  equal power splitter and it is shown in figure 4.4.

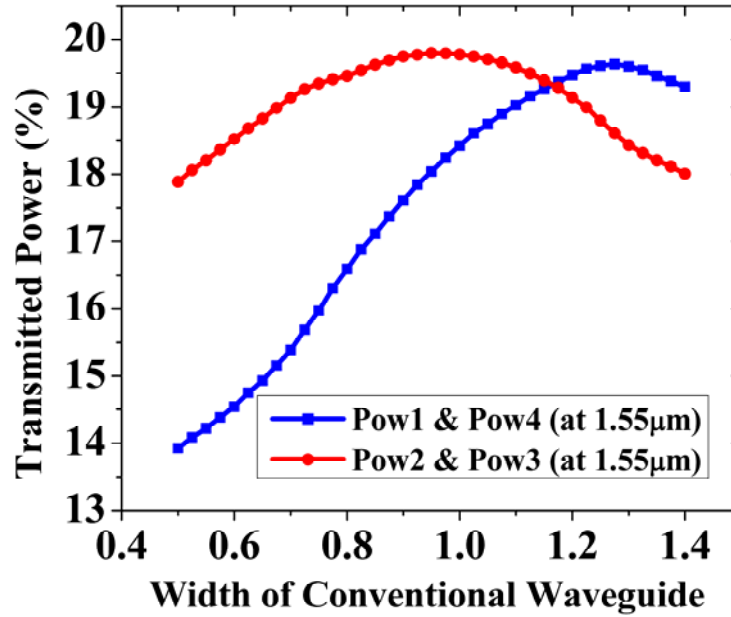
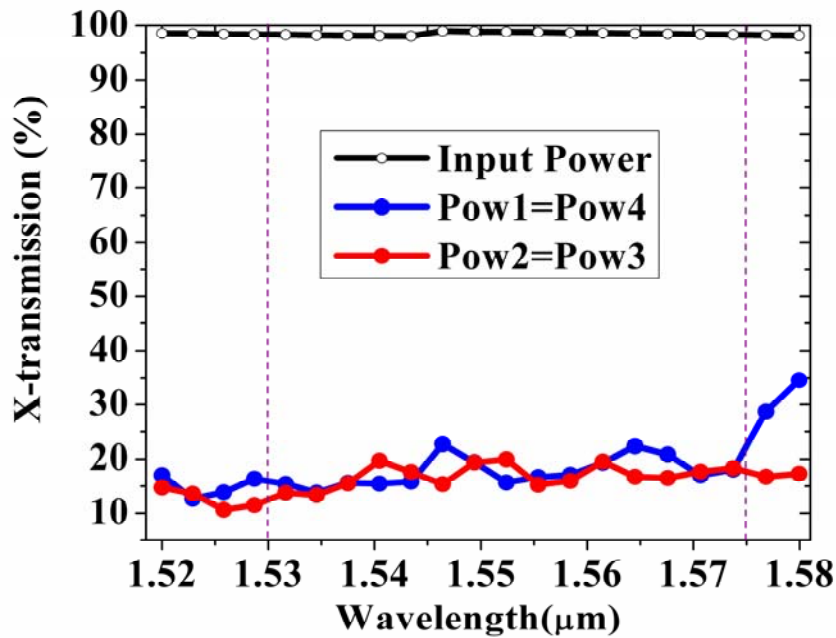


Figure 4.6 Normalized output transmission spectra at four channels with  $L_{\min}= 93.5\mu\text{m}$ ,  $W_c= 14.20\mu\text{m}$  and varying conventional waveguide width from  $0.5\mu\text{m}$  to  $1.4\mu\text{m}$

### 4.2.3 Analysis of power spectrum

Figure 4.7 show the whole output spectrum with respect to input. The normalized incident power is denoted by a white circle on black line and output transmitted power is denoted by solid circle on blue and red line. The total transmitted power is achieved more than 19% at each output channel at  $1.55\mu\text{m}$  wavelength. Whereas more than 15% power is achieved at each output channel in the frequency range of  $1.530\mu\text{m}$ - $1.575\mu\text{m}$  (with bandwidth about 45nm), indicated by purple dash line, with highest peak value of 22% power for channel 1 and 4 and 19% power for channel 2 and 3. The abrupt dip in the output spectrum is due to anti-crossing between different order modes.



**Figure 4.7** Normalized output transmitted power at each channel with respect to incident power

The length of the multimode region and input conventional waveguide width plays an important role in achieving the wider bandwidth. The result can be shown by the figure 4.7. The total output transmittance of more than 77% was achieved with respect to incident power at 1.55μm wavelength. Not only we have reached at our basic aim i.e. to achieve 1×4 equal power splitter but also have attained nearly flat transmission over the frequency range of 1.530μm-1.575μm. In this power splitter the output channels are well separated, so that there is no chance of crosstalk between the output signals. The length of the multimode region and PC line defect waveguides is about 102.3μm which is not as compact as compared to other researcher’s design [6, 8, 53]. Apart from its degree of compactness, the rest of the design topology of the device is comparable with the other’s work in terms of broadband, easy fabrication and practical implementation [6, 8, 33, 53]. The whole structure is identical in the sense that there is no need to tune the hole size for

optimization. The proposed design has no  $120^\circ$  junction as well as  $60^\circ$  bend. As a consequence the single mode operation is not suffered. The entire structure is formed by triangular lattice of dielectric hole so the vertical confinement is better than the triangular lattice of dielectric rod structure. In account of having all these advantages, the entire design can be considered as a 2-D slab PC configuration. The following section will elaborately discuss the method of designing the  $1 \times 4$  power splitter in 2-D slab PC configuration.

### **4.3 Design of 2-D Slab Photonic Crystal Line Defect Waveguides Integrated with MMI for Power Splitter Application**

Achieved a good result on 2-D base PC LDWs integrated with MMI for power splitter application, then the next stage is investigated the same structure on 2-D slab PC. The entire structure is simulated through 3-D FDTD method.

#### **4.3.1 Basic structure of MMI**

The structure of MMI block is already explained in section 4.1.1. For the calculation of the length and the width of the MMI, the same formula is used what has already been used for 2-D MMI configuration purpose.

#### **4.3.2 Device design**

The 2-D slab PC base power splitter consists of triangular lattice of air holes with its radius  $r = 0.25 * a$ , where  $a = 0.400 \mu\text{m}$  is the lattice constant. This triangular lattice consist of air holes etched into the dielectric substrate with a refractive index of silicon  $n = 3.47$ . The length and width of the MMI block is determined by using equation 4.1 and 4.2.

According to working principle of MMI, the folded images of the multimode region depends on its length i.e.  $L_{\min}$ . On the other hand, the location of the output channels depends on the  $L_{\min}$  and PC line defect waveguides integrated correctly to those locations. The calculated value of the  $L_{\min}$  is  $59.4\mu\text{m}$  and width of the ( $W_e$ ) is  $11.08\mu\text{m}$  shown in figure 4.8a. The whole structure is investigated through 3-D FDTD computation method where thickness of the slab is finite ( $300\mu\text{m}$ ).

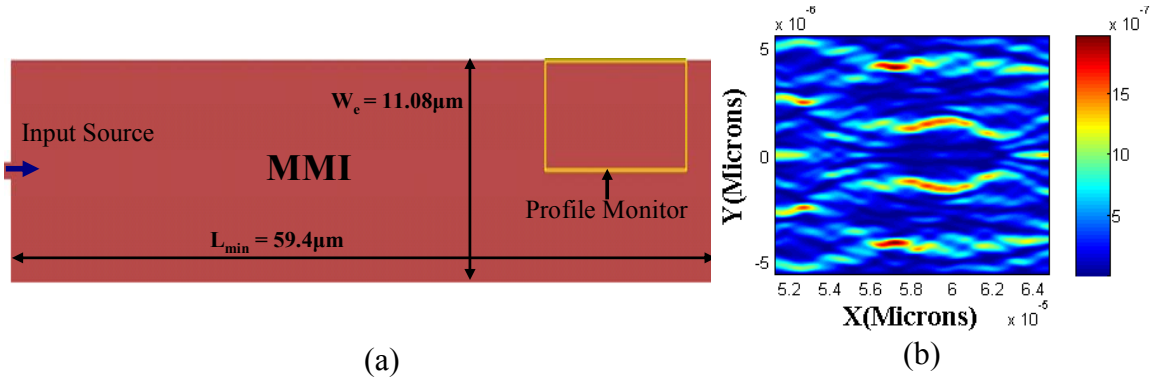


**Figure 4.8 (a) Initial structure of 2-D slab MMI block integrated with conventional waveguide (b) FDTD simulation of electric field profiles at the output edge of MMI. The operating wavelength of this excitation is  $1.55\mu\text{m}$**

### 4.3.3 FDTD simulation parameter for entire structure

The propagation of modes inside the MMI block is analyzed and the position where the mode pattern splits is estimated. By using the symmetric and anti-symmetric boundary, the overall region is reduced to half of the original size of the entire structure. The whole configuration of the proposed structure (Figure 4.9a) is then examined by 3-D FDTD computational domain with PML absorbing boundary condition with high mesh resolution for investigating the transmitted output power. The mesh size of this simulation is  $0.0166\mu\text{m}$  (dx)  $\times$   $0.0164\mu\text{m}$  (dy)  $\times$   $0.0165\mu\text{m}$  (dz). For power splitting application, a 3-D profile monitor is helpful for integration of PC LDWs with MMI, is

located at the output edge of the MMI to record 3-D profile. The entire structure is built in the 3-D FDTD simulation which is represented by the figure 4.9b.

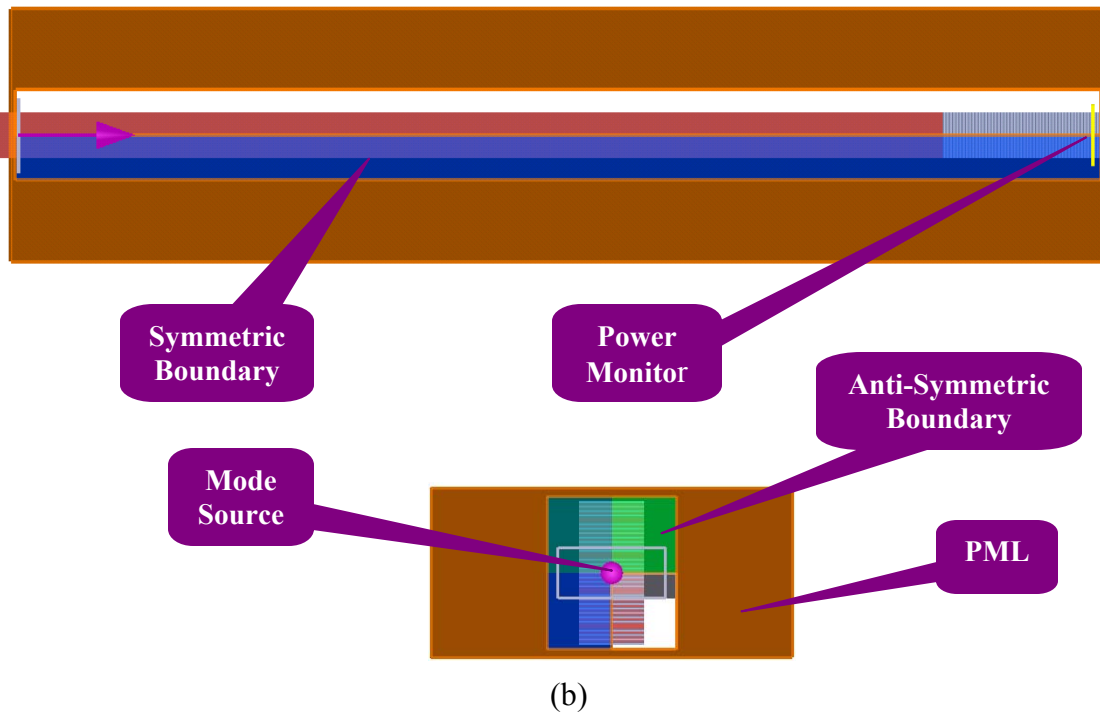
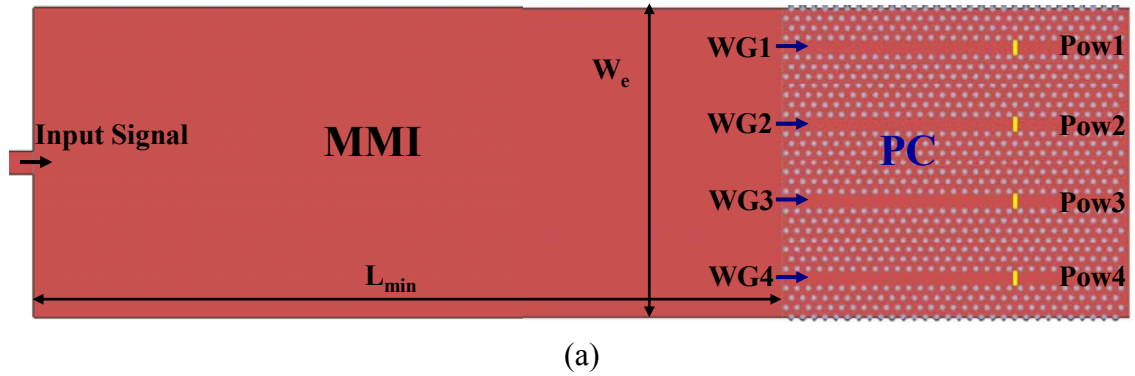


**Figure 4.9 (a) Basic structure of proposed power splitter, consist of input conventional waveguide, multimode interference region and PC line defect waveguides; (b) FDTD simulation setup for the entire structure**

#### 4.3.4 Mode profile analysis

A mode source is applied to generate the multiple modes inside the MMI region. When multiple modes are propagated through the MMI region they interfere with each other

and produce four spots at the output edge of the MMI block. These spots are well separated from each other and smoothly coupled into the PC line defect waveguides. The distribution of the mode is captured by the profile monitor whose result is illustrated in figure 4.8b. After that we have integrated the PC line defect waveguides with the region where the mode is divided and calculated the output power at each output channel of PC line defect waveguides.

## **4.4 Optimization Process**

In order to achieve maximum power as well as equal power splitting at each output channel the design of the proposed power splitter has been optimized. In the optimization process, first we simulated the output transmitted power with respect to varying length of the MMI to obtain maximum power. Secondly, the power flow propagating through the PC line defect waveguide is optimized with respect to varying the width of the input conventional waveguide in order to get equal power at each output channel.

#### 4.4.1 Optimization of MMI length

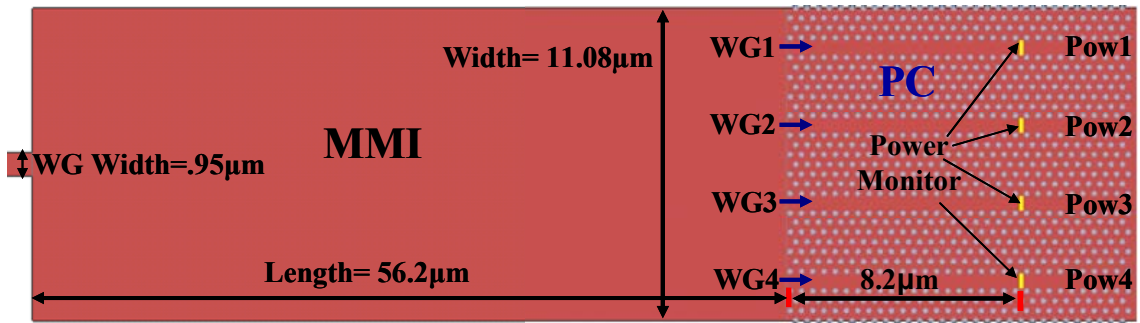
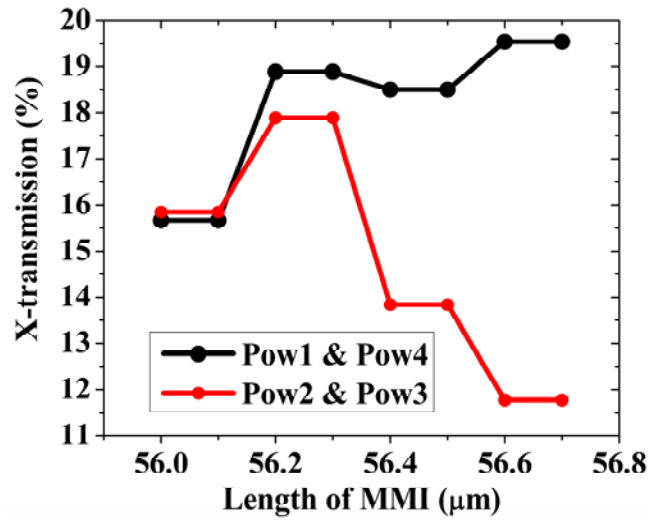


Figure 4.10 Optimized structure of 1 to 4 power splitter with length of multimode region is  $56.2\mu\text{m}$ . The width of the MMI region is  $11.08\mu\text{m}$

Figure 4.10 shows the optimized device structure after modifying the original power splitter. The method of optimization is done in two stages. At first, the transmitted output power has been maximized with respect to multimode region length and secondly the equal amount of power at each output channel is achieved after optimization of the structure with respect to width of the input conventional waveguide. According to numerical consideration, the length of the multimode region is optimally set to  $56.2\mu\text{m}$  (the result is shown in figure 4.11).





**Figure 4.11** Normalized output transmission spectra at four channels with different  $L_{\min}$  values and maximum energy transfer when  $L_{\min} = 56.2\mu\text{m}$

#### 4.4.2 Optimization of conventional waveguide width

In order to achieve equal amount of power at each output channel we have simulated the entire structure (Figure 4.10) with variable conventional input waveguide width. The entire simulated result is shown in figure 4.12 and it is indicated that when conventional waveguide width is  $0.95\mu\text{m}$ , the input energy is equally divided at each output channel i.e.  $\text{Pow1}=\text{Pow4}=18.9\%$  and  $\text{Pow2}=\text{Pow3}=18.9\%$  respectively and the overall output spectrum is shown in figure 4.13. Based on this result, it has been possible to achieve  $1\times 4$  equal power splitter. The numerical simulation for  $1\times 4$  power splitter shows that the splitter have achieved 75.7% of input power at a target wavelength of  $1.55\mu\text{m}$  with a uniform bandwidth of 46nm.

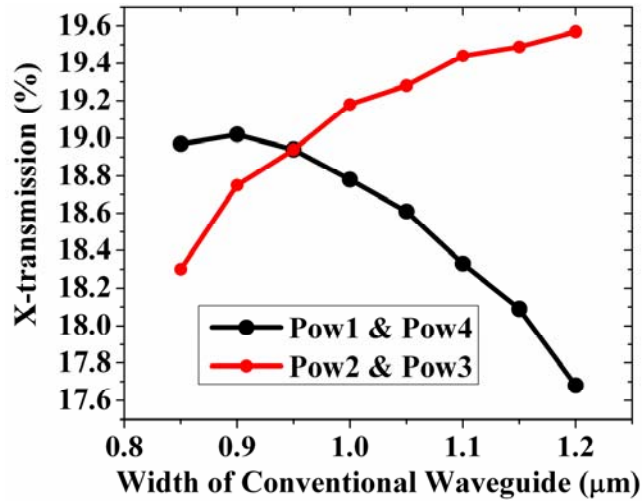


Figure 4.12 Normalized output transmission spectra at four channels with  $L_{\min}= 56.2\mu\text{m}$ ,  $W_c= 0.95\mu\text{m}$  and varying conventional waveguide width from  $0.85\mu\text{m}$  to  $1.2\mu\text{m}$

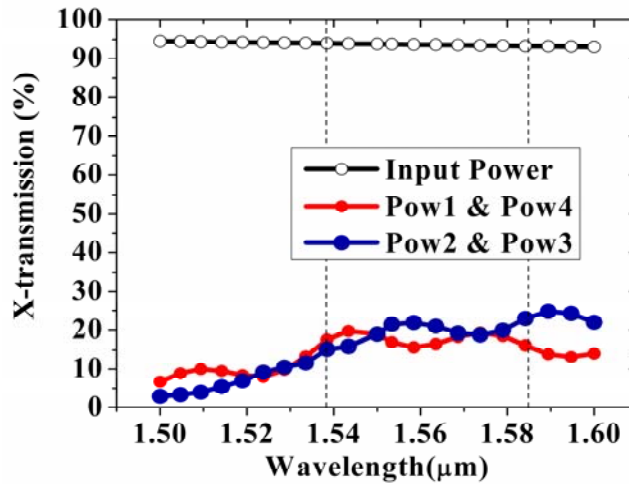


Figure 4.13 Normalized output transmitted power at each channel with respect to incident power

#### 4.4.3 Analysis of overall result

In order to achieve the wider bandwidth, the length of multimode region and input conventional waveguide width plays an important role. The result is shown in figure 4.13. Total 73.5% power is achieved with respect to incident power at  $1.55\mu\text{m}$  wavelength. Not only we have achieved our basic aim i.e. to obtain  $1\times 4$  equal power splitter but also

achieve flat transmission over the frequency range of  $1.538\mu\text{m}$ - $1.584\mu\text{m}$ . In 2-D slab configuration power splitter, the output channels are well separated, therefore crosstalk between the output signals does not occur. The length of the multimode region is less than the 2-D configuration of MMI region but it is not compact as compared to other researcher's design [6, 8, 53]. Barring compactness, the entire design topology of the device is comparable with the other's people's work in regard of broadband, easy fabrication and practical implementation [6, 8, 32, 53]. The whole structure is identical which means there is no need to tune hole size for optimization. The entire design is similar to the 2-D counter part. Therefore, there are no  $120^\circ$  junction and  $60^\circ$  bend and for that single mode operation is not affected. The entire structure is formed by the triangular lattice of dielectric hole so the vertical confinement is better than the triangular lattice of dielectric rod structure. In account of having all of these advantages, the entire design will be fabricated in our future work.

## **Summary**

The  $1\times 4$  power splitter which is based on PC line defect waveguide, integrated with MMI, has broad spectrum output and the power is equally divided. The only disadvantage is the length of the device is comparatively larger. Therefore, our next step is to make the device more compact. In the next chapter our focus was on the reduction of the length of the device and we investigated structures with reduced length that would provide the equal power splitting with broad spectrum at each output channel.

# Chapter 5

## Multiple Line Defect Based Power Splitter

Several Optical devices based on photonic crystals have been proposed and are expected to play an important role in future optical and optoelectronics circuits. Numerous planar photonic crystal optical components have been investigated theoretically and experimentally by several researchers for guiding and routing through bends, branches and waveguide crossings [6, 8, 33, 43, 54-56]. PC based power splitter is one of the members of optical component. The most common and simple design for a power splitter is a Y-junction structure. It has  $120^\circ$  junction and  $60^\circ$  bend two output channels [33]. This leads to mismatch and bending loss. To overcome these problems many researchers have theoretically investigated PC arrays of dielectric rods in air. The waveguide which is made by dielectric rods is single mode and the light traveling around the sharp bends with high transmission is relatively straight forward [6, 57]. Unfortunately, the rod in air approach does not provide vertical confinement and it is very difficult to implement as a practical device. However, as per our knowledge, none have so far focused on  $1 \times 4$  power splitter based on cascading of multiple line defect waveguides. These waveguides are based on 2-D PC triangular lattice of dielectric air hole.

This chapter focuses on  $1 \times 4$  and  $1 \times 3$  power splitter which is based on cascading of multiple line defect waveguides of 2-D and 2-D slab PC. We have investigated the power splitter structure with different configuration of multiple line defect waveguides. In the

first section, we will discuss briefly the computational methods implemented, while second section will be dealt with optimization of cascaded multiple line defect waveguides for 1×4 power splitter application and the last investigation part is related to 1×3 power splitter which is based on 2-D slab PC multiple line defect waveguides.

## 5.1: Principles and Computational Methods

### 5.1.1 Maxwell's equations for PCs

For isotropic, non-dispersive, non-magnetic and lossless materials, which is the case of our material systems, the Maxwell's for harmonic wave in MKS units can be written as [1]:

$$\nabla \cdot \vec{H}(\vec{r}) = 0 \quad (5.1)$$

$$\nabla \cdot [\varepsilon(\vec{r})\vec{E}(\vec{r})] = 0 \quad (5.2)$$

$$\nabla \times \vec{H}(\vec{r}) = -j\omega\varepsilon(\vec{r})\varepsilon_0\vec{E}(\vec{r}) \quad (5.3)$$

$$\nabla \times \vec{E}(\vec{r}) = j\omega\mu_0\vec{H}(\vec{r}) \quad (5.4)$$

By substituting  $\vec{E}(\vec{r})$  from (5.3) into (5.4), Hermitian eigenfunctions are obtained:

$$\nabla \times \left\{ \frac{1}{\varepsilon(\vec{r})} \nabla \times \vec{H}(\vec{r}) \right\} = \frac{\omega^2}{c^2} \vec{H}(\vec{r}) \quad (5.5)$$

This is referred to as the “master equation” for PCs. In PCs, dielectric constant  $\varepsilon(\vec{r})$  is a periodic vectorial function which implies

$$\varepsilon(\vec{r} + \vec{a}_i) = \varepsilon(\vec{r}), \text{ for } i = 1, 2, 3 \quad (5.6)$$

where  $\vec{a}_i$  are elementary lattice vectors of the PCs, as shown in figure 5.1(a) for a 2-D

triangular lattice PC. Any periodic function could be expanded into linear combination of Fourier series so that

$$\frac{1}{\varepsilon(\vec{r})} = \sum_{\vec{h}} \kappa(\vec{h}) e^{j\vec{h} \cdot \vec{r}} \quad (5.7)$$

In (3.7),  $\vec{h}$  is the reciprocal lattice vector defined by  $\vec{h} = l_1 \vec{b}_1 + l_2 \vec{b}_2 + l_3 \vec{b}_3$ , where  $l_1, l_2, l_3$  are integers and  $\vec{b}_1, \vec{b}_2, \vec{b}_3$  are elementary reciprocal lattice vectors defined by  $\vec{a}_i \cdot \vec{b}_j = 2\pi \delta_{ij}$ . The reciprocal for 2-D triangular lattice PC is shown in figure 5.1 (b). The yellow color region is the first Brillouin zone while the green color region is the irreducible first Brillouin zone.

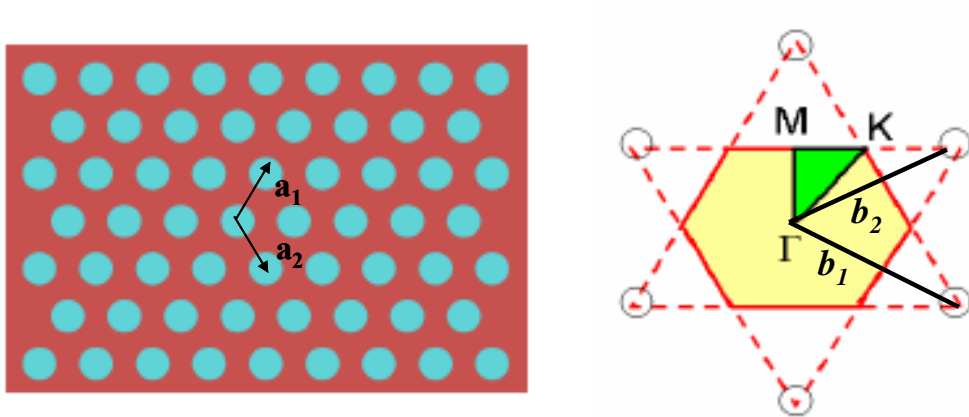


Figure 5.1 2-D triangular lattice and its reciprocal lattice

### 5.1.2 Bloch's theorem

In periodic system, Bloch's theorem proves that eigenmodes can be expressed as a plane wave modulated by a periodic function [12]. Each mode can be characterized by a mode number  $n$  and a wave vector  $\vec{k}$  in the first Brillouin zone. Thus we have eigen PC modes expressed as:

$$\vec{H}(\vec{r}) = \vec{H}_{n\vec{k}}(\vec{r}) = \vec{u}_{n\vec{k}}(\vec{r}) e^{j\vec{k} \cdot \vec{r}} \quad (5.8)$$

where  $\vec{u}_{n\vec{k}}(\vec{r})$  is a periodic function on the lattice:  $\vec{u}_{n\vec{k}}(\vec{r}) = \vec{u}_{n\vec{k}}(\vec{r} + \vec{a}_i)$ .

### 5.1.3 Plane wave expansion method

PWE method solve eigenvalue problem in periodic systems by expanding the eigenmode into linear combination of plane waves [58]. The simulation is done on a unit cell of the periodic structures. So both eigenvalues and eigenmodes are obtained.

Since  $\vec{u}_{n\vec{k}}(\vec{r})$  is periodic function, so it can expand into Fourier series combinations of plane waves as what we did for the dielectric constant in (5.7). The eigen PC modes become

$$\vec{H}_{n\vec{k}}(\vec{r}) = \sum_{\vec{h}} \vec{H}_{n\vec{k}}(\vec{h}) e^{j(\vec{k} + \vec{h}) \cdot \vec{r}} \quad (5.9)$$

By substituting (5.7) and (5.9) into equation (5.5), we could write (5.5) into a summation of expanded plane waves as

$$\frac{\omega_{n\vec{k}}^2}{c^2} \vec{H}_{n\vec{k}}(\vec{h}) = - \sum_{\vec{h}-\vec{h}'} \kappa(\vec{h} - \vec{h}') (\vec{k} + \vec{h}) \times \{(\vec{k} + \vec{h}') \vec{H}_{n\vec{k}}(\vec{h}')\} \quad (5.10)$$

For 2-D PCs, the periodicity is only in two dimensions which means wave vector  $\vec{k}$  and reciprocal vector  $\vec{h}$  both have in-plane components only. In addition, for simulating TE modes, the magnetic field of the eigenmode only has component in z direction. This (5.10) can be simplified into the form as

$$\frac{\omega_{n\vec{k}_{\parallel}}^2}{c^2} \vec{H}_{z,n\vec{k}_{\parallel}}(\vec{h}_{\parallel}) = \sum_{\vec{h}_{\parallel}} \kappa(\vec{h}_{\parallel} - \vec{h}_{\parallel}') (\vec{k}_{\parallel} + \vec{h}_{\parallel}) \bullet (\vec{k}_{\parallel} + \vec{h}_{\parallel}') H_{z,n\vec{k}_{\parallel}}(\vec{h}_{\parallel}') \quad (5.11)$$

To solve equation (5.11) analytically for a given wave vector  $\vec{k}_{\parallel}$ , infinite number of  $\vec{h}_{\parallel}$  and  $\vec{h}_{\parallel}'$  have to be taken into the formulation and this is not possible for complex

geometries of unit cell. However, we could solve this equation numerically by taking into account sufficiently large number of plane waves and the equation will become linear algebraic equation with  $H_{z,n\vec{k}_{\parallel}}(\vec{h})$  as eigenvector and  $\frac{\omega_{n\vec{k}_{\parallel}}^2}{c^2}$  as eigenvalues.

For 2-D PCLDWs, which are homogeneous and infinite in the third dimension, the waveguide modes can be simulated by 2-D PWE method by assuming an arbitrary periodicity of a “super cell” with a line defect surrounded by several layers of PC walls. If the super cell is large, the line defects in the imagined periodicity will be away from each other and coupling between them will be very weak. Under this circumstance, the 2-D PC LDW modes can be solved with high accuracy by 2-D PWE method. Though method is accurate and efficient, it has two major drawbacks. One is inability to treat loss and other is inability to treat material dispersion.

#### **5.1.4 Effective refractive index**

2-D PCLDW in slab retains or approximates the properties of a 2-D PCLDW. Therefore, rather than simulating line defect modes of 2-D PCLDWs in slab using 3-D PWEM, we can simulate line defect modes of 2-D PCLDWs using 2-D PWE method. 2-D PC structure is infinitely extended in the third dimension while 2-D PC slab light can confine by TIR at slab interface. In the process of using 2-D PWEM simulation, the influence of the slab confinement on the line defect modes must be taken into consideration. This can be approximated by using an effective refractive index of the slab. In this way the 3-D PWEM simulation can be reduced into 2-D simulations.

The effective index depends on the fundamental mode, thickness of the slab waveguide structure, working wavelength, slab index and cladding material index. The



material system used in this thesis is a 300nm thick silicon slab clad by materials with index equal to 1.4. Since we intend to design TE like symmetric PCLDW modes, the fundamental TE slab mode is therefore used in effective index calculation. The working wavelength is 1.55 $\mu$ m. These parameters give an effective index of 3.0189. Hence, in our calculation using 2-D PWEM, the index contrast of 3.0189: 1.4 is used on the PCLDW patterns to simulate the line defect modes. The effective index is an approximation for the slab confinement on the LDW modes.

### **5.1.5 Finite Difference Time Domain (FDTD) method**

The electromagnetic wave propagating through a periodic medium is (such as photonic crystal) exhibit the formation of allowable modes and their corresponding gaps. As propagation of the electromagnetic wave through a periodic structure like PC is different from that of homogeneous material, the used simulation technique should be accurate and fast enough to analyze structures from bulk to nanometer- scaled periodic structures.

The FDTD method has been one of the most widely used numerical techniques for solving electromagnetic boundary value problems. The essence of the method is the direct computational implementation of the Maxwell curl equation, which approximates all derivatives, both spatial and temporal [48]. The computational space is sampled at intervals that are small compared with all wavelengths under consideration, and material properties are specified at each sample point. The fields are calculated directly for all space points at successive time steps where the time increment between steps is small compared to the reciprocals of all frequencies under consideration.

The FDTD simulation tool offers appropriate boundary conditions and source. When the input signal can be set to be continuous wave (CW) or pulsed, the source is excited

and propagated through the structure by time stepping through the entire grid repeatedly. Boundary conditions are critical to analyze PC structure since any computational resource can only deal with finite size of matrix and the simulation region has to be terminated by boundaries. Perfectly matches layer (PML) was chosen to determine the leaky modes above the light line. The PML boundary condition in the Z-direction can be used without affecting the accuracy and any wave reaching out of the supercell will be absorbed and not give rise to an artificial resonance within it [59]. FDTD method has two primary advantages; first, this method computational requirements scale is linear with the size of the problem, which permits the analysis of larger, irregular structures in addition to perfectly periodic structures. Second, this method is simple to implement for complicated scattering structures.

## **5.2 Modeling of Multiple Line Defect Waveguides for 1×4 Power Splitter**

Design of 1×4 power is based on cascading of multiple line defect waveguides. For efficient power splitting, it is important to keep the whole structure symmetric with respect to the input waveguide. The proposed scheme considers two structures which are divided into five regions, one single mode input region, two multimode regions (MR), one separation region (SR) and one output region. In the first structure, MR is based on seven line defect waveguides (7-LDWs) where the central waveguide is used as an input port and output region consist of one pair of three line defect waveguides (3LDWs) in the second structure the only differences from the first one is its multimode region which is

based on five line defect waveguides (5-LDWs). In the proposed scheme the two structures are investigated by 2D FDTD simulation method.

### 5.2.1 2-D FDTD simulation parameter

In our FDTD simulations of PC multiple line defect waveguides some of the important parameters and assumptions are given below:

- Although, in 2-D FDTD method the structures is considered to be infinite height by using the effective index of the dielectric slab ( $N_{\text{eff}}$ ) instead of using the actual refractive index ( $N_{\text{slab}}$ ), yet, we can estimate the characteristics associated with structures of finite height.
- The grid size is chosen in such a way that it is always less than the  $\lambda / (10 * N_{\text{slab}})$  limit, where  $\lambda$  is the target wavelength. This limit will ensure that the grid size would be small enough to resolve the smallest feature in the fields and structures being simulated.

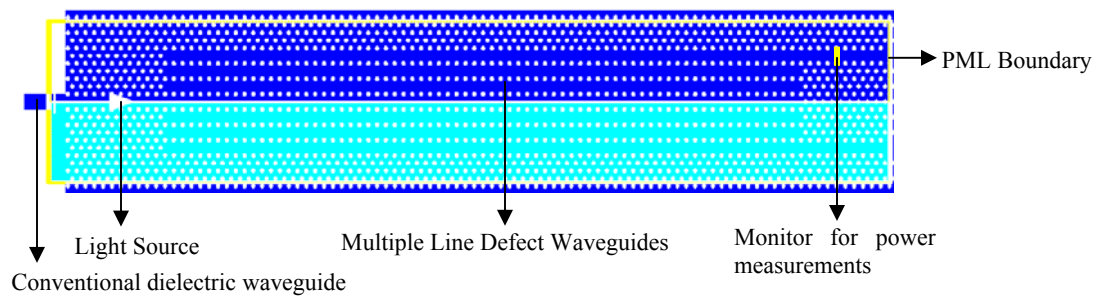


**Figure 5.2 2-D FDTD simulation setup**

- For characterizing the multiple line defect waveguides, the transmission spectrum of the multiple line defect waveguides is calculated initially. Then a modal source of small bandwidth set by a pulse-width of 200 femtosecond (fs) and an offset of 500fs are launched at the input through a conventional dielectric waveguide as shown in

Figure 3.2. The input pulse is centered at a frequency corresponding to maximum peak in the transmission spectrum so as to enable connection between the transmitted and reflected pulses along the waveguide.

- A PML layer boundary condition is applied to all sides of the PC multiple line defect waveguides structure which allows the radiation to leave the boundary without reflecting back.
- Total power transmission (normalized to the launch) is calculated at the end of the output channel of multiple line defect waveguides.

### **5.2.2 Design of PC multiple line defect waveguides**

The configuration of the structure is based on 2D PCs consisting of an array of dielectric air holes with a triangular lattice depicted in Figure 5.3 (a) and (b). The waveguides are oriented along the  $\Gamma$ -K direction of the triangular lattice of air holes with lattice constant 'a' and radius  $r = 0.25a$ . This triangular lattice of air holes are etched into the dielectric substrate with an effective index ' $n_{\text{eff}} = 2.847$ ' which is compatible with silicon micro-fabrication technology. In this structure, the lattice has a photonic bandgap with the normalized frequency ( $a/\lambda$ ) ranging from 0.22972 to 0.26851 for TM polarization (electric field parallel to air holes), where  $\lambda$  is wavelength in free space. While designing the proposed structure, the multiple photonic crystal line defect waveguides (PCLDWs) has been formed in the  $\Gamma$ -K direction by removing several entire rows air-holes and adjacent photonic crystal waveguides are separated by a row of air-holes.

### 5.2.2.1 Analysis of multimode PC line defect waveguides using self-imaging phenomenon

The mechanism of the whole device is divided into five regions according to their function; a single mode input photonic crystal waveguide (PCW), two MR, separation region (SR) between two MR and one output region, as shown in Figure 5.3 (a) and (b) respectively. In the first MR, the injected input field is propagating through the middle PCW and is identically coupled into the six and four PCLDWs at both sides (Figure 5.3(a) and (b)), and then in the separation region where the coupled power is transferred into the next MR. This region consists of one pair of 3-PCLDWs. In this region, the coupled power is propagating through the middle PCW and then transferred to the output waveguides without any cross talking from one waveguide into another at designed frequency range (in the vicinity of  $a/\lambda=0.264$ ).

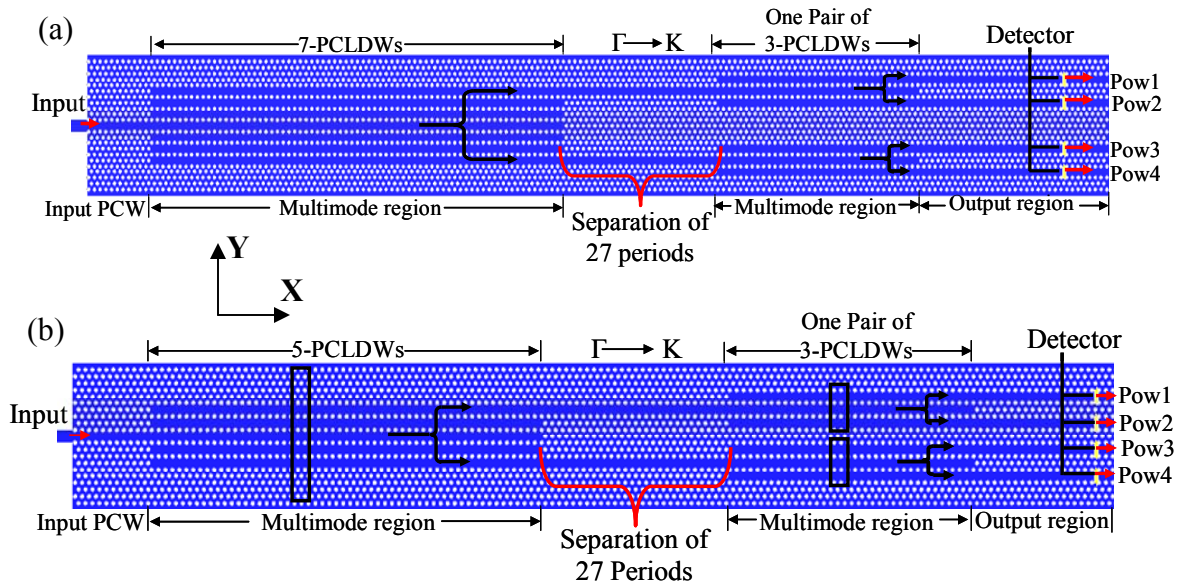


**Figure 5.3** Geometry of photonic crystal multiple line defect waveguides power-splitters: (a) Combination of seven and one pair of three PCLDWs; (b) Combination of five and one pair of three PCLDWs and setup for the FDTD method. The device is divided into five regions, as labeled at the bottom. Black boxes indicated super-cell for PWE calculation. White holes represent air-holes etched on Si ( $n_{\text{eff}}=2.847$ )

Here the length of the device depends on the multimode region's (MRs) length, since at the multimode region modes are divided and combined at periodic intervals which are directly related to the length of the device. As the proposed structures have two MRs and one SR therefore it's better to analyze these regions separately instead of taking into consideration the whole structure initially. We would be able to investigate the whole structure only after determining the length of the MRs. Therefore in this section we first analyzed the MRs with the help of the dispersion curve. This dispersion curve of the MRs is investigated by plane wave expansion (PWE) method as shown in figure 5.4. PWE computational super-cells of the MRs are depicted by black boxes in figure 5.3 (a) and (b) and enlarged view of these boxes is shown in insets of figure 5.4 (a), (b) and (c) respectively. This analysis has shown that MR supports fourteen, nine and six guided modes for 7-PCLDWs, 5-PCLDWs and 3-PCLDWs respectively at the operating frequency of  $0.264(a/\lambda)$  which is denoted by dashed lines in Figure 5.4 (a), (b), (c). These guided modes have their own symmetry with respect to the propagation axis ( $x = 0$ ) as shown in figure 5.3. All these modes in the multi-mode region PCLDWs are operated at the frequency of  $0.264(a/\lambda)$  which is excited by the input field.

The different configurations of the MR (7-PCLDWs, 5-PCLDWs and 3-PCLDWs) are transferred to the FDTD computational domain (Figure 5.5) to investigate the steady state electric field. So it helps to calculate the MR length which is the minimum distance between the input field and the folded images formed by splitted input field. According to proposed design the folded images should appear at the top and bottom of the waveguide of MR. The above mentioned MR is surrounded by twelve perfectly matched layers to absorb the outgoing waves. A continuous optical pulse is injected into the center

waveguide of each multiple line defect waveguides (MLDWG) as shown in figure 5.5. To capture the steady-state electric field distribution on the multimode region, a profile monitor is placed which is shown in figure 5.5 (a), (b) and (c) respectively.

The distribution of steady-state electric fields are obtained after sufficient steps, which is shown in figure 5.6. It is clearly seen that a single image and folded images are reproduced alternatively at constant intervals along the propagation direction in the MR. The distance between the single and folded images is called the coupling length. To calculate the coupling length, the normal mode theory and self imaging principal was employed [51, 60].

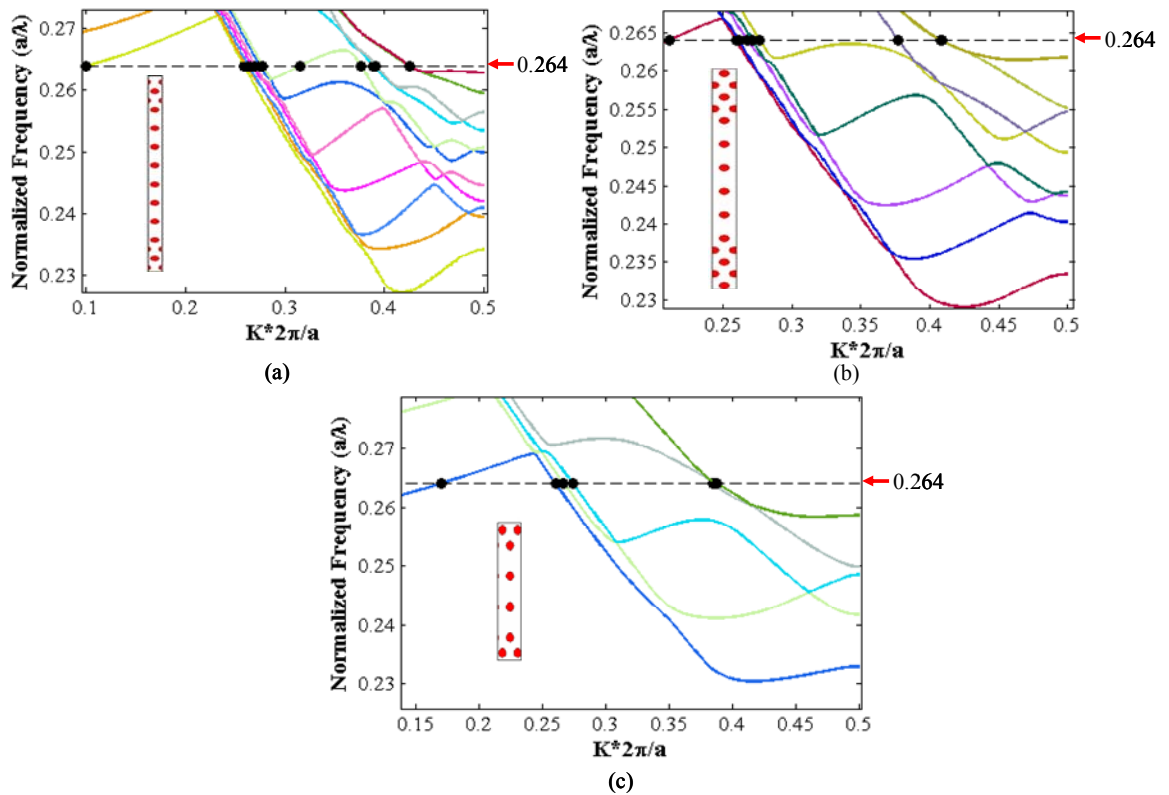


**Figure 5.4** The dispersion curves for (a) 7-PCLDWs (b) 5-PCLDWs and (c) 3-PCLDWs and computational super-cell (inset)

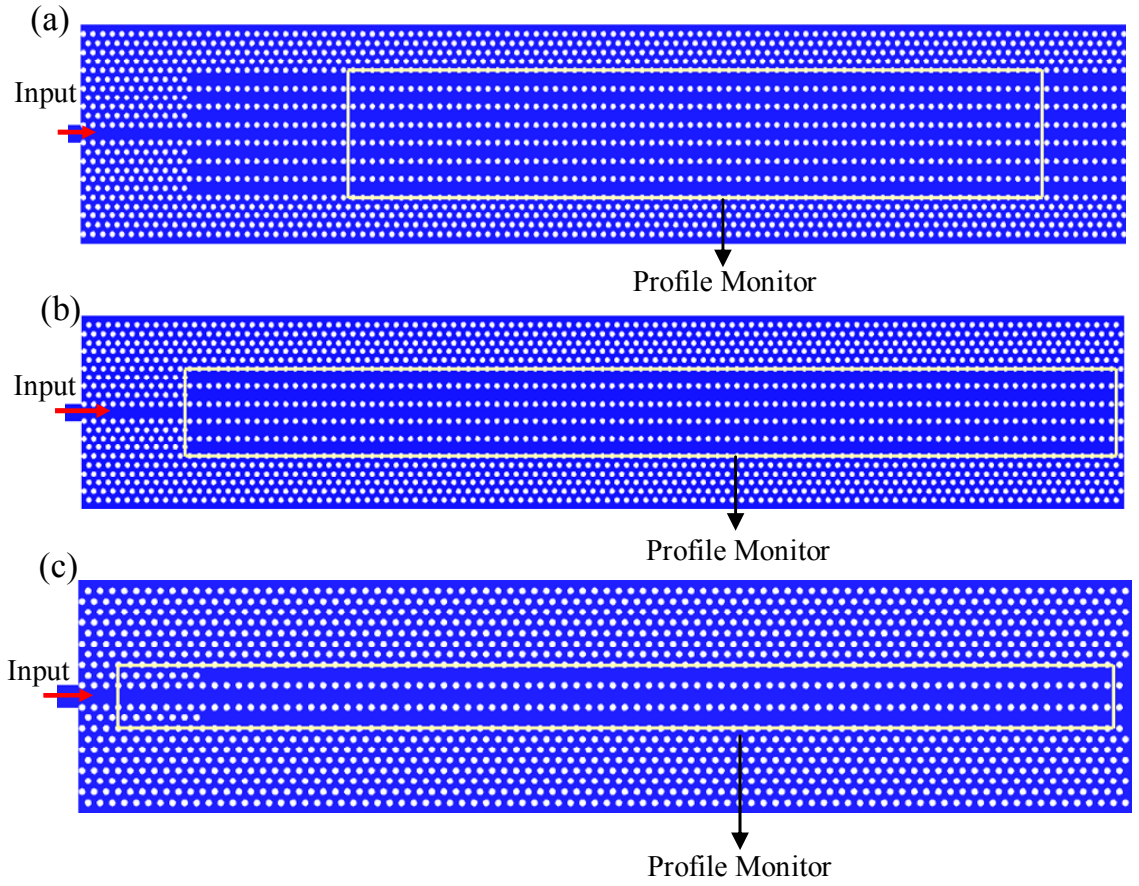


**Figure 5.5 Schematic diagrams of multiple line defect waveguides (a) 7-PCLDWs, (b) 5-PCLDWs (c) 3-PCLDWs with profile monitor on multimode region**

The total field  $\Psi(x, y)$  in the coupling region can be divided into the guided modes and expressed as:

$$\Psi(x, y) = \sum_{n=0}^{p-1} C_n \varphi_n(y) e^{-i\beta_n x} \quad (5.12)$$

Where  $C_n$  is the field excitation coefficient,  $\varphi_n(y)e^{-j\beta_n x}$  is the modal field distribution with a propagation constant  $\beta_n$ ,  $p$  is the number of modes, and the subscript  $n$  denotes the order of the mode ( $n = 0, 1, 2, \dots, p-1$ ).



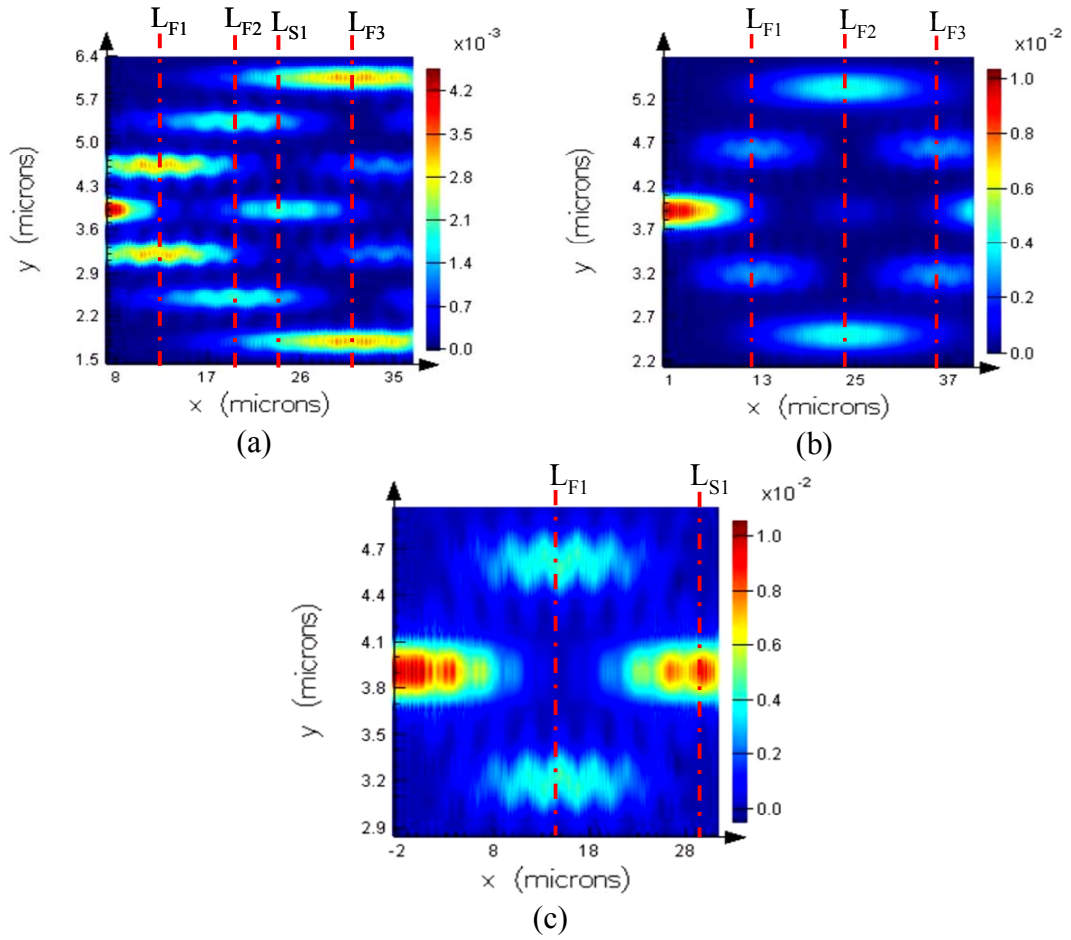


**Figure 5.6 FDTD simulated results of steady-state electric field distribution in the multi mode regions of (a) 7-PCLDWGs, (b) 5-PCLDWs and (c) 3-PCLDWGs at  $0.264(a/\lambda)$**

The total field at a distance  $L$  can be written as a superposition of all guided mode fields:

$$\begin{aligned}
 \Psi(L, y) &= \sum_{n=0}^{p-1} C_n \varphi_n(y) e^{-j\beta_n L} \\
 &= C_0 \varphi_0(y) e^{-j\beta_0 L} + C_1 \varphi_1(y) e^{-j\beta_1 L} + \\
 &C_2 \varphi_2(y) e^{-j\beta_2 L} + C_3 \varphi_3(y) e^{-j\beta_3 L} + \dots
 \end{aligned} \tag{5.13a}$$

For the simplicity, the initial phase of the input field at  $x = 0$  is assumed to be 0, therefore the input field at  $x = 0$  is

$$\begin{aligned}
\Psi(0,0) &= \sum_{n=0}^{p-1} C_n \varphi_n(0) \\
&= C_0 \varphi_0(0) + C_1 \varphi_1(0) + \\
&C_2 \varphi_2(0) + C_3 \varphi_3(0) + \dots
\end{aligned} \tag{5.13b}$$

Then term by term comparison with  $\Psi(L, y)$  is done. By comparing the phase factors between terms in equation 5.13(a) and 5.13(b), the condition for the single image, either a direct image or a mirrored image at  $x = L$  is expressed as

$$\beta_n L = K_n \pi \quad \text{for } n \text{ even, with } K_n = 1, 2, \dots \tag{5.14}$$

$$\beta_n L = (K_n - \frac{1}{2})\pi \quad \text{for } n \text{ odd; with } K_n = 1, 2, \dots \tag{5.15}$$

From equation (5.14) and (5.15) we calculated the folded images. To calculate the folded images, first step is to find out the single image at  $x = L = L_S$  and is expressed as

$$\beta_n L_S = K_n \pi \quad \text{with } K_n = 1, 2, 3, \dots \tag{5.16}$$

$L_S$  is periodical and has a constant interval of  $L_{S1}$ , therefore at  $L_{S1}$  the first single image is reproduced, so it can be written as

$$L_S = K_n L_{S1} \quad \text{with } K_n = 1, 2, 3, \dots \tag{5.17}$$

The first folded image is symmetrically located along the x-axis and can be obtained at  $x = L_{F1}$  by linear combination of symmetric modes which is excited by the input field, therefore  $L_{F1}$  can be expressed as

$$L_{F1} = \frac{L_{S1}}{2} \tag{5.18}$$

And all other folded images can also be considered as a linear combination of symmetric modes excited by the single image fields, therefore the folded images can be found at  $x = L_F$ , where  $L_F$  satisfies

$$L_F = \left(K - \frac{1}{2}\right)L_{S1} \quad \text{with } K_n = 1, 2, 3, \dots \quad (5.19)$$

So, the folded image distribution is also periodical and with the same interval as the single images. By using equation 5.16 to equation 5.19, imaging position can be described [50]. Table 1, 2 and 3 are the calculated imaging position of 7-PCLDWs, 5-PCLDWs and 3-PCLDWs respectively.

To verify the calculated length of the MR, we start terminating the middle portion of the waveguides which is depicted in figure 5.7 and simulated with 2D FDTD computation method. The output transmitted power varies with respect to the number of periods which is shown in figure 5.8. The result of maximum transmitted power at each output channel of seven, five and three PCLDWs is mentioned in the table 4. In this way we verified our calculated MR length.

**Table 5-1. Parameter used to calculate the folded images position of 7-PCLDWs at 0.264(a/λ)**

n	$K_n$	$\beta_n(2\pi/a)$	$L = 2K_n\pi/\beta_n$ for n even $(2K_n-1)\pi/\beta_n$ for n odd
0	14	0.0999	70.07a
1	37	0.2568	70.57a
2	37	0.2609	70.90a
3	37	0.2632	69.33a
4	37	0.2667	69.36a
5	38	0.2701	69.41a
6	40	0.2745	72.85a
7	40	0.2773	71.24a
8	46	0.3149	73.03a
9	56	0.3760	73.80a
10	58	0.3883	74.68a
11	58	0.3914	73.45a
12	64	0.4247	75.34a
13	64	0.4249	74.72a
Mean value of $L = 72.05a$			

**Table 5-2. Parameter used to calculate the folded images position of 5-PCLDWs at 0.264 (a/λ)**

n	$K_n$	$\beta_n(2\pi/a)$	$L= 2K_n\pi/\beta_n$ for n even $(2K_n-1)\pi/\beta_n$ for n odd
0	22	0.2106	52.23a
1	28	0.2592	53.04a
2	29	0.2612	55.51a
3	30	0.2674	55.16a
4	31	0.2713	57.13a
5	32	0.2765	56.96a
6	44	0.3773	58.30a
7	48	0.4077	58.25a
8	49	0.4085	59.97a
Mean value of $L = 56.28a$			

**Table 5-3. Parameter used to calculate the folded images position of 3-PCLDWs at 0.264(a/λ)**

n	$K_n$	$\beta_n(2\pi/a)$	$L= 2K_n\pi/\beta_n$ for n even $(2K_n-1)\pi/\beta_n$ for n odd
0	12	0.1698	35.33a
1	19	0.2601	35.56a
2	19	0.2667	35.62a
3	19	0.2737	33.79a
4	28	0.3845	36.41a
5	28	0.3875	35.48a
Mean value of $L = 35.36a$			

**Table 5-4. Multiple line defect waveguides transmitted output power**

Waveguides	Periods	Power at each O/P Channel
7-PCLDWs	72	7P1=7P2=47%
5-PCLDWs	56	5P1=5P2=48%
3-PCLDWs	35	3P1=3P2=45%

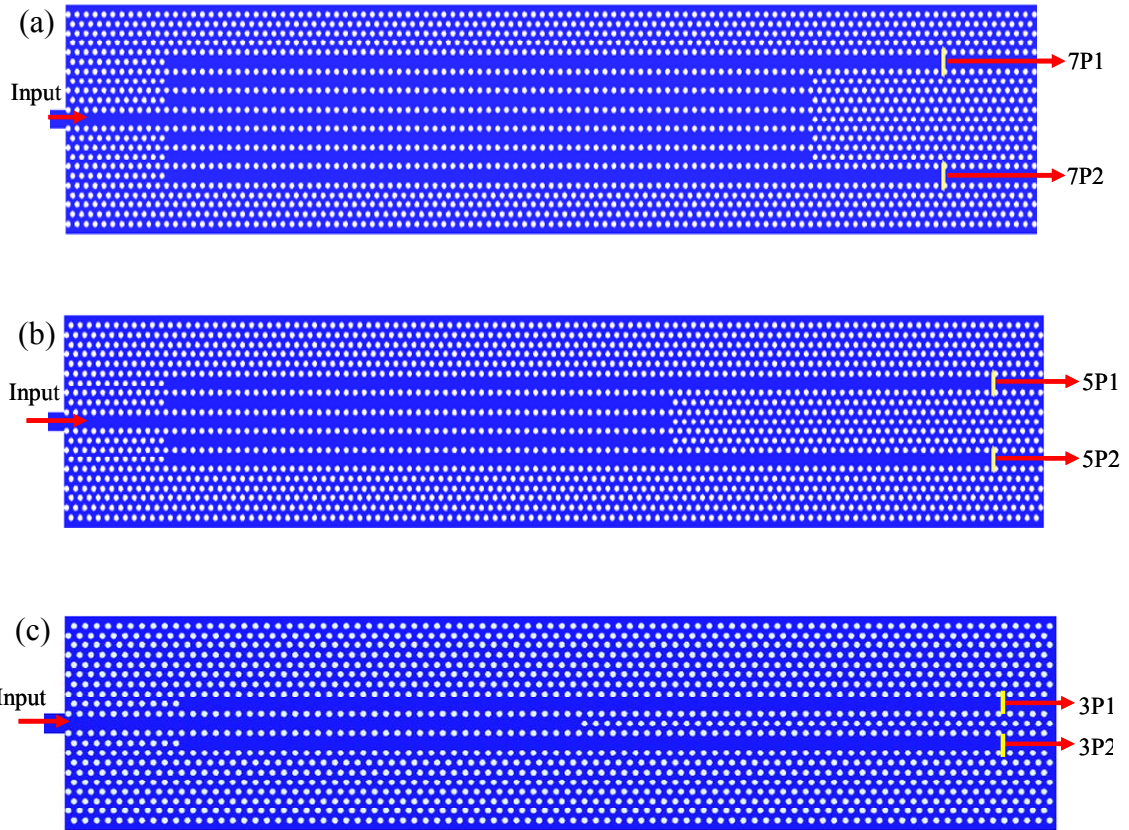


**Figure 5.7 Input waveguide divided into two output channel with MR of (a) 7-PCLDWs, (b) 5-PCLDWs and (c) 3-PCLDWs**

### 5.2.2.2 Design of power splitter structure

To achieve a  $1 \times 4$  power splitter of our proposed structure which is shown in figure 5.3, we only consider the folded images of the respective MLDWGs which are analyzed in the previous section. These MLDWGs are integrated together to achieve our desired splitter which we have proposed. In both the  $1 \times 4$  power splitters, the outputs PCWs are indicated by Pow1, Pow2, Pow3 and Pow4 respectively. In these proposed devices, first input beam is divided into 2 output channels with MR of length  $29.52\mu\text{m}$  ( $72 \cdot a$ ) and  $22.96\mu\text{m}$  ( $56 \cdot a$ ) of 7-PCLDWs and 5-PCLDWs respectively. These output channels are considered as an input to next stage i.e. one pair of 3PCLDWs. At this stage the input

beams are divided into 4 output channels with MR length of  $14.35\mu\text{m}$  (35a) of one pair of 3-PCLDWs respectively. After integration, the whole device is simulated by 2D FDTD computational method to determine the length of the separation region which is placed between two MRs. The computational domain of the whole structure is surrounded by twelve perfectly matched layers to absorb the outgoing waves. A continuous optical pulse is injected into the middle waveguide as shown in figure 5.9 (a) and (b).

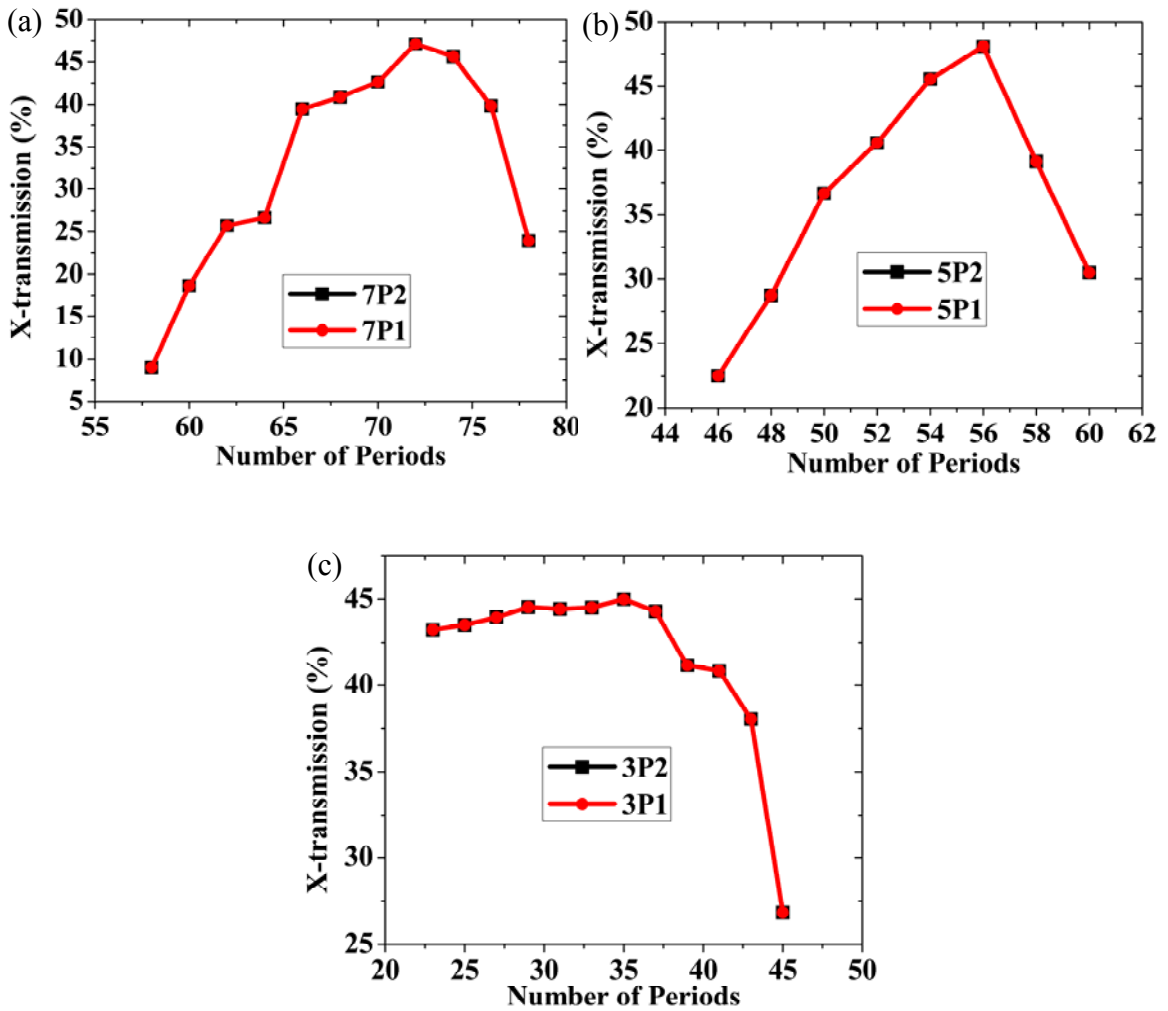


**Figure 5.8** Transmitted output power of MRs after FDTD computation as a function of the number of periods: between 58 period to 78 period (a) in 7-PCLDWs , between 46 period to 60 period (b) in 5-PCLDWs, between 23 period to 45 period in (c) 3-PCLDWs

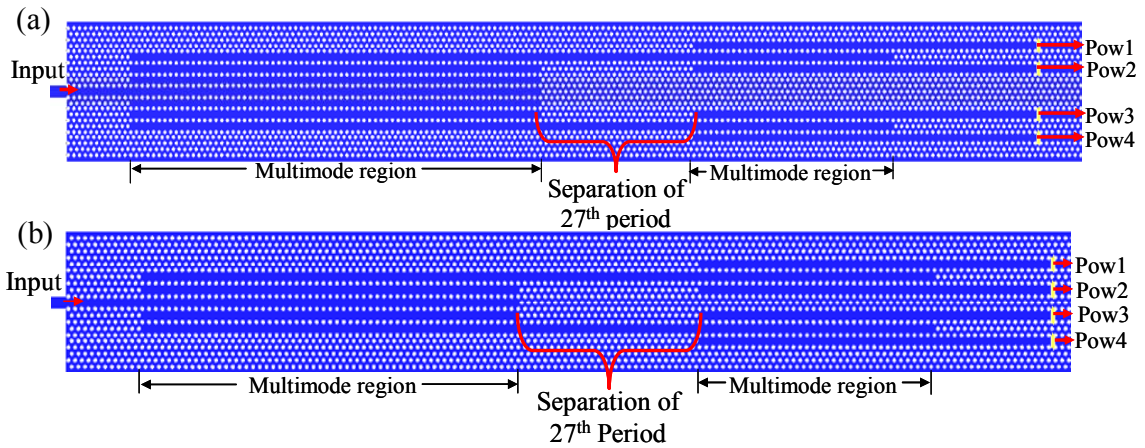


**Figure 5.9** Schematic diagram of two 1×4 power PC power splitter with same separation region; (a) combination of seven and one pair of three PCLDWs;(b) combination of five and one pair of three PCLDWs

### 5.2.2.3 Determination of separation region

To determine the SR, we calculated the transmitted output power with respect to input at variable periods of SR while value of 7-PCLDWs of MR is  $72*a$  and one pair of 3-PCLDWs of MR is  $35*a$  whereas the value of 5-PCLDWs of MR is  $56*a$  and one pair of 3PCLDWs of MR is  $35*a$ . It is found that at 27<sup>th</sup> period of SR the output power is maximized and it is almost equally splitted in each channel as shown in figure 5.10(a) and (b).

**Table 5-5. Transmitted output power of the devices**

Devices transmitted	Output power at each channel
1. Combination of seven and one pair of three line defect waveguides.	Pow1=Pow4=22.6%; Pow2=Pow3=22.9%
2. Combination of five and one pair of three line defect waveguides.	Pow1=Pow4=23.9%; Pow2=Pow3=23.5%

In order to reconfirm the position of period of SR at which maximum output power is achieved, we measured the output power with variable periods of one pair of 3-PCLDWs while periods of MR of 7-PCLDWs, 5-PCLDWs and period of SR are fixed. It is observed that at 35<sup>th</sup> period of one pair of 3-PCLDWs, the output power is maximized (Figure 5.11) for both of the devices and it is similar to the previous result when seven, five and one pair of three line defect waveguides periods and fixed and only period (i.e. from 25 to 30) of separation region is varied. The result of the transmitted output power at each channel of both of the devices is shown in table 5. Therefore, the total output transmitted power of first device is 91.1% and second device is 94.9% at target wavelength of 1.55 $\mu$ m. In addition more than 11% power is achieved at each output channel of the first structure in the frequency range of 1.547 $\mu$ m-1.557 $\mu$ m (with bandwidth about 10nm) whereas second structure transmit more than 15.8% power at each output channel in the frequency range of 1.538 $\mu$ m-1.569 $\mu$ m (with bandwidth about 31nm), indicated by blue dash line in figure 5.12. Thus the proposed structures are well suited for equal power splitting technique.



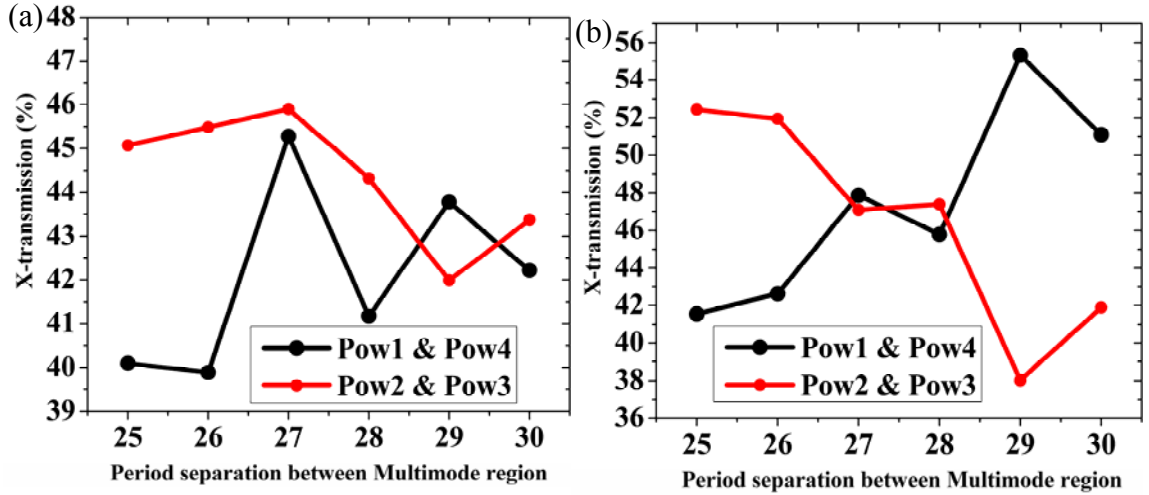


Figure 5.10 Transmitted power at the output channels with variable separation region; (a) 1x4 splitter denotes combination of 7-PCLDWs and one pair of 3-PCLDWs; (b) 1x4 splitter denotes combination of 5-PCLDWs and one pair of 3-PCLDWs

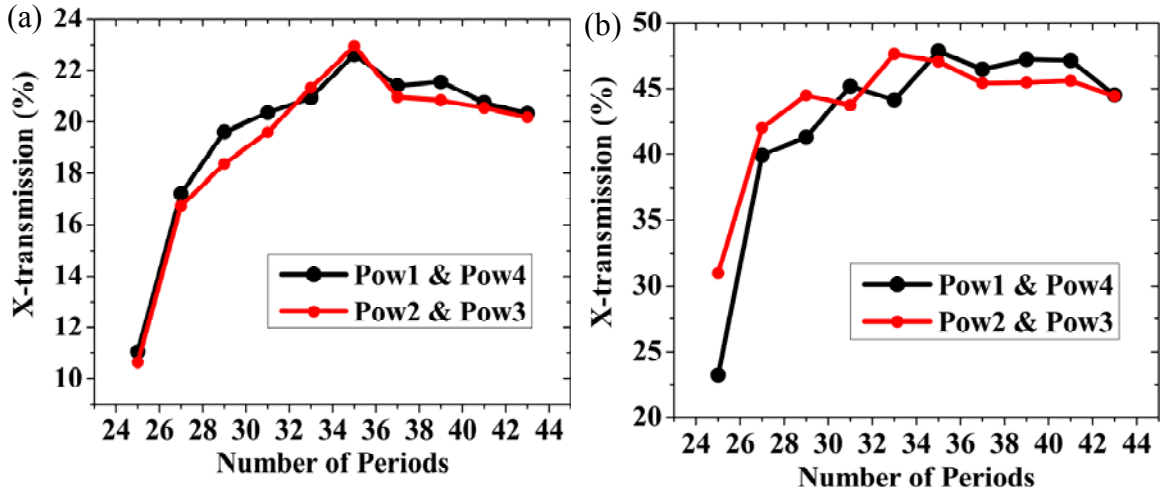
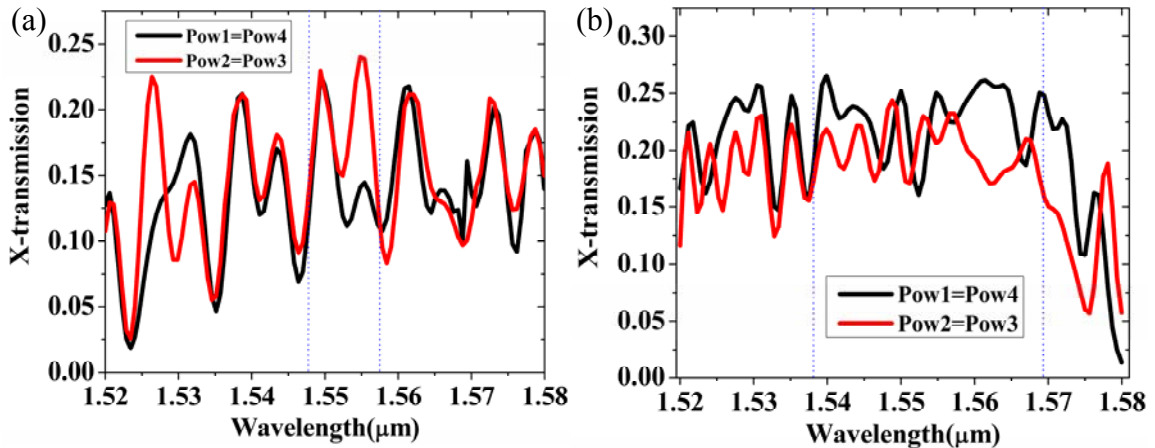


Figure 5.11 Normalized output power of all the output ports with variable one pair of 3-PCLDWs of the proposed splitters: (a) 1x4 splitter when 7-PCLDWs and SR period is fixed; (b) 1x4 splitter when 5-PCLDWs and SR period fixed

### 5.2.2.4 Merits and demerits of the multiple line defect waveguides structure

From all the output power distribution, it is clearly observed that equal power splitting technique depends on the number of periods in two MR which means coupling length and

number of periods in SR. This SR region plays an important role in this power splitting technique. Due to SR, the power is redistributed at the output region with uniform power at each output channel. The whole structure of the device is identical and also it does not have any  $120^\circ$  junction as well as  $60^\circ$  bend output waveguide so that the single mode operation does not suffer. The entire structure of the design is formed by triangular lattice of dielectric holes. Therefore, the proposed design is feasible to be transferred to a 2D slab photonic crystal; so the vertical confinement will be better as compared to the triangular lattice of dielectric rod structure. From the fabrication aspect it will be easier to fabricate on the slab structure as compared to Y-junction and T-junction splitter. The length of the device is somewhat larger when compared to the ultracompact multiway beam splitters and directional coupling based power level splitter, which is one drawback. The advantage is that the design is simple and there is no need to modify the MR holes size to get equal splitting of power at the output.



**Figure 5.12** Normalized output power after 2D FDTD computation of (a) combination of seven and one pair of three PCLDWs; (b) combination of five and one pair of three PCLDWs

A novel technique, using the  $1 \times 4$  power splitter based on multiple line defect photonic crystal waveguides, is investigated in this section. The input field is equally

divided into four output channels. This equal distribution of power is possible due to the length of two multimode regions and the length of the separation region. The transmitted power of first device is 91.1% and for the second is 94.9%. Due to high power transmission in 2-D configuration of PC we try to implement same technique into 2-D slab PC configuration. So, in next section we explain how to design the multiple line defect waveguides into 2-D slab PC for power splitting application.

## **5.3 Modeling of Multiple Line Defect Waveguides for 1×3 Power Splitter**

So far we have investigated multiple line defect waveguides configuration with triangular lattice of air holes on 2-D PC. In this section we extended our analysis of multiple line defect waveguides on 2-D slab PC configuration (Figure 5.13 (a)). The methodology of this power splitting technique is similar to the 2-D based multiple LDWs based power splitting scheme but there is some differences. In this scheme power is divided into 1 to 3 ways which involves 3-PCLDWs MR, 5-PCLDWs MR and one SR. Before considering the whole structure for simulation, it is better to choose all parts individually. The whole structure is investigated by FDTD method.

### **5.3.1 3-D FDTD simulation parameter**

From 3-D FDTD simulation, the time domain electromagnetic field is obtained. The whole structure is simulated by a mode source located on the conventional waveguide which is launched by the waveguide mode. Figure 5.13 (b) shows the structure built in the FDTD simulations. The center part of the multiple line defect waveguides of PC slab is connected with conventional waveguide. The design of 2-D slab PC multiple line

defect waveguides is created in the simulation region. In order to excite the waveguide mode, perfectly matched layer (PML) boundaries are used according to the mode symmetry of the waveguide mode. These boundaries help to reduce the simulation region by half without any loss of accuracy. Three power monitors are placed on the output channel of the waveguides in order to record the transmission of power.

In order to obtain convergent simulation results and to reduce the numerical dispersion, a fine mesh is critical. In our study, the grid size  $d$  is chosen such that  $d < \frac{\lambda}{20n}$ , where  $\lambda$  is the minimum wavelength of the source spectrum and  $n$  is the refractive index of the slab. This mesh configuration ensures the convergence and high accuracy of the simulations. The stability factor  $S$  is defined as  $S = \frac{c\Delta t}{d}$ , where  $c$  is the speed of light in vacuum and  $\Delta t$  is the time step. In this simulation,  $S$  is set to be equal to 0.99, satisfying the stability condition of the 3-D FDTD simulations.

### **5.3.2 Design of multiple line defect waveguides on 2-D PC slab**

In order to obtain a photonic band structure with a wide spectrum and high transmission, the lattice constant, hole size and the height of the slab were adjusted through a series of simulations. The parameters of the 2-D planar PC are tuned to lattice constant  $a = 400\text{nm}$ , radius of the air holes  $r = 0.25*a$ , height of the slab  $h = 300\text{nm}$  is shown in Figure 5.13 (a). The dielectric air holes are etched into the slab with a refractive index of silicon. In this structure, the lattice has a photonic bandgap with the normalized frequency  $(a/\lambda)$  ranging from 0.24006 to 0.28242, where  $\lambda$  is the wavelength in free space. While designing the proposed structure, the multiple photonic crystal line defect waveguides (PCLDWs) is formed in the  $\Gamma$ -K direction by removing several entire rows air holes and

adjacent photonic crystal waveguides are separated by a row of air-holes. The splitting mechanism is similar to what has been described in section 5.2.2.1 but only difference is device configuration. In order to that first MR consist of 3-PCLDWs, second MR build with 5-PCLDWs and both MRs separated by 9 periods and the output region consist of three PCW that helps to divide the equal amount of power into their respective output PCWs i.e. CH1, CH2, and CH3 (Figure 5.13a). The innovative part in this device is the splitting technique which is without any changes in holes size in both MRs. According to our best knowledge, such a PC multiple line defect waveguides based  $1 \times 3$  power splitter in 2-D slab configuration has not been investigated yet.

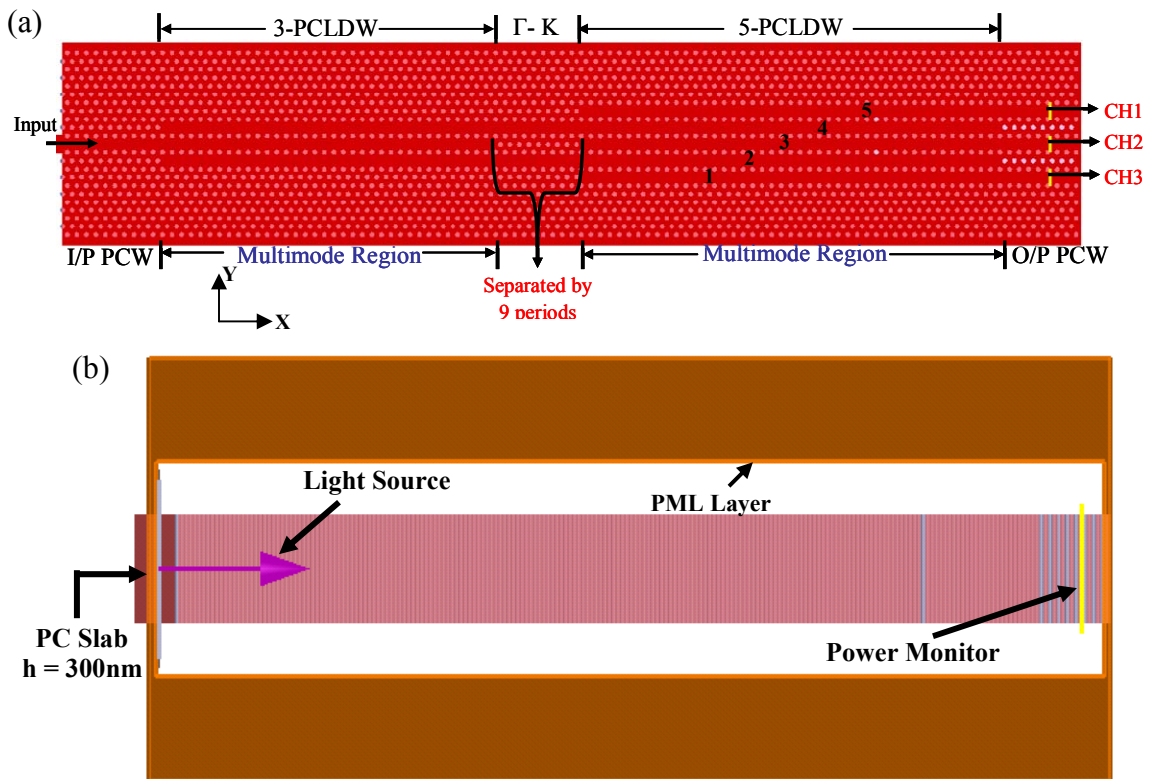


**Figure 5.13 (a) Schematic diagram of power splitter based on 2-D slab PC multiple line defect waveguides. It is a combination of three and five PCLDWs. (b) Design figure in FDTD simulation**

### 5.3.2.1 Methodology of 1×3 power splitting technique

The mechanism of this power splitting technique is similar to the 2-D based multiple LDWs based power splitter scheme but there is some difference. In this scheme the whole device is divided into five regions which are input PCW, two MR, SR and one output region, as shown in figure 5.13 (a). The first MR region consists of 3-LDWs and second MR is consist of 5-LDWs. The two MR is separated by 9 periods. In the first MR, the injected input field is propagating through the middle PCW and is identically coupled into the top and bottom of the PCLDWs, and then in the SR where the coupled power is transferred into the next MR. This region consists of 5-PCLDWs and coupled power is transmitted through the second and fourth PCLDWs and then transferred to the output channels without any cross talking from one waveguide into another at the designed frequency range (in the vicinity of  $a/\lambda = 0.258$ ).

Here the length of the device depends on the multimode region's (MRs) length, since at the multimode region modes are divided at periodic intervals which are directly related to the length of the device. As the structure has two MRs and one SR therefore it's better to analyze these regions separately instead of taking into consideration the whole structure initially. We would be able to investigate the whole structure only after determining the length of the MRs. Therefore, in this section, we first analyzed the MRs with the help of the dispersion curve. This dispersion curve of the MRs is investigated by plane wave expansion (PWE) method as shown in figure 5.14. This analysis has shown that MR supports six and nine guided modes for 3-PCLDWs and 5-PCLDWs respectively at the operating frequency of  $0.258(a/\lambda)$  which is denoted by dashed lines in figure 5.14 (a), (b). These guided modes have their own symmetry with respect to the propagation

axis ( $x = 0$ ) as shown in figure 5.13 (a). All these modes in the multi-mode region PCLDWs are operated at the frequency of  $0.258(a/\lambda)$  which is excited by the input field.

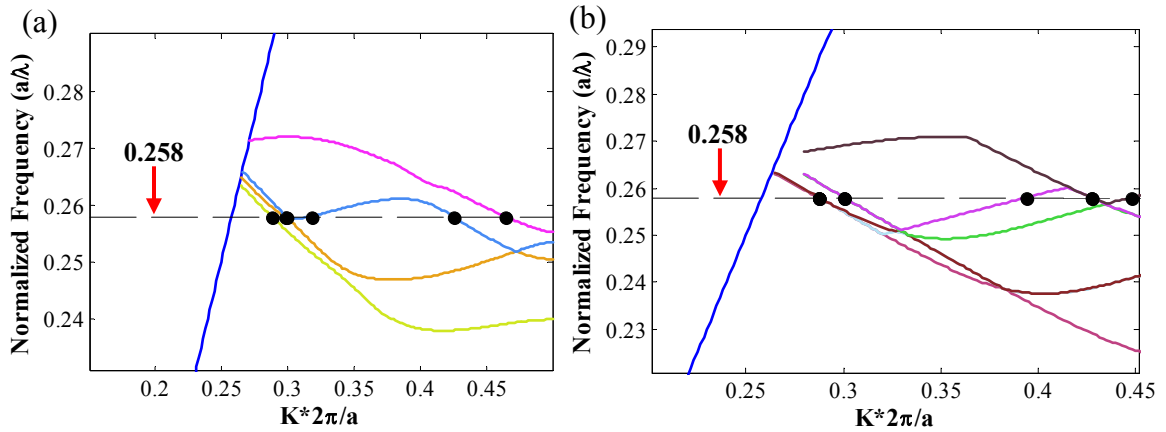


**Figure 5.14** The dispersion curves for (a) 3-PCLDWs and (b) 5-PCLDWs

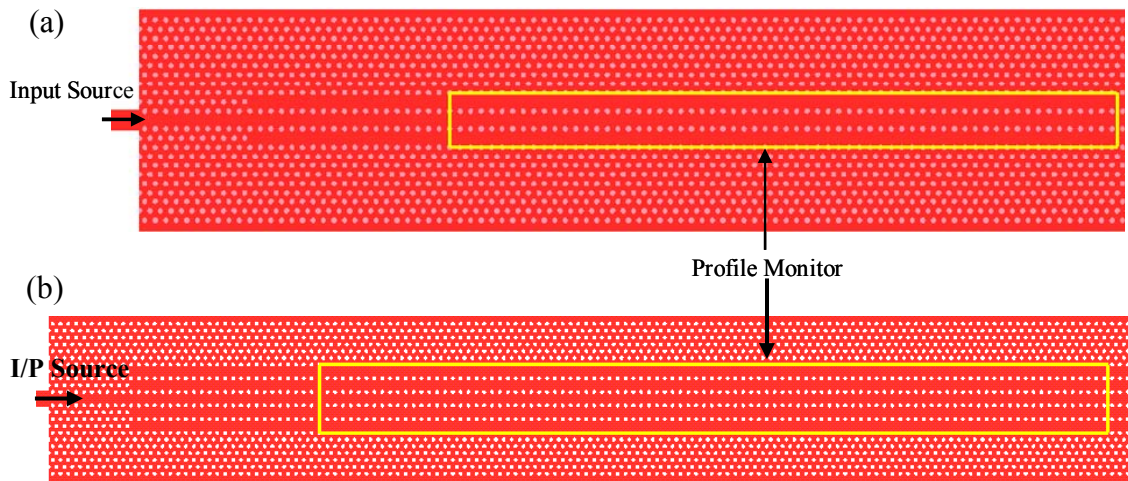


**Figure 5.15** Schematic diagrams of multiple line defect waveguides (a) 3-PCLDWs, (b) 5-PCLDWs with profile monitor on multimode region

To find the field distribution, the MR (3-PCLDWs and 5-PCLDWs) waveguides are transferred to the 3-D FDTD computational domain (Figure 5.15 (a) and (b)). So from this investigation it helps to calculate the length of the MR. This length is the minimum distance between the input field and the folded images formed by splitted input field. According to proposed design the folded images should appear at the top and bottom of

the waveguide of MR. The simulation region of MR is surrounded by twelve PML which offers minimal reflection into the simulation region. A continuous optical pulse is injected into the center waveguide of each multiple line defect waveguides (MLDWG) as shown in figure 5.15. To capture the steady-state field distribution on the multimode region, a profile monitor is placed which is shown in figure 5.15 (a) and (b) respectively.

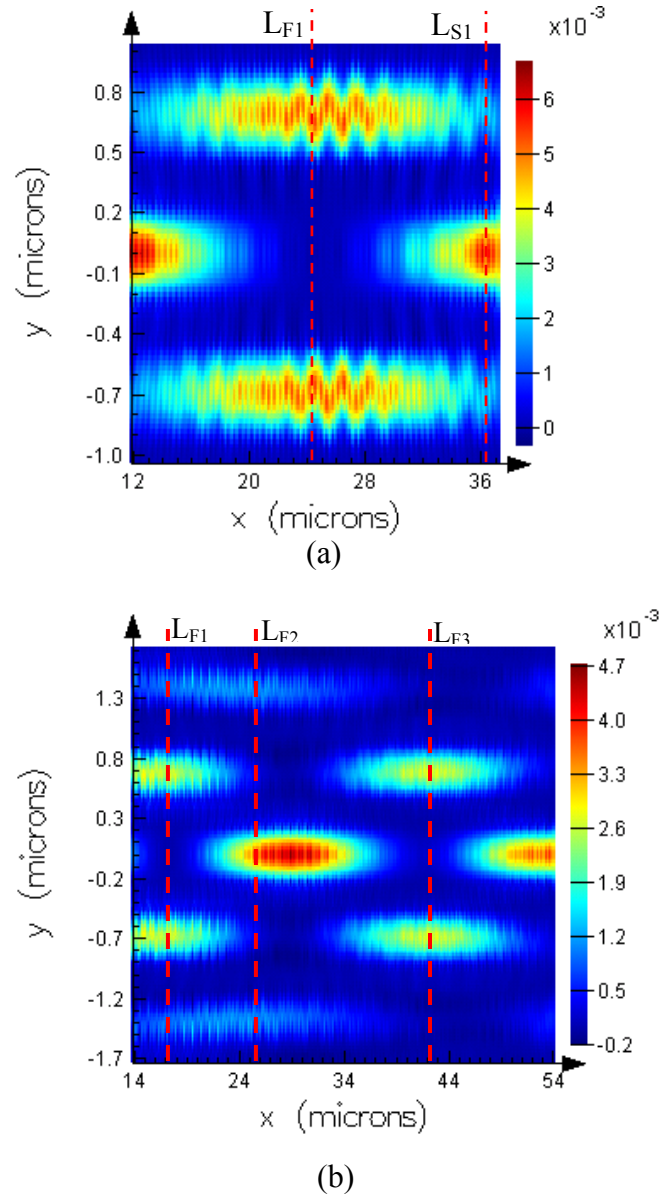


**Figure 5.16 FDTD simulated results of steady-state electric field distribution in the multi mode regions of (a) 3-PCLDWs and (b) 5-PCLDWs at  $0.258 (a/\lambda)$**



The distribution of steady-state electric fields are obtained after sufficient steps, which is shown in figure 5.15. It is clearly seen that a single image and folded images are reproduced alternatively at constant intervals along the propagation direction in the MR. The distance between the single and folded images is called the coupling length. The normal mode theory and self imaging principal is employed to calculate the coupling length [51, 60]. By using equation 5.16 to equation 5.19 imaging position can be described [50]. Table 5-6 and 5-7 are the calculated imaging position of 3-PCLDWs and 5-PCLDWs respectively.

**Table 5-6. Parameter used to calculate the folded images of 3-PCLDWs at 0.258(a/λ)**

n	$K_n$	$\beta_n(2\pi/a)$	$L= 2K_n\pi/\beta_n$ $(2K_n-1)\pi/\beta_n$	for n even for n odd
0	11	0.2883	38.15a	
1	12	0.2985	38.52a	
2	13	0.2994	43.42a	
3	14	0.3178	42.47a	
4	19	0.4251	44.69a	
5	21	0.4644	44.14a	
Mean value of $L= 41.89a$				

**Table 5-7. Parameter used to calculate the folded images of 5-PCLDWs at 0.258(a/λ)**

n	$K_n$	$\beta_n(2\pi/a)$	$L= 2K_n\pi/\beta_n$ $(2K_n-1)\pi/\beta_n$	for n even for n odd
0	12	0.2871	41.79a	
1	12	0.2876	39.98a	
2	12	0.2877	41.71a	
3	13	0.3004	41.61a	
4	13	0.3004	43.27a	
5	18	0.3937	44.45a	
6	20	0.4272	46.81a	
7	21	0.4274	47.96a	
8	22	0.4476	49.15a	
Mean value of $L= 44.08a$				

To verify the calculated length of the MR, we start terminating the middle portion of the waveguides which is depicted in Figure 5.17 and simulated with 3-D FDTD

computation method. The output transmitted power varies with respect to the number of periods which is shown in Figure 5.18. The result of maximum transmitted power at each output channel of three and five PCLDWs is mentioned in the table 5-8.

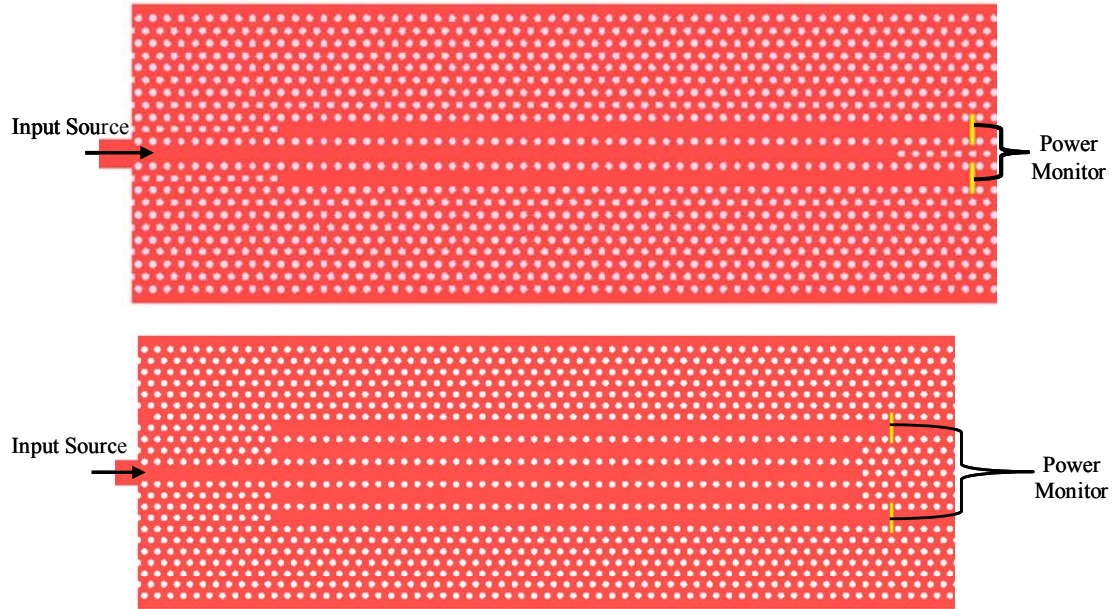


Figure 5.17 Input waveguide is divided into output channel with the help of MRs of (a) 3-PCLDWs and (b) 5-PCLDWs

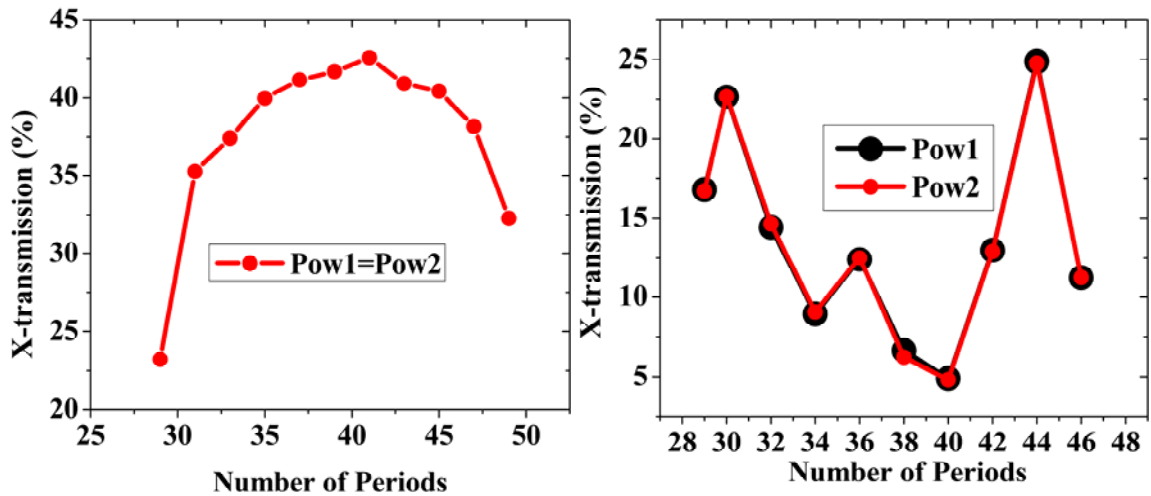


Figure 5.18 Transmitted output power of MRs after the FDTD computation as function of the number of periods: between 29 periods to 45 periods (a) 3-PCLDWs, between 29 periods to 46 period (b) 5-PCLDWs

**Table 5-8. Multiple line defect waveguides transmitted output power**

Waveguides	Periods	Power at each O/P Channel
3-PCLDWs	41	Pow1=Pow2 = 42.5%
5-PCLDWs	44	Pow1= 24.9%, Pow2 = 24.7%

### 5.3.2.2 Analysis of 1×3 power splitter design

To achieve a 1×3 power splitter of our proposed structure which is shown in figure 5.13 (a), we only consider the folded images of the respective MLDWGs which are investigated in the previous section. These MLDWGs are integrated together to achieve our desired splitter which we have proposed. In both of the 1×4 power splitters, the outputs PCWs are indicated by CH1, CH2 and CH3 respectively. In these proposed devices, first input beam is divided into 2 output channels with MR of length  $16.4\mu\text{m}$  ( $41*a$ ) of 3-PCLDWs. These output channels are considered as an input to next stage i.e. 5-PCLDWs. At this stage the input beams are divided into 3 output channels with MR length of  $17.6\mu\text{m}$  ( $44*a$ ) of 5-PCLDWs. After integration, the whole device is simulated by 3-D FDTD computational method to determine the length of the separation region which is placed between two MRs. This separation region is very important to divide the power equally at each output channel. The computational domain of the whole structure is surrounded by twelve perfectly matched layers to absorb the outgoing waves. A continuous optical pulse is injected into the middle waveguide as shown in figure 5.13(a).

To determine the SR, we calculated the transmitted output power with respect to input at variable periods of SR while value of 3-PCLDWs of MR is  $41*a$  and 5-PCLDWs of MR is  $44*a$ . It is found that at the 9<sup>th</sup> period of SR the output power is almost equally divided in each channel as shown in figure 5.18(a). In order to reconfirm the position of period of SR at which maximum output power is achieved, we measured the output

power with variable periods of one pair of 5-PCLDWs while periods of MR of 3-PCLDWs and period of SR are fixed. It is observed that at 44<sup>th</sup> period of 5-PCLDWs, the output power is maximized (figure 5.18(b)) and it is similar to the previous result when three and five line defect waveguides periods are fixed and only period (i.e. from 0 to 13) of separation region is varied. The result of the transmitted output power at each channel is depicted in table 10. Therefore the total output transmitted power of 1×3 splitter is 72.8% at target wavelength of 1.55μm. In addition more than 16.4% power is achieved at each output channel in the frequency range of 1.546μm-1.556μm (with bandwidth about 10nm), indicated by blue dash line in figure 5.20. Therefore 1×3 power splitter structure is well suited for equal power splitting technique.

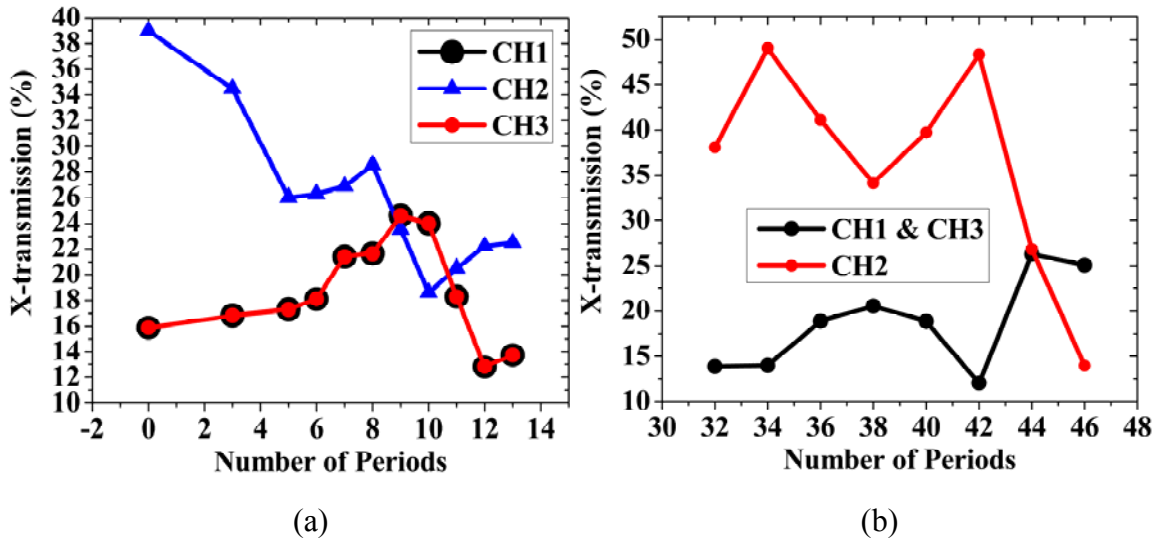
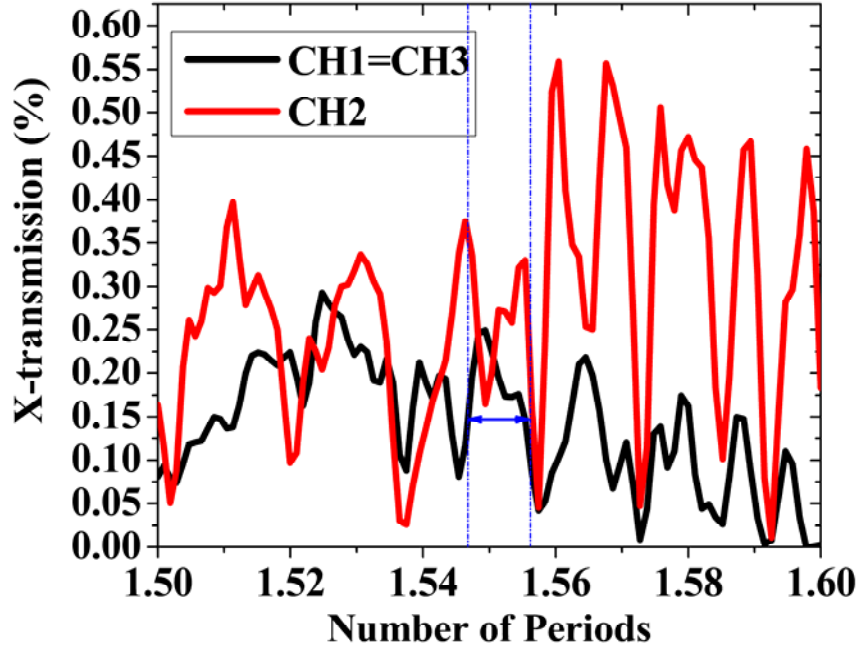


Figure 5.19 (a) Transmitted power at the output channels with variable separation region of 1×3 splitter combination of 3-PCLDWs and 5-PCLDWs; (b) Normalized output power of all the output channel with variable periods of 5-PCLDWs of 1×3 splitter

**Table 5-9. Transmitted output power of 1×3 splitter**

Output Port	Output Power
CH1	24.6%
CH2	23.5%
CH3	24.6%



**Figure 5.20 Normalized output power after 3-D FDTD computation of combination of three and five PCLDWs with a separation region of 9<sup>th</sup> periods**

### **5.3.2.3 Advantage and disadvantage of multiple line defect waveguides structure**

Distribution of equal power depends on the number of periods in two MRs which means the coupling length and the number of periods in SR. It is lucidly observed from all the output power distribution. The SR plays an important role in this power splitting scheme. Due to SR, the power is redistributed at the output region with uniform power at each output channel. The whole structure is identical and also it does not have any 120<sup>0</sup> junction as well as 60<sup>0</sup> bend output waveguide so that single mode operation is not affected. As far as the fabrication is concerned, it will be easier to fabricate on the slab structure as compared to Y-junction and T-junction splitter. The length of the device is

somewhat larger when compared to the ultracompact multiway beam splitter and Y-junction based power splitter. This is considered as one of the drawbacks. However the positive side of the structure is that it is designed simply and there is no need to modify the holes in MRs to achieve the equal power at each output channel.

A novel technique based on multiple line defect PC waveguides, is investigated by using  $1 \times 3$  power splitter. This equal distribution of power is possible due to the optimized length of both of the two multimode regions and separation region. The total transmitted power is 72.8%. So, in next chapter we will compare all our proposed power splitting result.

## **Summery**

$1 \times 4$  power splitter based on 2D PC multiple line defect waveguides transmitted equal amount of power at each output channel. This design does not contain any junction, bending waveguide and defect holes. So this design can potentially be implement on a 2-D slab PC. The design of  $1 \times 4$  power splitter on 2-D slab presented still. It has vertical loss and the mode is not well coupled from one waveguide to another. However the  $1 \times 3$  splitter investigated on 2-D slab PC has equal splitting at each channel. The spectrum however is narrower.

Each design has some merit and demerits. The next chapter compares the designs presented in more detail.

# Chapter 6

## Analysis and Comparison of Different Power Splitter Configuration

In this thesis we have designed four different types of PC based power splitter which are the Y-junction based power splitter, 2-D and 2-D slab PCLDWs integrated with MMI block for  $1 \times 4$  power splitter,  $1 \times 4$  power splitter based on 2-D PC multiple line defect waveguides (multiple LDWs based on 5 & 7 and cascaded with one pair of 3-LDWs) and  $1 \times 3$  power splitter based on 2-D slab PC multiple LDWs (combination of 3-PCLDWs and 5-PCLDWs). We have investigated the power transmission and the bandwidth with the help of FDTD computational method. Here in this chapter we have analyzed and compared the advantages and disadvantages of each design and also compared with the results of published literatures.

We have found two literatures to be well suited for comparing with our proposed design. The results obtained by R. Wilson et al [61] and T. Yu et al [6] are used as benchmarks to analyze this thesis' work.

## 6.1 Comparison of 1×2 Power Splitter on 2-D Slab Photonic Crystal Configuration

**Table 6.1 Comparison between Y-junction based power splitter and literature benchmark**

<b>Parameter</b>	<b>Y-junction based 1×2 power splitter</b>	<b>Efficient PC Y-junction [61]</b>
<b>Configuration</b>	Holes with triangular lattice etched into a dielectric slab	Holes with triangular lattice etched into a dielectric slab
<b>Power Transmission</b>	84.4%	80%
<b>Equal Splitting</b>	Each channel achieved 42.2% of input power	Each channel achieved 40% of input power
<b>Device Size</b>	Length 10.2μm and width 12.7μm	Length 10μm and width 10μm
<b>Spectrum</b>	42nm broad	40nm broad

From the above table it is clearly understood that power transmission of investigated design is more than the literature and also the output spectrum. The maximum power transmission is possible due to the optimization of 120° junction and 60° bend. The new design of 1×2 Y-junction based power splitter solved the bending loss and mode mismatch problem.



## 6.2 Comparison of 1×4 Power Splitter on 2-D Photonic Crystal Configuration

Table 6.2 Comparison between proposed designs with literature benchmark

Parameter	2-D PC line defect waveguides integrated with MMI block 1×4 power splitter	1×4 power splitter based on 2-D PC multiple LDWs (multiple LDWs based on 5 & 7 and cascaded with one pair of 3 LDWs)	Ultracompact multiway beam splitters using multiple coupled PCW [5]
<b>Configuration</b>	Holes with triangular lattice etched into a dielectric slab	Holes with triangular lattice etched into a dielectric slab	Rods with triangular lattice etched into a dielectric slab
<b>Power Transmission</b>	77.3%	94.9% (combination of 5 and one pair of 3 LDWs) and 91.1% (combination of 7 and one pair of 3LDWs)	94.8%
<b>Equal Splitting</b>	Each channel achieved 19.2% of input power	Combination of 5 and one pair of 3 LDWs for 1×4 splitter; each channel achieved 23.5% of input power and Combination of 7 and one pair of 3 LDWs for 1×4 splitter; each channel achieved 22.6% of input power.	Each channel achieved 23.7% of input power by changing the radius of the rod i.e. $R_M = 0.143a$
<b>Device Size</b>	Length 102.3 $\mu\text{m}$ and width 14.2 $\mu\text{m}$	48.3 $\mu\text{m}$ for combination of five and one pair of three line defect waveguides and 54.94 $\mu\text{m}$ for combination of seven and one pair of three line defect waveguides	Length= 6.82 $\mu\text{m}$
<b>Spectrum</b>	45nm broad	32nm broad for combination of five and one pair of three line defect waveguide and 10nm broad for seven and one pair of three line defect waveguides	8nm broad

**Note:** Rod in air approach does not provide vertical confinement and it is very difficult to implement as a practical device.

Table 6.2 shows the comparison between investigated designs with published literature result. From the above table it is clearly understood that combination of multiple line defect waveguides (i.e. combination of 5 and one pair of 3 LDWs) of 1×4 power splitter transmits maximum amount of power i.e. 94.9%. The device is larger than the designs investigated in the literature. The entire design is based on hole with triangular lattice structure. As a result, it is feasible to be transferred into 2-D slab configuration where as the design of literature is based on rod with triangular lattice structure. So, it lacks vertical confinement and is very difficult to implement in 2-D slab PC configuration. The other investigated structure which is based on 2-D PC line defect waveguides integrated with MMI has broad output spectrum (i.e. 45nm) but it transmits less amount of power which is 77.3%. In this structure the PC configuration is hole with triangular lattice so it is also feasible to be transferred into a 2-D slab configuration.

### 6.3 Comparison of 1×4 Power Splitter on 2-D Slab Photonic Crystal Configuration

**Table 6.3 Comparison between two proposed designs**

<b>Parameter</b>	<b>2-D slab PC LDWs integrated with MMI block for 1×4 power splitter</b>	<b>Y-junction based 1×4 power splitter</b>
<b>Configuration</b>	Holes with triangular lattice etched into a dielectric slab	Holes with triangular lattice etched into a dielectric slab
<b>Power Transmission</b>	75.7%.	58.3%.
<b>Equal Splitting</b>	each channel achieved 18.9% of input power	Power is not equally divided
<b>Device Size</b>	Length 64.4μm and width 11.08μm	Length 16.2μm and width 14.2μm
<b>Spectrum</b>	46nm broad	5nm broad

The above table shows the result of investigated 1×4 power splitter design. From this result it is clearly understood that 2-D slab PC LDWs integrated with MMI block transmits more power as compared to Y-junction based 1×4 power splitter. Though the MMI based power splitter is a little bit larger than Y-junction based design, yet from the design point of view, it is less complicated. This design does not have 120° junction and 60° bend. Therefore, splitter does not face any mode mismatch and bending loss problem.

# Chapter 7

## Conclusion and Suggestions for Future Work

The goal of this thesis is to analyze the power distribution characteristic of the different types of power splitter configuration which is formed in 2-D and 2-D slab photonic crystals. To achieve the equal power at each output channel all configurations are optimized by 2-D and 3-D FDTD computational method. Photonic crystal based power splitter can be used in wide application area such as on-chip optical interconnect, data control in high speed optical communication link and also beam formation in Phased Antenna Array (PAA). This chapter summarizes the work presented in this thesis and the future work will follow to successfully implement some of the applications mentioned.

### 7.1 Summary

Y-junction based  $1 \times 2$  and  $1 \times 4$  power splitter formed in 2-D slab PC is analyzed primarily by using 3-D FDTD computational method.  $120^\circ$  junction and  $60^\circ$  bend are optimized for obtaining maximum power transmission in  $1 \times 2$  Y-junction based power splitter. As a consequence, 84.4% of input power is transmitted with 42nm broad spectrum. Therefore, optimized fundamental unit of Y-junction is further used for dividing the power in  $1 \times 4$  ways. This  $1 \times 4$  power splitter divider is not able to transmit enough power from input to output side. In order to that we proposed a novel design which is based on MMI block integrated with PC LDWs for  $1 \times 4$  power splitter application.

In this section we have first designed the 2-D configuration of  $1\times 4$  power splitter based on MMI block integrated with PC LDWs. The entire configuration is examined by 2-D FDTD computational method. MMI length plays an important role to maximize the power from input to output. In this scheme, 77.3% of input power transmitted at the output. The length of the device is somewhat big but the output spectrum (45nm broad) and transmitted power is promising. As a result, the design is successfully extended on 2-D slab configuration. In this configuration, qualitative amount of power i.e. 75.7% power is transmitted with 46nm broad spectrum. The length and width of the device is  $56.2\mu\text{m}$  and width  $11.08\mu\text{m}$  respectively.

Multiple LDWs are used for  $1\times 4$  power splitter application. This power is based on combination of seven and one pair of three LDWs and another one five and one pair of three line defect waveguides. The branching topologies of these power splitters are very simple. In the case of seven and one pair of three LDWs structure transmits 91.1% of input power with 10nm broad spectrum. The amount of power is less than the results obtained from the literature review. So, in an attempt to improve this result, another structure which is based on the five and one pair of three LDWs is examined by 2-D FDTD simulation method. Simulation results of these architectures transmit 94.9% of input power with 32nm broad spectrum and the result can be comparable with the results of the literature review result which have already been discussed in chapter 6. By using this architecture concept we have explored  $1\times 3$  power splitter on 2-D slab PC. The splitter is a combination of three and five LDWs. The entire structure is examined by 3-D FDTD method. The branching topology of this power splitter is optimized to increase the

overall power transmitted into the branch. The input power is transmitted equally through all output branches.

## 7.2 Suggestion for Future Work

**MMI and multiple line defect waveguides for 1×4 power splitter:** For the future, it is worthwhile to improve the 1×4 power splitter design (Figure 7.1). This design can be achieved the better power transmission by optimizing the multiple LDWs.

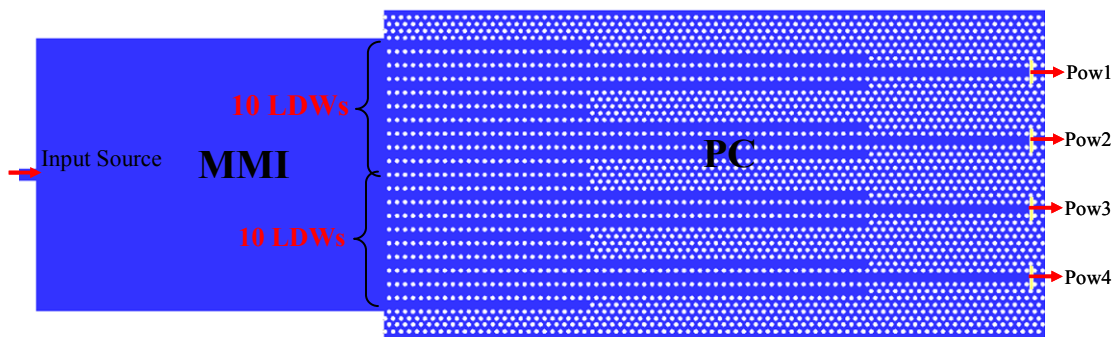


**Figure 7.1 Multiple line defect waveguides integrated with MMI for 1×4 power splitter application**

The design is based on one pair of ten multiple LDWs integrated with MMI. This one pair of ten LDWs is ended up with four LDWs as an output channel. We will analyze the whole structure with 2-D FDTD method for improving the power transmission from input side to output.

**Fabrication and Measurements:** We would like to fabricate the 2-D slab PC 1×4 MMI based power splitter and 1×3 power splitter based on 2-D slab PC based multiple LDWs and also to conduct experiments to verify the simulation results of power transmission and spectrum bandwidth.

**Photonic crystal based MMI power splitter:** The four channel power splitter architecture implemented in chapter 3, 4 and 5 is based on 2-D and 2-D slab PC.

Although we have achieved better power transmission on the respective design which is already discussed in chapter 3, 4 and 5 yet we will investigate PC based MMI structure  $1 \times 4$  power splitter to improve the power transmission and to reduce the length of the device. The proposed structure is shown in figure 7.2

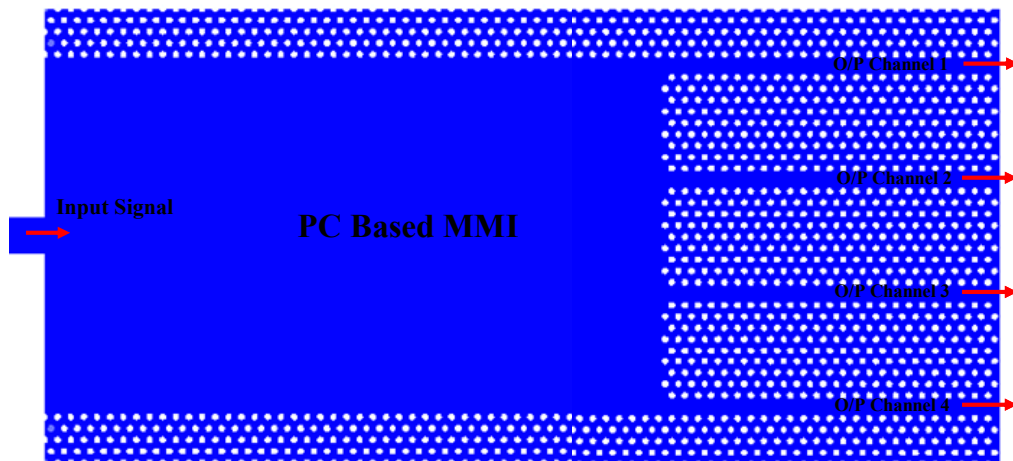


**Figure 7.2 2-D PC based MMI for  $1 \times 4$  power splitter application**

# Bibliography

- [1] J.D.Joannopoulos, R.D.Meade and J.N.Winn, Photonic Crystals: Molding the flow of light, (Princeton University Press, New York, 1995).
- [2] C.M.Soukoulis, Photonic Crystals and light Localization in the 21<sup>st</sup> century, (Kluwer Academic Publishers, 2000).
- [3] E.Yablonovitch, “Photonic crystal: Semiconductor of light”, Scientific American, pp. 47-55, 2001.
- [4] S.John, “Strong localization of photons in certain disordered dielectric super lattices,” Phys.Rev. Lett. vol.58, pp 2286, 1987.
- [5] S. Boscolo, M. Midrio, and T.F. Krauss, “Y junction in photonic crystal channel waveguides: high transmission and impedance matching,” Opt. Lett. vol. 27, pp. 1001-1003, 2002
- [6] T. Yu, H. Zhou, J. Yang, X. Jiang, and M. Wang, “ Ultracompact multiway beam splitters using multiple coupled photonic crystal waveguides,” J. Phys.D:Appl. Phys. vol.41, pp. 1-5, 2008.
- [7] S. Fan, S.G. Johnson, J.D. Joannopoulos, C. Manolatu, and H. A. Haus, “ Waveguide branches in photonic crystals”, J. Opt. Soc. Am. B. vol 18, pp 162-165, 2001.
- [8] A. Ghaffari, M. Djavid, and M.S. Abrishamian, “ Power splitters with different output power levels based on directional coupling”, Appl. Optics, vol. 48, pp. 1606-1609, 2009.
- [9] S. Wei, and X. Kang, “Optimal design of a multi-mode interference splitter based on SOI”, Optoelectronics Lett., vol. 4, pp. 0092-0095, 2008.



- [10] M. Forbes, J. Goulay, and M. Desmulliez, “Optically interconnected electronic chips: A tutorial and review of the technology”, *J. Elect. And Comm. Engg.*, vol. 13, pp 221-223, 2001.
- [11] E. Cassan, D. Marris, M. Rouviere, L. Vivien, and S. Suzanne, “Comparison between electrical, optical global clock distributions for CMOS integrated circuits”, *optical Engineering*, vol. 44, pp 105402, 2005.
- [12] P. Kapur, and K. Saraswat, “Optical interconnects for future high performance integrated circuits”, *Physica E*, vol. 16, pp. 620-627, 2003.
- [13] A. Keeler, E. Nelson, D. Agarwal, C. Debaes, C. Helman, A. Bhatnagar, and A.B. Miller, “The benefits of ultrashort optical pulses in optically interconnected systems”, *IEEE J. Sel. Topics in Quantum Electronics*, vol. 9, pp. 477-485, 2003.
- [14] T. Yamashita, and J. Summers, “Evaluation of self-collimated Beams in photonic crystal for optical interconnects”, *IEEE J. Sel. Areas in Comm.* vol. 23, pp 1341-1347, 2005.
- [15] J. D. Joannopoulos, “Manipulating light with PCs”, *Proceedings of CPIOE*, vol. 4253, pp. 1-10, 2001.
- [16] C. M. Soukoulis, “Photonic Crystals and Light localization in the 21<sup>st</sup> Century”, Kluwer Academic Publishers, ISBN: 978-0-7923-6947-9, 2000.
- [17] K. Inoue, K. Ohtaka, “Photonic Crystals” *Physics, fabrication and Applications*”, Springer, Berlin 2004, ISBN 3-540-20559-4, 2004.
- [18] D.W. Prather, S.Shi, A.S.J.Murakowski and G. Schneider, *Photonic Crystals Theory, Application, and Fabrication*, Wiley, New Jersey, 2009.

- [19] G.Johnson, P.R. Villeneuve, S. Fan and J.D. Joannopoulos, “Linear waveguides in photonic-crystal slab”, *Physical Review B*, vol. 62 (12), pp. 8212-8222, 2000.
- [14] J. D. Joannopoulos, “Manipulating light with PCs”, *Proc. of SPIE*, vol. 4253, pp 1-10, 2001.
- [20] C. Jamois, R.B. Wehrspohn, L.C. Andreani, C. Hermann, O. Hess and U. Gösele, “Silicon-based two-dimensional photonic crystal waveguides”, *Photonics and Nanostructures- Fundamentals and Application*, vol.1, pp. 1-13, 2003.
- [21] H. Kurt, “Photonic crystals: analysis, design and biochemical sensing application”, PhD thesis, Georgia Institute of technology, 2006.
- [22] D. Cassagne, A. Barra, and C. Jouanin, “Defects and Diffraction in Photonic Crystals”, *Superlattice. Micros.*, vol. 25, pp. 343-346, 1999.
- [23] R.D. Pradhan and G.H. Watson, “Impurity Effects in Coaxial-Connector Photonic Crystal: A Quasi-One-Dimensional Periodic System,” *Phys. Rev. B*, vol. 60, pp. 2410-2415, 1999.
- [24] G.J. Schneider, S. Hanna, J.L. Davis, and G.H. Watson, “ Defect Modes in Coaxial Photonic Crystals,” *J. Appl. Phys.*, vol. 90, pp. 2642-2649, 2001.
- [25] S.Y. Lin, J.G. Fleming, M.M. Sigalas, R. Biswas, and K.M. Ho, “Photonic Bandgap Microcavities in Three Dimensions,” *Phys Rev. B*, vol. 59, pp. R15579-R15582, 1999.
- [26] T. Ueta, K. Ohtaka, N. Kawai, and K. Sakoda, “ Limits on Quality Factors of Localized Defect Modes in Photonic Crystals due to Dielectric Loss,” *J. Appl. Phys.*, vol. 84, pp. 6299-6304, 1998.
- [27] A. Yariv, *Optical Electronics in Modern Communication*, 5th ed. New York: Oxford University Press, 1997.

- [28] M. Agio, E. Lidorikis, and C.M. Soukoulis, "Impurity Modes in a Two-Dimensional Photonic Crystal: Coupling Efficiency and Q Factor," *J. Opt. Soc. Am. B*, vol. 17, pp. 2037-2042, 2000.
- [29] O. Painter, R. K. Lee, A. Yariv, A. Scherer, J. D. O'Brien, P. D. Dapkus, and I. Kim, "Two-dimensional photonic band-gap defect mode laser," *Science*, vol. 284, pp. 1819-1821, June 1999.
- [30] J. Sabarinathan, P. Bhattacharya, P-C. Yu, and S. Krishna, "An electrically injected InAs/GaAs quantum-dot photonic crystal microcavity light emitting diode," *Appl. Phys. Lett.*, vol. 81 (20), pp. 3876-3878, 2002.
- [31] E. Chow, A. Grot, L. W. Mirkarimi, M. Sigalas, and G. Girolami, "Ultra compact biochemical sensor built with two-dimensional photonic crystal microcavity," *Optics Lett.*, vol. 29, no. 10, pp. 788-789, May 15, 2004.
- [32] M. Soltani, A. Haque, B. Momeni, A. Adibi, Y. Xu, R. k. Lee, "Designing complex optical filters using photonic crystal microcavities," *Proceedings of the SPIE*, vol. 5000, pp. 257-265, 2003.
- [33] L.H. Frandsen, P.I. Borel and Y.X. Zhuang, A. Harpøth, M. Thorhauge, M. Kristensen, W. Bogaerts, P. Dumon, R. Baets, V. Wiaux, J. Wouters, and S. Beckx, "Ultralow-loss 3-dB photonic crystal waveguide splitter," *Opt. Lett.*, vol.29, pp. 1623-1625, 2004.
- [34] I. Park, H. S. Lee, H. J. kim, K M. Moon, S.G. Lee, B. H. O, S. G. Park, and E. H. Lee, "Photonic crystal power-splitter based on directional coupling," *Opt. Express*, vol. 12, pp. 3599-3604, 2004.

- [35] Z. Ma, and K. Ogusu, "Power splitter based on cascaded multimode photonic crystal waveguides with triangular lattice of air holes," *Opt Commun.* vol. 282, pp. 3473-3476, 2009.
- [36] E. Yablonovitch, "Inhibited spontaneous emission in solid-state physics and electronics," *Phys. Rev. Lett.* vol.58, pp 2059, 1987.
- [37] A. Chutinan and S. Noda, "Waveguides and waveguides bends in two-dimensional photonic crystal slabs," *Phys. Rev.B.* vol.62, pp 4488, 2000.
- [38] W. Yang, X. Chen, X. Shi, and W. Lu, "Design of a high transmission Y-junction in photonic crystal waveguides," *Physica B*, vol.405, pp 1832, 2010.
- [39] T. F. Krauss, R. M. Delarue, and S. Brand, "Two-dimensional photonic-bandgap structures operating at near-infrared wavelengths," *Nature*, vol.383, pp 699, 1996.
- [40] M. Loncar, D. Nedeljkovic, T. Doll, J. Vuckovic, A. Scherer, and T. P. Pearsall, "Waveguiding in planar photonic crystals," *Appl.Phys.Lett.* vol.77,pp 1937, 2000.
- [41] E. Chowm S. Y. Lin, S. G. Johnson, P. R. Villeneuve, J. D. Joannopoulos, J. R. Wendt, G. A. Vawter, W. Zubrzycki, H. Hou, and A. Alleman, " Three-dimensional control of light in a two-dimentional photonic crystal slab," *Nature*, vol. 407, pp 983, 2000.
- [42] M. Notomi, A. Shinya, K. Yamada, J. Takahashi, C. Takahashi, and I. Yokohama, " Singlemode transmission within photonic bandgap of width-varied single-line-defect photonic crystal waveguides on SOI substrates," *Electron.Lett.* vol.37, pp 293, 2001.
- [43] H.S.Zhen, T.Jie,R.Cheng,X.X.Sheng, L.Z.Yuan, C.B.Ying, and Z.D.Zhong, " A Y-branch photonic crystal slab waveguides with an ultrashort interport interval," *Chin.Phys.Lett.* vol.22, pp 1934, 2005.

- [44] P.I.Borel, L.H.Frandsen, A.Harpøth, M. Kristensen, J.S.Jensen, and O.Sigmund, "Topology optimized broadband photonic crystal Y-splitter," *Electron. Lett.* vol.41, pp 69, 2005.
- [45] L.Dekkiche, and R.Naoum, "Improved transmission for photonic crystal Y-junctions," *Electrical Engineering*, vol.89, pp 71, 2006.
- [46] R.Wilson, T.J.Karle, I.Moerman, and T.F.Krauss, "Efficient photonic crystal Y-junctions," *J.Opt.A:Pure Appl.Opt.* vol.5, pp S76, 2003.
- [47] M. Koshiba, Y.Tsuji, and M.Hikari, "Time-domain beam propagation method and its application to photonic crystal circuits," *J.Lightwave Technol.* vol.18,pp102,2000.
- [48] A.Taflove, S.C Hagness, *Computational Electrodynamics: The Finite-Difference Time-Domain Method*, Artech House, 2000.
- [49] A. Mekis, JC. Chen, I.Kurland, S. Fan, PR. Villeneuve, and JD.Joannopoulos, "High transmission through sharp bends in photonic crystal waveguides," *Phys Rev. Lett.* vol.77,pp3787,1996.
- [50] Y. Zhang, Z. Li, and B. Li, "Multimode interference effect and self-imaging principle in two-dimensional silicon photonic crystal waveguides for terahertz waves", *Opt. Express* 14, 2679-2689 (2006),
- [51] H.J. Kim, I. Park, B.H.O, S.G. Park, E.H. Lee, and S.G. Lee, "Self-imaging phenomena in multi-mode photonic crystal line defect waveguides: application to wavelength de-multiplexing", *Opt. Express* 12, 5625-5633 (2004),
- [52] L.B. Soldano, and E. C. M. Pennings, "Optical multi-mode interference devices based on self-imaging: Principles and Applications", *J. Lightwave Technol.* 13, 615-627 (1995).

- [53] M.H. Ibrahim, N.M. Kassim, A.B. Mohammad, M.K. Chin, S.Y. Lee, "Polymeric optical splitter based on multimode interference mechanism", SCORed, 58-60 (2006).
- [54] A. Ghaffari, M.Djavid, and M.S. Abrishamian, "Bi-periodic photonic crystal Y-splitter," *Physica E*. vol.41, pp. 1495-1499, 2009.
- [55] J. Zimmermann, M. Kamp, A. Forchel, and R. März, "Photonic crystal waveguide directional couplers as wavelength selective optical filters", *Opt.Commun.* vol.230, pp.387-392, 2004.
- [56] H. Chen, Y. Xu, J. He, and Z. Hong, "A polarization splitter based on self-imaging phenomena in an anisotropic photonic crystal with an absolute photonic bandgap", *Opt.Commun.* vol.282, pp.3626-3629, 2009.
- [57] A. Ghaffari, M. Djavid, F. Monifi, and M.S. Abrishamian, "Photonic crystal power splitter and wavelength multi/demultiplexer based on directional coupling," *J.Opt.A:Pure Appl.Opt.*vol.10, pp. 1-7, 2008.
- [58] K. Sakoda, *Optical Properties of photonic Crystals*, Springer, 2001.
- [59] D.W. Prather, S. Shi, J. Murakowski, G. J. Schneider, A. Sharkawy, C. Chen, B. Miao, " Photonic crystal structures and applications: perspective, overview and development," *IEEE Journal of Selected Topics in Quantum Electronics*, vol. 12, 2006.
- [60] A. Yariv, and P. Yeh, *Optical Waves in Crystals*, Wiley, New York, 1984.
- [61] R. Wilson, T. J. Karle, I. Moerman, and T. F. Krauss, "Efficient photonic crystal Y-junctions," *J. Opt. A: Pure Appl. Opt.*, vol. 5, pp. 76-80, 2003.

# Appendix A: Gold deposition on alignment marks through lift off process

Gold is deposited on alignment marks through the lift off process. After that photolithography is done for conventional waveguide. Then the sample is ready for e-beam lithography for aligning and writing for photonic crystal patterns with conventional waveguide. After that whole sample is ready for dicing. This appendix focuses on the gold deposition on alignment marks through life off process.

**Table A-1: Recipe for gold deposition on alignment marks through lift off process**

1. Silicon must go through cleaning process prior to photo-resist coating. The silicon is placed in a nanostrip at 80<sup>0</sup>C for 3 minutes.
2. Rinse and dryer.
3. HMDS deposition for adhesive of photo-resist with silicon substrate.
4. LOR is used as a lift off resist:
  - i) Spread speed of 300rpm for 5 second.
  - ii) Spin speed of 3500rpm for 45 second.
  - iii) Prebake at 170<sup>0</sup>C for 150 second.
5. Shiply 1805:1827 at 1:1 ratio is used as a photo-resist:
  - i) Spread speed of 500rpm for 5 second.
  - ii) Spin speed of 4500rpm for 45 second.
  - iii) Prebake at 115<sup>0</sup>C for 3 minute.
  - iv) Aligment marks are exposed to UV (Ultraviolet) rays in MA6 machine for 5.8 second of channel at 6mW/cm<sup>2</sup> and developed in MF 319 for 50 second and hard baked at 120<sup>0</sup>C for 5 minute and then developed for 90 second in MF 319 and gently rinsed in water and dried with soft blow of air.
6. Samples is then descummed using STS RIE machine using the recipe descum.
7. Cr of 2nm and gold of 100nm is deposited using e-beam evapouration technique.
8. The lift off process is continued with PG remover at 60<sup>0</sup>C to remove lift off resist and photo-resist and obtain gold alignment marks.

# Appendix B: Photolithography with conventional waveguide and etching for conventional waveguide

This appendix represents the process of fabrication of conventional waveguide. After achieving the gold alignment marks on the sample the next steps is fabrication of conventional waveguide on the sample which will be integrated with Y-junction base structure for launching the light.

**Table B -1: Recipe for conventional waveguide etching**

- 1) HMDS deposition for adhesive of photo-resist with silicon substrate
- 2) Spin coating of Shipley 1805:
  - i) Spread speed of 500rpm for 5 second.
  - ii) Spin at 3000rpm for 40 second.
  - iii) Pre bake at 113<sup>0</sup>C on hot plate for 3 minute.
  - iv) Alignment marks is exposed to UV rays in MA6 machine for 3.4 second of channel 2 at 18mW/cm<sup>2</sup> and developed in MF 319 for 1minute.
- 3) Samples are placed in deep silicon etch machine for etching silicon (etch rate is about 16.67nm/sec) for conventional waveguides.
- 4) PG remover is used for cleaning photoresist at 60<sup>0</sup>C with ultrasonic bath.
- 5) The sample is removed from the PG remover then it placed in a nanostrip at 80<sup>0</sup>C for 3 minute for cleaning process and then rinsed with lot of water and dry air.



# Appendix C: E-beam Lithography

Zep520A D.R = 1.4 is dispensed onto the wafer and spun rapidly to produce a 200nm uniformly thick layer at 300rpm for 3second and 3500rpm for 120 second. Comparing to PMMA, it has an advantage of 3-4 times faster and has good dry etch resistance. It has the disadvantages of poor adhesion and normal exposure does result in re-entrant pattern profiles. The photoresist-coated wafer is then prebaked to drive off excess solvent, typically 180<sup>0</sup>C for 3 minutes.

For high resolution lithography, writing conditions of e-beam lithography needs to be optimized. To write the PC waveguides coupled to conventional waveguide, the parameters were set to be:

**Table C-1: Parameters of E-beam**

<b>Parameters of E-beam Lithography</b>
1) Accelerating Voltage: 30kV
2) Aperture: 10 $\mu$ m
3) Beam Current: ~28pA
4) Magnification: 800X
5) Line Spacing: 20nm
6) Centre to centre distance: 20nm
7) Dose: Varied from 57 $\mu$ C/cm <sup>2</sup> to 78 $\mu$ C/cm <sup>2</sup>

## Appendix D: Recipe for Bosch etching

The 40 seconds etching process for individual sample consisted of two alternating steps. First, plasma etching is using SF<sub>6</sub> for 1 second. Second, passivation by C<sub>4</sub>F<sub>8</sub> for 2 second.

Table below shows the optimized parameters for ICP Alcatel system to achieving high etch rate and high aspect ratio.

**Table D-1: Recipe for ICP etch**

<b>ICP Etch</b>
1) RF power for Plasma generation: 1000 Watts
2) Substrate RF power: 50 Watt
3) Chamber Pressure: 1.3E-3mBar to 9E-2mBar
4) Chamber Temperature: 20 <sup>0</sup> C
5) Helium Pressure: 1E+1mBar
6) SF <sub>6</sub> Flow: 100sccm
7) C <sub>4</sub> F <sub>8</sub> Flow: 100sccm

# Curriculum Vitae

Name: Rajat Dey

Education: Post Graduate Diploma in Electronics,  
Royal Melbourne Institute of Technology, Australia, 2006

Master of Engineering in Microelectronics,  
Royal Melbourne Institute of Technology, Australia, 2006

Bachelor of Engineering in Electronics,  
Nagpur University, India, 2002

Awards: Western Engineering Scholarship (UWO), 2007-2011

Related Work Teaching Assistant, UWO, 2007-2010  
Research Assistant, UWO, 2007-2011

## Publication:

- [1] R. Dey and J. Sabarinathan, "Comparison between 2-D Slab Photonic Crystal Based Y-Junction and MMI Power Splitter", International Conference on Frontier Topics in Nanostructures and Condensed Matter Theory, March 2011.
- [2] R. Dey, J. Sabarinathan, "1 to 3 Power splitter Based on 2-D Slab Photonic Crystal Multiple Line Defect Waveguides", Photonic North Conference, May 2011.
- [3] R. Dey, A. Bakhtazad, and J. Sabarinathan, "1×4 Power Splitter Based on 2-D Slab Photonic Crystal Line Defect Waveguides Integrated with MMI", Information Photonics, May 2011.
- [4] R. Dey, A. Gujjula, J. Sabarinathan, "Optical Delay Lines Using Photonic Crystal Coupled Cavity Waveguide", (Poster) WINS workshop, University of Western Ontario, 2008.
- [5] R. Dey, A. Bakhtazad, and J. Sabarinathan, "Power splitter based on 2-D photonic crystal multiple line defect waveguides", J. Phys D: Appl. Phys, Submitted
- [6] R. Dey, A. Bakhtazad, and J. Sabarinathan, "Two dimensional photonic crystal line defect waveguides integrated with multimode interference block for power splitter application", Optics Express, Submitted
- [7] R. Dey, and J. Sabarinathan, "2-D slab photonic crystal Y-junction based 1 to 2 power splitter," Prepared.